UNIVERSIDADE DE SÃO PAULO

YONARA DE GOUVEIA CORDEIRO

Contribuições para o estudo da heterogeneidade inter e intratumoral em neoplasias mamárias em cadelas

Pirassununga

2020

YONARA DE GOUVEIA CORDEIRO

Contribuições para o estudo da heterogeneidade inter e intratumoral em neoplasias mamárias em cadelas

Versão Corrigida

Tese apresentada à Faculdade de Zootecnia e Engenharia de Alimentos da Universidade de São Paulo, como parte dos requisitos para a obtenção do título de Doutor em Ciências do programa de pós-graduação em Biociência Animal.

Área de Concentração: Genética, Biologia Celular e Molecular

Orientador: Prof. Dr. Heidge Fukumasu

Pirassununga

2020

Ficha catalográfica elaborada pelo
Serviço de Biblioteca e Informação, FZEA/USP,
com os dados fornecidos pelo(a) autor(a)

Cordeiro, Yonara de Gouveia
C794c Contribuições para o estudo da heterogeneidade inter e intratumoral em neoplasias mamárias em cadelas / Yonara de Gouveia Cordeiro ; orientador Heidge Fukumasu. -- Pirassununga, 2020.
93 f.

Tese (Doutorado - Programa de Pós-Graduação em Biociência Animal) -- Faculdade de Zootecnia e Engenharia de Alimentos, Universidade de São Paulo.

1. Biomarcadores tumorais. 2. Carcinomas mamários caninos. 3. Heterogeneidade tumoral. 4. Oncologia Comparada. I. Fukumasu, Heidge, orient. II. Título.

UNIVERSIDADE DE SÃO PAULO
Faculdade de Zootecnia e Engenharia de Alimentos
Comitê de Ética em Pesquisa da FZEA

CERTIFICADO

Certificamos que a proposta intitulada "Estudo da heterogeneidade intratumoral de neoplasias mamárias em cadelas", protocolada sob o CEUA nº 8632101017, sob a responsabilidade de **Yonara de Gouveia Cordeiro** - que envolve a produção, manutenção e/ou utilização de animais pertencentes ao filo Chordata, subfilo Vertebrata (exceto o homem), para fins de pesquisa científica ou ensino - está de acordo com os preceitos da Lei 11.794 de 8 de outubro de 2008, com o Decreto 6.899 de 15 de julho de 2009, bem como com as normas editadas pelo Conselho Nacional de Controle da Experimentação Animal (CONCEA), e foi **aprovada** pela Comissão de Ética no Uso de Animais da Faculdade de Zootecnia e Engenharia de Alimentos da Universidade de São Paulo - FZEA/USP (CEUA/FZEA) na reunião de 19/12/2017.

We certify that the proposal "Intratumoral heterogeneity in canine mammary carcinomas", utilizing 10 Dogs (10 females), protocol number CEUA 8632101017, under the responsibility of **Yonara de Gouveia Cordeiro** - which involves the production, maintenance and/or use of animals belonging to the phylum Chordata, subphylum Vertebrata (except human beings), for scientific research purposes or teaching - is in accordance with Law 11.794 of October 8, 2008, Decree 6899 of July 15, 2009, as well as with the rules issued by the National Council for Control of Animal Experimentation (CONCEA), and was **approved** by the Ethic Committee on Animal Use of the School of Animal Science and Food Engineering - (São Paulo University) (CEUA/FZEA) in the meeting of 12/19/2017.

Finalidade da Proposta: Pesquisa (Acadêmica)

Vigência da Proposta: de 07/2017 a 01/2019 Área: Biociência Animal

Origem:	Animais de proprietários						
Espécie:	Cães	sexo:	Fêmeas	idade:	0 a 20 anos	N:	10
Linhagem:	Sem especificações			Peso:	1 a 60 kg		

Resumo: O câncer é uma doença complexa e multifatorial, que apresenta diversos subtipos celulares geneticamente diferentes mesmo entre clones de uma mesma massa tumoral, compreendendo a heterogeneidade intratumoral. Estudos recentes têm ajudado a definir as interações entre as diferentes subpopulações celulares necessárias à evolução desse sistema complexo, porém os modelos de desenvolvimento neoplásico propostos até o momento ainda não permitem um completo entendimento de como acontece esta evolução. A iniciação e progressão das neoplasias sólidas, como no caso dos cânceres de glândula mamária na medicina humana ou veterinária, ainda é um tema controverso.

Local do experimento: Hospital Veterinário e laboratórios da FZEA/USP

Pirassununga, 18 de janeiro de 2018

Profa. Dra. Daniele dos Santos Martins
Coordenadora da Comissão de Ética no Uso de Animais
Faculdade de Zootecnia e Engenharia de Alimentos da
Universidade de São Paulo - FZEA/USP

Profa. Dra. Cristiane Gonçalves Titto
Vice-Coordenadora da Comissão de Ética no Uso de Animais
Faculdade de Zootecnia e Engenharia de Alimentos da
Universidade de São Paulo - FZEA/USP

FOLHA DE APROVAÇÃO

Nome: Yonara de Gouveia Cordeiro

Título: Contribuições para o estudo da heterogeneidade inter e intratumoral em neoplasias mamárias em cadelas

Tese apresentada à Faculdade de Zootecnia e Engenharia de Alimentos da Universidade de São Paulo, como parte dos requisitos para a obtenção do título de Doutor em Ciências do programa de pós-graduação em Biociência Animal.

Área de Concentração: Genética, Biologia Celular e Molecular

Data: ____/____/_____

BANCA EXAMINADORA

Prof. Dr. _____

Instituição: _____ Julgamento: _____

Prof. Dr. _____

Instituição: _____ Julgamento: _____

Prof. Dr. _____

Instituição: _____ Julgamento: _____

Prof. Dr. _____

Instituição: _____ Julgamento: _____

Prof. Dr. _____

Instituição: _____ Julgamento: _____

AGRADECIMENTOS

À Deus, sempre e em primeiro lugar. Por nunca ter soltado a minha mão, me conduzindo ao longo dos caminhos tortuosos da vida;

À minha mãe, Ana Maria, a base forte da minha estrutura e meu modelo. A razão por eu ter chegado até aqui.

À minha família. Meus avós e anjos-da-guarda Zé Carro e Jandira, que de onde estiverem olham por mim e me acompanham. Minhas amadas tias, Nice, Tereza e Iolanda. E todos os meus tios, primos e primas. A vida não seria tão doce sem vocês;

Ao Joost, presente que a Holanda me deu. Que mesmo a um oceano Atlântico de distância se fez sempre presente. Ik hou van jou, kleine leeuw.

Ao Prof. Heidge, que desde 2011 me recebeu, me acompanhou e me orientou neste mundo apaixonante da pesquisa em câncer. Tenho muito orgulho por ter sido sua orientada durante todos estes anos, e grata pela oportunidade de evoluir junto com o LOCT;

Aos professores e amigos Prof. Ricardo de F. Strefezzi, e Prof. José Bento S. Ferraz, que sempre me inspiraram pessoal e profissionalmente, e sempre estiveram à disposição para ajudar e ensinar;

Aos colegas e amigos do LOCT. Em especial à Arina, Pedro e Pedrinho, companheiros de tantos anos. Aos pós-graduandos Taismara, Jéssika, Gabriela, Sacha, Júlia, Roberta e Thiago, todos os ICs e demais novos integrantes, que vocês possam um dia olhar pra trás e sentir o mesmo orgulho e realização que eu sinto hoje, por ter feito parte desta "família";

À todos os amigos. Em especial a minha migles e eterna *roomie* Pâmela, e também à Lídia. Choramos, rimos, celebramos, trabalhamos, reclamamos, nos ajudamos... Enfim, vivemos e sobrevivemos. Meu coração se enche de alegria a cada conquista de vocês;

Ao Prof. Manfred Wührer, por ter aceitado o meu estágio no exterior, e a todos do Centro de Proteômica e Metabolômica do LUMC. Ao grupo de espectrometria de massas por imagem que me recebeu tão bem, Hans, Renée, Fanny, Leandra, Walter, Cristina, e em especial ao Dr. Bram Heijs, que me supervisionou durante todo o trabalho. Não poderia ter pedido por uma experiência melhor;

Ao programa de Biociência Animal e à FZEA/USP, por permitirem o desenvolvimento deste trabalho. À CAPES pela bolsa (processo nº 88882.376316/2007-1) e à FAPESP pelo auxílio financeiro (processo nº 2014/02493-7);

E enfim, à Becca, minha sempre companheira de quatro-patas, pelo seu amor incondicional.

Obrigada!

“A vida é uns deveres que nós trouxemos para fazer em casa.

Quando se vê, já são 6 horas; há tempo.
Quando se vê, já é 6ª-feira.
Quando se vê, passaram 60 anos...
Agora, é tarde demais para ser reprovado.

E se me dessem – um dia – uma outra oportunidade,
eu nem olhava o relógio
Seguia sempre, sempre em frente

E iria jogando pelo caminho a casca dourada e inútil das horas.”

- Seiscentos e sessenta e seis, Mário Quintana

RESUMO

CORDEIRO, Y.G. **Contribuições para o estudo da heterogeneidade inter e intratumoral em neoplasias mamárias em cadelas.** 2020. 99f. Tese (Doutorado). Faculdade de Zootecnia e Engenharia de Alimentos. Universidade de São Paulo. 2020.

As neoplasias mamárias estão entre as mais frequentes em cães assim como em humanos. São consideradas excelentes modelos para o estudo da biologia do câncer, uma vez que algumas semelhanças, como sua apresentação espontânea, são difíceis de replicar em outros modelos animais. As diferenças entre os subtipos tumorais, bem como o alto grau de heterogeneidade inter e intratumoral, exigem marcadores mais precisos para melhorar o diagnóstico e prognóstico destas neoplasias. Além disso, novas informações sobre mecanismos moleculares podem levar a novos alvos terapêuticos, aprimorando o cuidado dado aos pacientes. Este trabalho teve como principais objetivos: (i) Associar a expressão gênica global à tumorigenicidade e potencial de invasão em linhagens celulares derivadas de carcinomas mamários caninos, a fim de estabelecer um modelo *in vitro* para pesquisas básicas e aplicadas; e (ii) Caracterizar subpopulações tumorais, em tecidos primários e metástases, a partir de alterações morfológicas e moleculares utilizando a espectrometria de massas por imagem (MALDI-MSI) para a determinação de alterações em vias associadas ao câncer. No primeiro capítulo, mostramos diferenças na expressão gênica entre as duas culturas celulares em comparação com o tecido normal da glândula mamária. Também, observamos maior invasão e potencial tumorigênico *in vivo* na linhagem M25, associados à maior expressão de genes envolvidos na adesão focal e comunicação com a matriz extracelular. Nos capítulos 2 e 3, identificamos alterações nos perfis de expressão de proteínas em subpopulações tumorais e metastáticas utilizando tanto o fenótipo morfológico, quanto o fenótipo molecular das populações indistinguíveis microscopicamente, relacionadas principalmente à vias associadas ao processamento de proteínas, componentes da matriz extracelular, adesão focal e regulação epigenética. Estes resultados em conjunto com aqueles encontrados no experimento *in vitro* demonstram a importância e complexidade dos carcinomas mamários heterogêneos em cães e devem direcionar a busca para a determinação de biomarcadores dos diferentes estágios da progressão tumoral.

Palavras chave: biomarcadores tumorais; carcinoma mamário; MALDI; transcriptoma

ABSTRACT

CORDEIRO, Y.G. **Contribution to the study of inter and intratumor heterogeneity in canine mammary carcinomas.** 2020. 99f. PhD Thesis. Faculdade de Zootecnia e Engenharia de Alimentos. Universidade de São Paulo. 2020.

Mammary tumors are among the most common types of cancer in dogs as well as in humans. Considered as excellent models for the study of cancer biology, similarities such as their spontaneous nature are difficult to be replicated in other animal models. Mammary tumors can be classified in many tumor subtypes, presenting a higher degree of inter and intratumoral heterogeneity. New insights on biomolecular mechanisms may lead to new therapeutic targets, improving diagnosis and prognosis and also improving patient care. Therefore, the main purposes of this work were: (i) To correlate global gene expression with tumorigenicity and invasion potential in canine mammary carcinoma cell lines, in order to establish an *in vitro* model for basic and applied oncology studies; and (ii) To characterize, using image mass spectrometry (MALDI-MSI), tumor subpopulations in primary tissues and metastasis through morphological and molecular features, in order to identify altered cancer-related pathways. In the first chapter, we showed differences regarding gene expression between two cell lines and a normal mammary gland tissue, as well as a higher invasion and *in vivo* tumorigenic potential of M25 cells associated to upregulation of genes involved in focal adhesion and extracellular matrix organization. In chapters 2 and 3, alterations in protein expression profiles of tumor and metastatic subpopulations were identified using both the morphological and the molecular phenotype of microscopically indistinguishable populations. Such differences were found mainly related to protein-processing pathways, extracellular matrix components, cell adhesion pathways and epigenetic regulations. These results should direct a search for the determination of biomarkers of populations in distinct levels of tumor progression.

Key words: cancer research; MALDI imaging; mammary carcinoma; transcriptomic, tumor biomarkers

SUMÁRIO

INTRODUÇÃO

A oncologia é uma área relevante tanto na medicina humana quanto veterinária, seja pelo aumento do número de casos diagnosticados a cada ano, ou por se tratar de doenças em sua maioria sem cura. Nos cães, as neoplasias mamárias podem ser classificadas em mais de 20 tipos histológicos diferentes, e com frequência, estes animais apresentam múltiplas formações simultâneas com classificações histopatológicas distintas, determinando a heterogeneidade intertumoral. Porém, sabe-se a tempos que somente a classificação histopatológica não é suficiente para a determinação do prognóstico clínico em todos os pacientes, e portanto, a caracterização molecular de genes e seus produtos se faz necessária para uma melhor compreensão da doença. Ainda, temos a presença de populações celulares com perfis moleculares diferentes em uma mesma massa tumoral, onde estas populações normalmente não são distinguíveis por métodos diagnósticos tradicionais. Esta heterogeneidade intratumoral advém do fato que alguns grupos de células adquirem características de forma diferenciada, podendo definir o curso da doença e influenciando na sobrevida e no bem-estar dos indivíduos.

As neoplasias mamárias em cadelas são muito semelhantes àquelas diagnosticadas em mulheres, o que as tornam excelentes modelos para o estudo em oncologia comparada. Entretanto, em medicina veterinária, a literatura é escassa quanto a estudos sobre a heterogeneidade intratumoral das neoplasias sólidas. Estudos *in vitro* utilizando linhagens celulares permitem importantes descobertas sobre a origem, fisiopatologia, alvos terapêuticos e biomarcadores tumorais. Além disso, são necessários para o rastreamento de substâncias com propriedades antitumorais, contribuindo para o desenvolvimento e aprimoramento de terapias. Porém, a maioria dos estudos é realizada em cultivos de células mantidas à longo prazo, os quais fornecem dados valiosos para a investigação do comportamento tumoral, mas ainda é um recurso limitado devido à perda da similaridade com o tecido primário. Neste contexto, a espectrometria de massas por imagem surge como uma abordagem nova e eficiente, uma vez que, sem a necessidade de marcadores específicos, como anticorpos por exemplo, é capaz de detectar a expressão de biomoléculas ao mesmo tempo em que mantém a integridade do corte histológico, economizando tempo e recursos por direcionar a busca por novos marcadores tumorais.

Esta tese apresenta o estabelecimento e a caracterização de linhagens celulares morfologicamente semelhantes, mas com diferenças quanto à malignidade; e também, investiga a heterogeneidade inter e intratumoral preservando a neoplasia primária, lançando mão de abordagens inovadoras e atuais para a área de oncologia comparada e translacional.

CAPÍTULO 1 - TRANSCRIPTOMIC PROFILE REVEALS MOLECULAR EVENTS ASSOCIATED TO FOCAL ADHESION AND INVASION IN CANINE MAMMARY GLAND TUMOR CELL LINES

CORDEIRO, Y.G.[1], XAVIER, P.L.P[1], ROCHETTI, A.L.[1], ALEXANDRE, P.A.[1], MORI C.M.C.[2], STREFEZZI, R.F.[1], FUKUMASU, H[1].

[1] Laboratory of Comparative and Translational Oncology, Department of Veterinary Medicine, School of Animal Science and Food Engineering, University of São Paulo, Pirassununga, Brazil

[2] Department of Pathology, School of Veterinary Medicine and Animal Science, University of São Paulo, São Paulo, Brazil

Vet Comp Oncol 16 (1), E89-E98 Mar 2018

ABSTRACT

The prevalence of cancer in animals has increased significantly over the years. Mammary tumors are the most common neoplasia in dogs, in which around 50% are presented in the malignant form. Hence, the development and characterization of in vitro models for the study of canine tumors are important for the improvement of cancer diagnosis and treatment. Thus, the aim of this study was to characterize cell lines derived from canine mammary gland neoplasias which could be further used for basic and applied oncology research. Samples of canine mammary carcinomas were taken for cell culture and two cell lines were established and characterized in terms of cell morphology, tumorigenicity and global gene expression. Both cell lines presented spindle-shape morphology and shown common malignant features as in vitro invasion potential and expression of epithelial and mesenchymal proteins. Also, we found gene expression patterns between the two cell cultures in comparison to the normal mammary gland tissue. Cells from M25 culture showed a higher invasion and in vivo tumorigenic potential, associated to the overexpression of genes involved in focal adhesion and extracellular matrix communication, such as FN1, ITGA8 and THBS2. The phenotypic characterization of these cells along with their global gene expression profile potentially determine new therapeutic targets for mammary tumors.

Key words: canine; gene expression; mammary cancer; next-generation sequencing; tumor biology

BACKGROUND

Dogs develop tumors spontaneously and unpredictably as humans, sharing a variety of features including histological appearance, genomic alterations, molecular targets, biological behavior and response to conventional therapies (PAOLONI; KHANNA, 2008). Malignant neoplasms are responsible for almost 50% of deaths of dogs over 10 years old (BAEK; MCENTEE; LEGENDRE, 2009), and as in women, mammary tumors are the most common corresponding to 52% of all types of tumors (QUEIROGA; LOPES, 2002), in which 50% of those are malignant (HELLMÉN, 2005).

Regarding mammary gland tumors, canine cancer cells are great experimental models for veterinary and comparative research. In vitro studies using primary and well-established cell lines allowed important discoveries on the origin, pathophysiology, therapeutic targets and cancer biomarkers (VAN STAVEREN et al., 2009). In addition, cancer cell lines are necessary for the screening of substances with anticancer properties, representing a rich database of growth inhibition systems and cytotoxic properties (SHOEMAKER, 2006).

Thus, the aim of this study was to establish canine mammary cancer cell lines, characterize their transcriptome, and identify potential new therapeutic targets associated to invasion and metastasis.

MATERIAL AND METHODS

Tumor samples

Mammary tumor samples were obtained from female dogs that underwent surgery at the Veterinary Hospital of the School of Animal Science and Food Engineering of University of Sao Paulo, and private veterinary clinics which agreed to participate in the present study (protocol approved by the Ethic Committee on Animal Use, University of Sao Paulo, protocol number CEUA/3094061014). Inclusion criteria consisted of animals that had primary neoplasms and were not subjected to any type of antitumor treatment. Tumor fragments were washed in sterile phosphate buffer solution (PBS) and placed in sterile transport medium consisting of DMEM F12 (Thermo Fisher, Fremont, CA, USA) at 5% penicillin/streptomycin (PenStrep, Thermo Fisher, Fremont, CA, USA) at 4° C until arrival at the laboratory. An aliquot of fragments was formalin fixed, processed and stained with hematoxylin and eosin (HE) for histological evaluation, and mammary tumors were classified following Goldschmidt et. al. (GOLDSCHMIDT et al., 2011).

Dissociation and cell culture

Fragments were minced with sterile scalpels to 1 mm³ pieces and placed into 50 mL tube containing 10mL DMEM-F12, 200U/mL Collagenase type I (Sigma Aldrich®, St. Louis, MO, USA), 100 U/ml de Hyaluronidase (Sigma Aldrich®, St. Louis, MO, USA) and 2% of antibiotics, at 37ºC and centrifuged at 100 rpm for 2 hours. The tube was centrifuged at 1200 rpm, supernatant was discharged, cells were suspended in 5mL of TrypLE Express Enzyme 1X (Thermo Fisher, Fremont, CA, USA) and maintained at 37ºC for an additional hour. Then, suspension was filtered through a 100µm filter followed by another filtration through a 40µm filter. Cells were washed twice with PBS and plated in DMEM-F12 supplemented with 5% fetal bovine serum (FBS) and 1% antibiotics, in 25cm³ flasks kept under controlled CO2 and temperature. Culture evolution was evaluated daily by optical microscopy (Eclipse TS100, Nikon, Japan) and culture medium was supplemented with 10% FBS after five passages.

Doubling-time and karyotyping

Cells in at least 7th passage were grown 5 x 104 cells per well, in 6-well plates, with supplemented culture medium as described above. The number of cells was counted using a hemocytometer at 24-hour intervals for a total period of 120 hours. The results were evaluated with the Doubling-Time Software (ROTH, 2006). For karyotyping, cells at passage ten, at least, were cultured in petri dishes and metaphases arrested by incubation with Colchicine (40 mM, Sigma Aldrich®, St. Louis, MO, USA) for 3 hours at 37ºC. Cells were detached, centrifuged and suspended in hypotonic solution (0,075M KCl) for 30 minutes at 37ºC. Then, 2 mL of ice-cold fixative (methanol/acetic acid 3:1) solution was added to the tube and the suspension was homogenized, followed by centrifugation at 1200 rpm for 10 minutes. The supernatant was carefully discarded and the pellet resuspended in cold fixative avoiding oversaturation. Slides were washed, dried and two drops of cell suspension were dispensed from a pipette to the glass slides. Slides were air dried and stained with Giemsa 10% solution for 10 minutes at room temperature. Chromosomes were photographed under optical microscope (MC 80 DX, Carl Zeiss, Germany) using 100x objective. Twenty metaphases per sample were counted.

Immunocytochemistry

Immunofluorescence of cytoskeleton filaments was performed with primary antibodies against cytokeratin (clone A1/A39, Dako, Carpinteria, CA, USA), vimentin (clone V99, Dako, Carpinteria, CA, USA) and α-smooth muscle actin (clone HHF3510, Dako, Carpinteria, CA,

USA). Cells (near passage 25) were grown on cover slips, fixed with 4% paraformaldehyde for 10 min at room temperature and blocked with a PBS solution containing 5% non-fat milk and 1% BSA. Primary antibodies were incubated overnight at 4ºC and were detected using Alexa Fluor® 488 Goat Anti-mouse IgG (H+L) secondary antibody (Thermo Fisher, Fremont, CA, USA). Coverslips were mounted with Hoechst 33342 (Thermo Fisher, Fremont, CA, USA) following manufacturer's recommendations.

Invasion assay

Cells were cultured for 24 hours in serum-free medium. The transwell inserts were placed in 24 well plates and filled with 100 µl of ECM gel (Sigma Aldrich®, USA) in PBS (1:5). After, 4 x 104 cells were resuspended in 100 µl serum-free medium and plated on inserts. The bottom well was filled with 600 µl of DMEM-F12 medium supplemented with 20% SFB, used as chemoattractant, and 24 hours later, a cotton swab was used to remove non-invasive cells from the top of the inserts. As fixative, 5% glutaraldehyde was used for 10 minutes at room temperature and inserts stained with 1% crystal violet in 2% ethanol for 2 minutes. The invasive cells were counted under optical microscope in five random fields at 100x magnification. The experiment was performed twice and in duplicates.

Tumorigenicity

In vitro tumorsphere formation.

Cells were grown in DMEM-F12 medium supplemented with 20 ng/mL EGF (PrepoTech, USA), 10 ng/mL FGF (PrepoTech, USA), 5 µl/mL bovine insulin (Sigma Aldrich, MO, USA) and 1% antibiotic/antimycotic (PenStep, Gibco, Life Technologies, USA). 24-well plates (Corning®, USA) were bottom covered with 0.5 mL/well of 0.6% agar diluted in DMEM-F12 medium, and submitted to UV polymerization for one hour before cell addition. Cell number was adjusted to a concentration of approximately 1000 cells/mL in 0.5 mL/well in order to avoid cell clumping. For cell culture maintenance, 50 µL/well of fresh medium was added every 48h. The tumorspheres were counted after seven consecutive days.

Tumor growth in immunodeficient mice

A total of six specific pathogen free (SPF) 5-wk-old female BALB/c nude (Foxn1sepe/Foxn1sepe) mice, were provided from the animal facility of the Department of Immunology, Institute of Biomedical Science, University of São Paulo, Brazil, and housed in IVC (Alesco Indústria e Comércio, Monte Mor, Brazil). They had unrestricted access to filtered sterile water and irradiated commercial pelleted diet (Nuvilab, Quimtia, Paraná, Brazil). At least

seven days before beginning the experiment, mice were transferred to the Department of Pathology, School of the Veterinary Medicine and Animal Science (FMVZ), University of São Paulo located in Pirassununga city, Brazil. They were housed under controlled room temperature (22-25°C) and humidity (55-65%) with a 12h/12h light/dark cycle. The protocols for the experimental studies were approved by the Ethic Committee of FMVZ under license number CEUA 3094061014. Cells were injected subcutaneously with a suspension of 5 x 106 cells in 0.05 mL of PBS (n=3 for each cell culture) and mice were humanely euthanized by isoflurane saturated atmosphere when the tumors reached 1 cm of diameter or after 120 days of transplantation if no tumor was visualized. Tumor mass and organs such as liver, lung, spleen, lymph nodes and pancreas were collected, fixed in formalin, processed and embedded in paraffin for histopathology.

Transcriptomic profile

RNA extraction and preparation for sequencing mRNA libraries

Total RNA of triplicate biological samples from each cell line was extracted with TRIZOLTM according to manufacturer's recommendation. RNA quality and quantity were assessed using automated capillary gel electrophoresis on a Bioanalyzer 2100 with RNA 6000 Nano Labchips (Agilent Technologies Ireland, Dublin, Ireland), and only samples which presented an RNA integrity number (RIN) above 8.0 were used for further analysis. Preparation of mRNA libraries was carried out using a TruSeq™ RNA Sample Prep Kit in accordance with TruSeq® RNA Sample Preparation v2 Guide (Illumina, USA). The libraries were evaluated and quantified using Agilent 2100 Bioanalyzer and qPCR with KAPA Library Quantification kit (KAPA Biosystems, Foster City, USA), and adapter-ligated cDNA fragment libraries were run on Illumina HiSeq 2500 equipment using TruSeq PE Cluster Kit and TruSeq SBS Kit (Illumina, USA) generating 100bp paired-end reads. Canine normal mammary gland RNA-seq data (LIU et al., 2014) was obtained at the Sequence Read Archive database (NAKAMURA et al., 2013).

Alignment and differential expression

Sequencing quality was evaluated by FastQC software (ANDREW, 2010). Once we obtained a high sequencing quality, each sample was aligned against the reference genome (CanFam3.1) using TopHat 2.0.9 and Bowtie 2.1.014, (TRAPNELL et al., 2012). PCR duplicates, not primary alignments and low quality reads were removed with Samtools (LI et al., 2009) and final reads were counted using HTSeq (ANDERS; PYL; HUBER, 2015). Differential gene expression between M5 and M25 cells as well as between cultured cells and

normal mammary gland tissue was performed using EdgeR package (ROBINSON; MCCARTHY; SMYTH, 2010) on R environment, based on negative binomial distribution. Transcripts with FDR ≤ 0.01 and log Fold Change >1 were considered differentially expressed (DE). Gene Ontology and KEGG (KANEHISA; GOTO, 2000) of DE genes between normal canine mammary gland tissue and cell cultures was performed using WEB-based Gene Set Analysis Toolkit (WANG et al., 2013), with gene stable Ensembl ID (YATES et al., 2016) as input data, and CanFam3.1 as the reference genome. In silico protein-protein interaction was assessed with STRING database (SZKLARCZYK et al., 2015). Sequence data can be found in Gene Expression Omnibus database repository (BARRETT et al., 2013), accession number GSE98482.

Statistical analysis

Invasion assay and in vitro tumorigenic assay were analyzed by Mann-Whitney test at the $P<0.05$ significance level. For functional enrichment analyses, P value was adjusted for multiple tests, and Benjamini & Hochberg method was used to test multiple categories in a group of functional gene sets.

RESULTS

Establishment and characterization of canine mammary cancer cell cultures

Following our protocol, two out of 49 primary cell cultures were successfully established from different canine mammary gland tumors (Table 1). One was originated from a canine mammary comedocarcinoma and the other from a carcinoma mixed-type, designated as M5 and M25, respectively. Both tumors presented epithelial and myoepithelial cell proliferation. The comedocarcinoma showed typical necrotic areas surrounded by viable neoplastic cell aggregates. In the carcinoma mixed-type, additional cartilage tissue was found (data not shown), along with the epithelial component arranged in tubules (Figure 1A and 1B). Microscopically, both cultures showed spindle-shape cells, with round to oval nuclei and some presenting multiple nucleoli (Figure 1C and 1D). Doubling time was estimated to 26.0h for M5 and 42.8h for M25 cells.

Table 1. Histopathological classification of primary tumors used for primary cell cultures

	# samples	**%**

Carcinoma-complex type	13	26.53
Carcinoma-mixed type	10	20.41
Carcinoma-simple	5	10.2
Carcinoma-solid	5	10.2
Benign neoplasm	4	8.16
Lobular hyperplasia	3	6.13
Comedocarcinoma	3	6.13
Squamous cell carcinoma	2	4.08
Carcinoma-anaplastic	1	2.04
Malignant myoepithelioma	1	2.04
Adenosquamous carcinoma	1	2.04
Mesenchymal neoplasm	1	2.04
Total	**49**	**100**

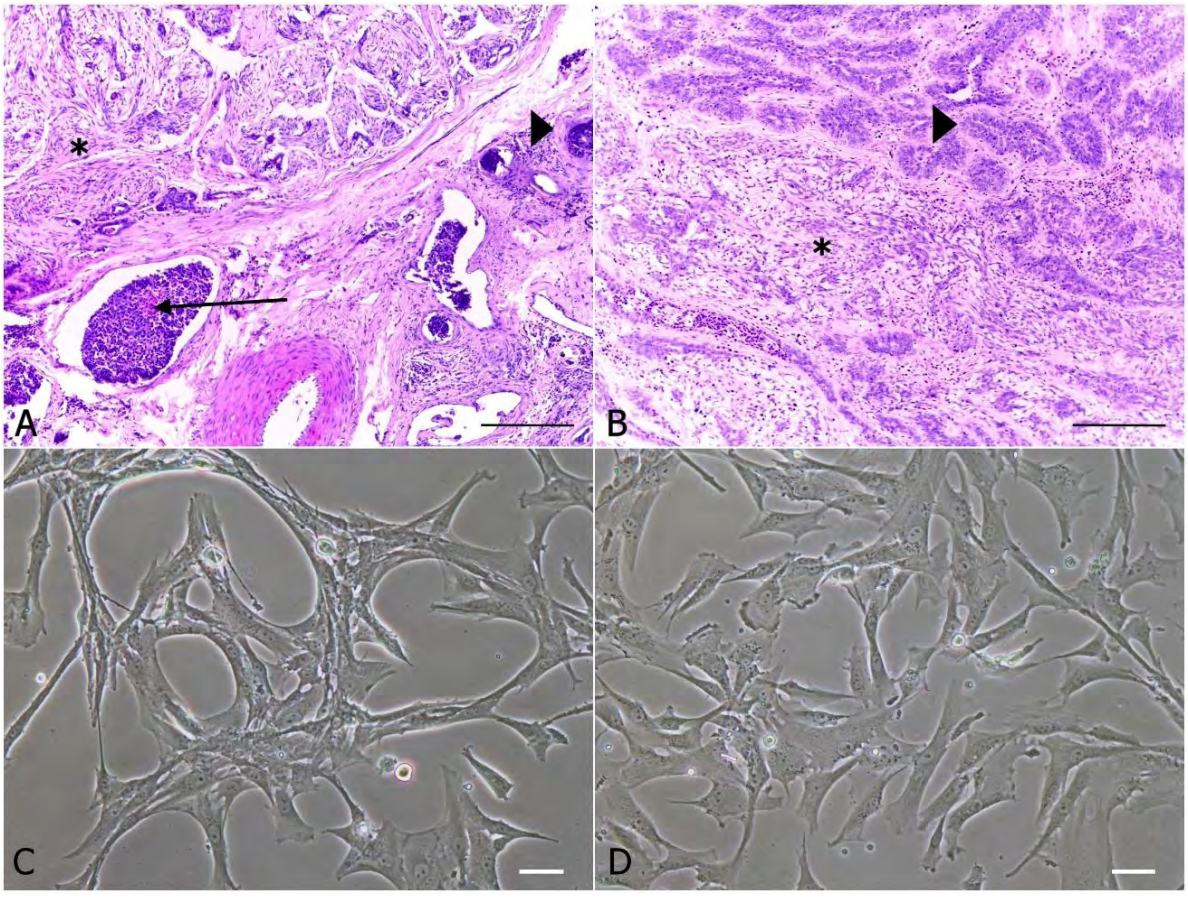

Figure 1: (A, B) Representative histology of M5 comedocarcinoma (A) and M25 mixed carcinoma (B) primary tumors. Myoepithelial (*) and epithelial (arrow head) proliferation is evident in both tissues. The necrotic area within the center of the neoplastic epithelial cell aggreagates common to comedocarcinomas is pointed (arrow). Scale bar: 200 µm. (C, D) Established cell cultures of canine mammary carcinomas. M5 (C) and M25 (D) presented a spindle-shape morphology with cells showing one or more nuclei. Scale bar: 100 µm.

Karyotype analysis showed moderate aneuploidy for both cell cultures (M5 77.55 ± 0.94 and M25 76.9 ± 2.84). Also, additional cytogenetic alterations could be found, for example, M25 cells showed monosomy of X chromosome (Figure 2). Immunocytochemistry analyses on both cell cultures showed expression of vimentin, cytokeratin and α-smooth actin, where cytokeratin was expressed heterogeneously in M5 cells (Figure 3A to 3F). Vimentin was expressed intensely in both cultures, corresponding to their mesenchymal-like morphology (Figure 3G and 3H).

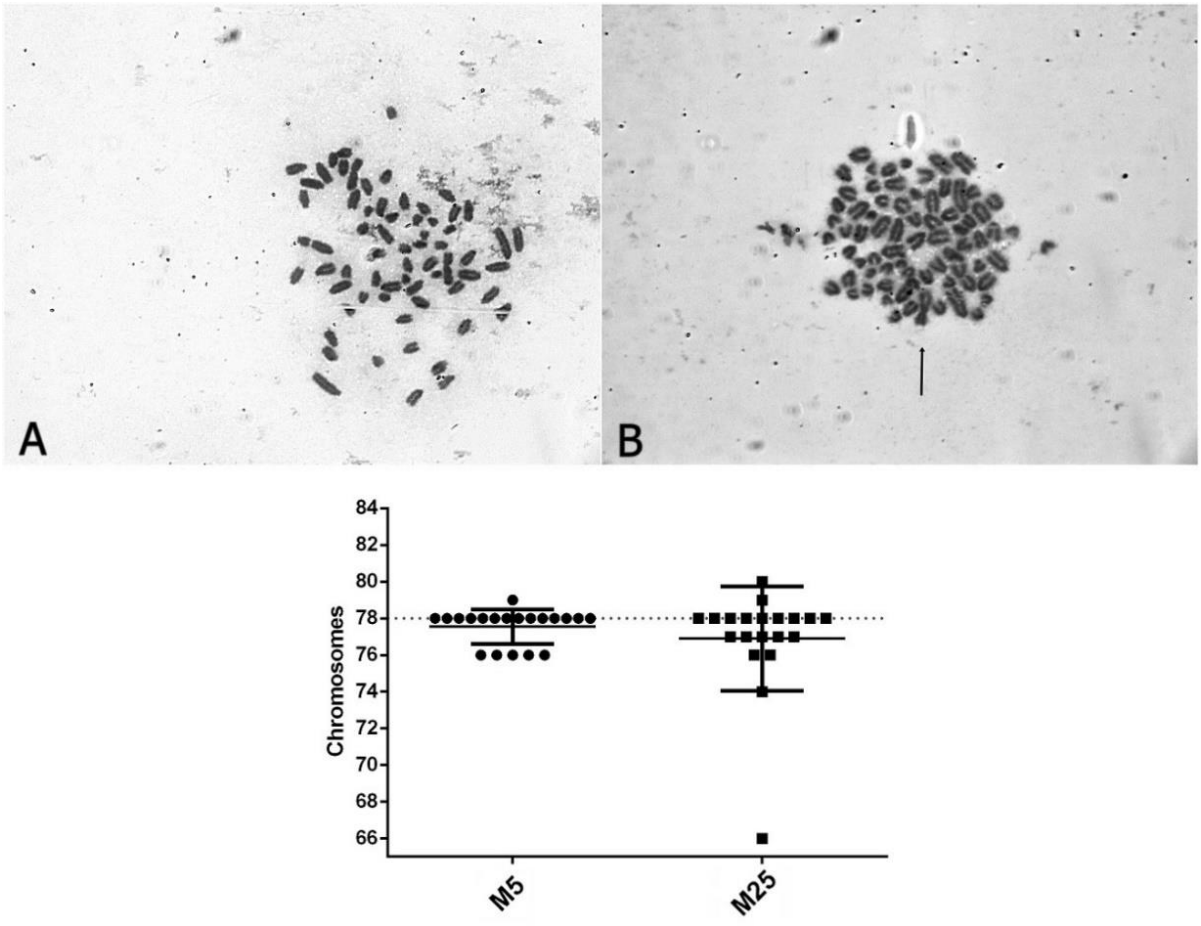

Figure 2: Aneuploidy found in cells from mammary carcinomas primary cultures. (A) Hypoploidy of a M25 cell showing a metaphase with 66 chromosomes. (B) M25 aneuploid cell presenting monosomy of X chromosome, indicated by the black arrow. Graph shows the numeric distribution of the twenty metaphasis analyzed in karyotyping. Magnification: 1000x.

In addition, both cell cultures were positive in the invasion assay (5M: 33.1 ± 4.93 cells and 25M: 60.4 ± 13.50 cells, per field). The M25 cells presented higher invasion potential in comparison to M5 cells ($p < 0.0001$) (Figure 4).

Tumorigenicity

Both M5 and M25 cells were similarly able to form tumorspheres under low-adherence conditions (Figure 5A and 5B) after seven days. *In vivo*, only 25M cells produced tumors after 120 days in our conditions. Histologically, the 25M cell nodules presented predominantly tubular arrangements with one to four layers of cubical cells. The tubular structures were composed of cells with round to oval nuclei, revealing moderate anisocariosis and common mitotic figures (Figure 5C and 5D). The architecture of the nodule formed was similar to the primary mammary gland tumor (Figure 1B). Therefore, considering the invasion potential and the *in vitro* tumorigenicity, the M25 cell line could be considered more malignant than M5 cell line.

Transcriptomic analysis of M5 and M25 cells

An average of 16.2 million 100 bp paired-end reads were sequenced per replicate (three for each cell culture), and after alignment, an average of 81.1% were considered concordant pair alignment rate (Table S1). A total of 11,260 genes presenting more than 1 count per million were detected in M5 cells and 11,476 genes in M25 cells. Also, we found 824 DE genes between M5 and M25 cell lines, in which 384 were upregulated and 440 were downregulated in M25 cells (Table S2). All enrichment analysis was made based upon the unique Ensembl entrez gene IDs.

Gene ontology (GO) from a gene set of 647 genes considered to enrichment analysis showed that DE genes between M5 and M25 cell cultures were related to biological and developmental processes as well as cell membrane components, such as genes involved in cell motility and extracellular matrix reorganization (Table 2, Figure S1). To further evaluate those processes, we mapped M25 upregulated genes using KEGG database, according to Canis familiaris reference genome. Most of genes were significantly enriched for pathways involved in drug metabolism and resistance, cell cycle control, DNA replication and extracellular matrix communication. Among them, we found an increased expression of genes related to cell adhesion molecules (CAMs) with a high in silico protein interaction score (0.7) such as FN1, THBS2 and ITGA8 (adjusted p value ≈ 1.51-53, 0, 4.64-197 and LogFC = 1.347, 3.867 and

2.852, respectively) suggesting that M25 cells have a more invasive potential than M5 cells, results that confirm the in vitro analysis of invasion.

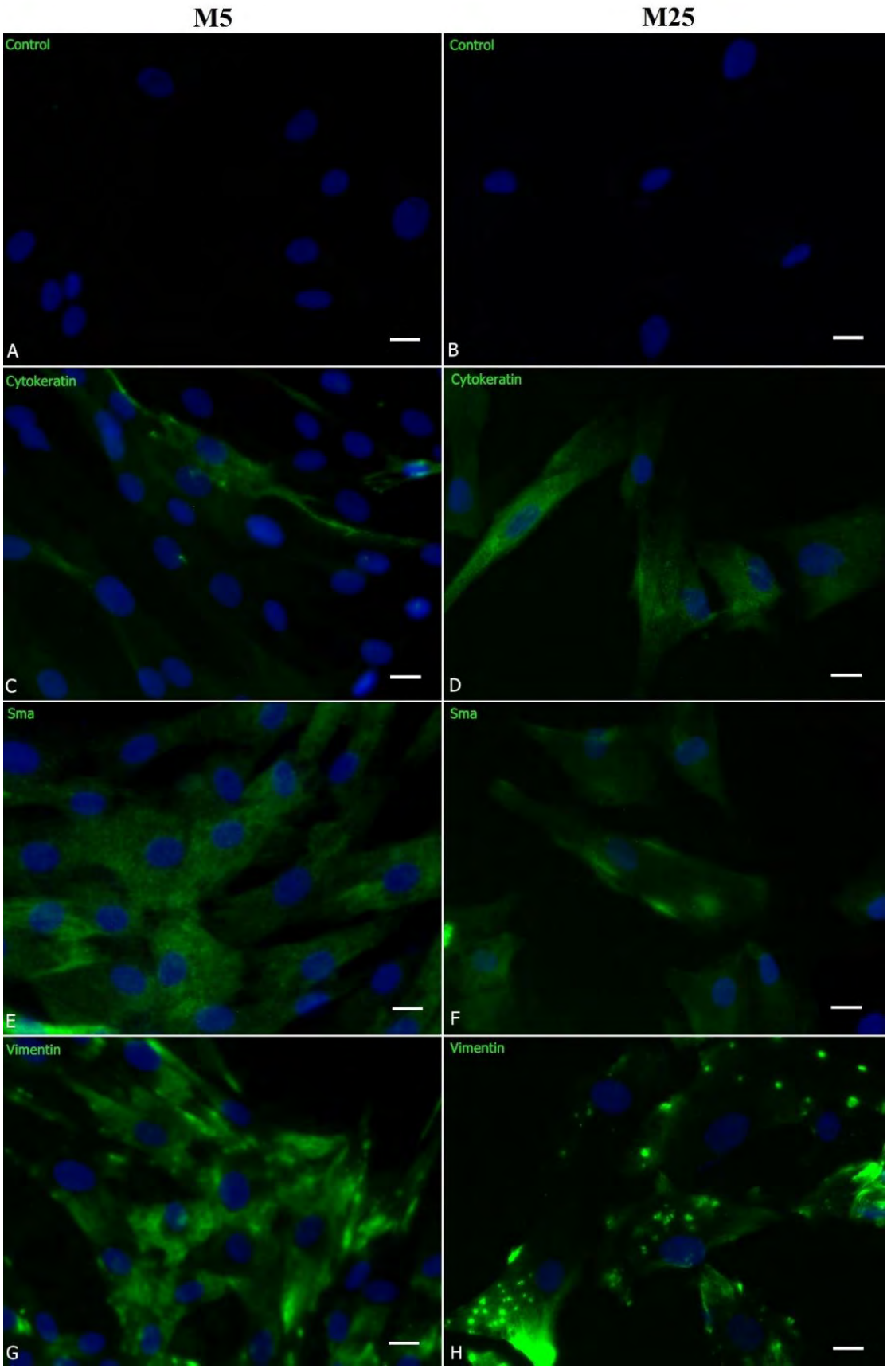

Figure 3: Immunocytochemistry of cytoskeleton filaments in M5 and M25 cells. (A, B) Control. (C to H) Both cultures expressed all three markers, although some M5 cells did not present cytokeratin expression (C). Scale bar: 20 µm.

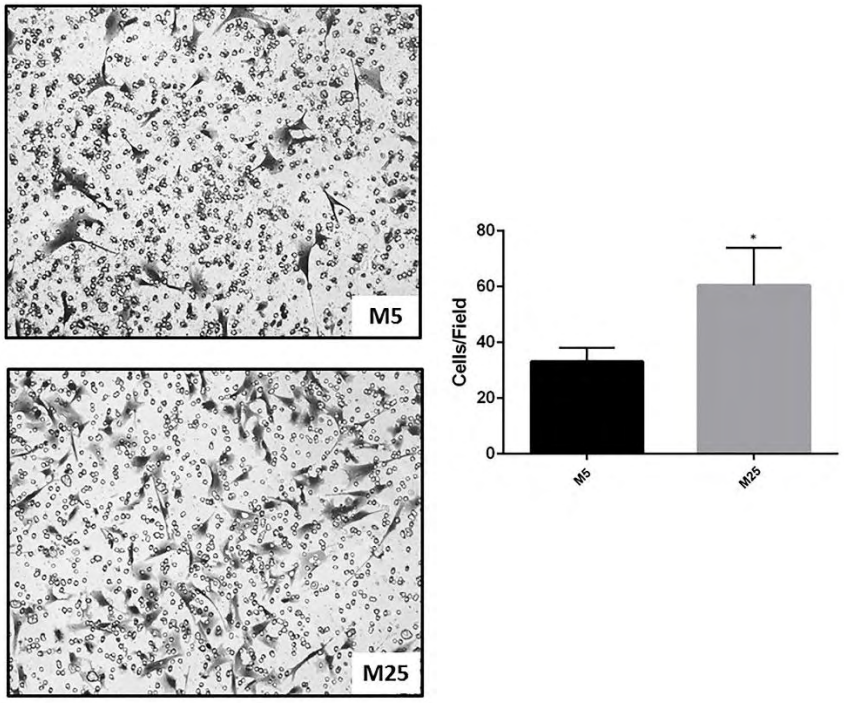

Figure 4. M25 cells exhibited higher invasive potential than M5 cells. Results are described as an average of number of cells per field ± SD of two independent experiments. *p < 0.0001.

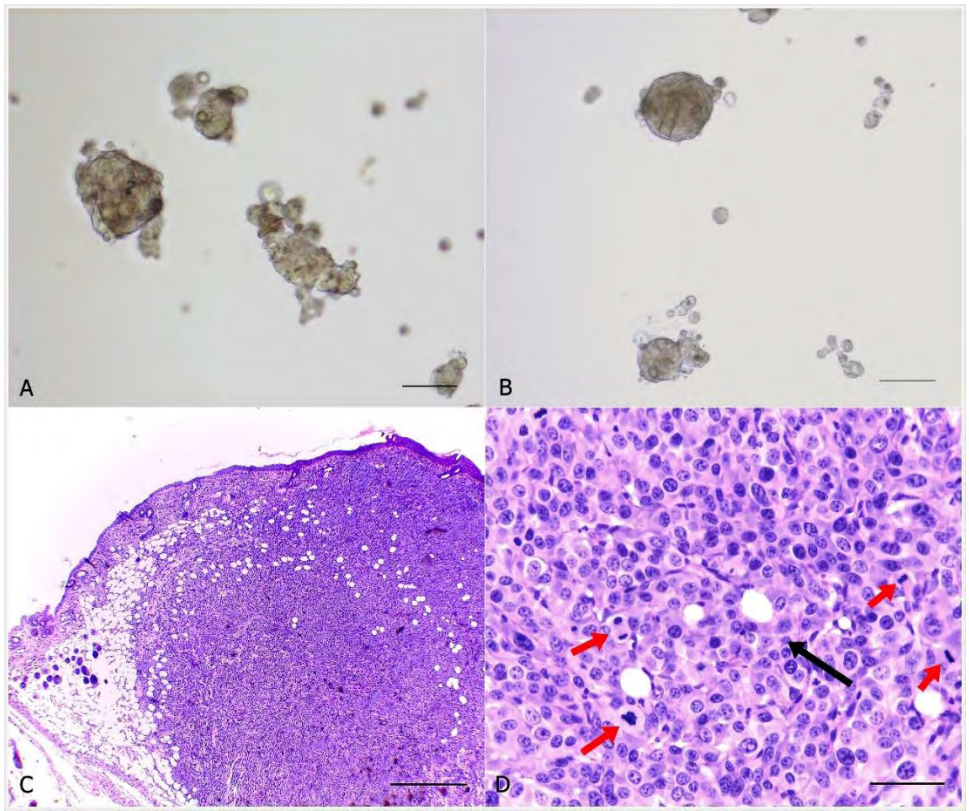

Figure 5: Tumorigenicity of M5 and M25 cell lines. (A, B) Tumorsphere formation under low-adherence conditions, M5 (A) and M25 (B) cell cultures. Scale bar: 100 µm. (C, D) Tumor mass after three weeks post-injection of M25 cells in nude mice. Note mitotic figures (red arrows) and tubule formation (black arrow). Scale bar: 500 µm (C) and 50 µm (D).

Table 2. Pathways identified in M5 and M25 DE genes used for functional enrichment analysis

	# genes*	***p value*****
ECM-receptor interaction	13	5.74^{-6}
One carbon pool by folate	5	0.34^{-2}
Focal adhesion	17	0.06^{-3}
Synthesis and degradation of ketone bodies	3	1.58^{-2}
Drug metabolism – cytochrome P450	6	1.58^{-2}
Pathways in cancer	17	3.32^{-2}
Retinol metabolism	5	3.32^{-2}

*number of genes enriched in the category
***p value* adjusted by the multiple test adjustment

In order to identify gene expression patterns specific of each cell line, we compared their transcriptome to one canine normal mammary gland tissue sample deposited in a public repository (NCBI SRX295056). A total of 7,311 and 7,407 DE genes were observed, respectively, for M5 and M25 cells (Table 3). Proto-oncogenes, tumor suppressor genes and some miRNAs were found to be differentially expressed (Tables S3 and S4). KEGG and gene ontology analyses of DE genes showed upregulation of genes involved in focal adhesion and ECM-receptors interactions, protein processing in endoplasmic reticulum, regulation of actin cytoskeleton and MAPK signaling pathway (Table 4 and Figures S2 and S3).

Table 3. Number of differentially expressed genes between neoplastic cells and a normal mammary gland

	M5	**M25**
Total DE genes*	**7311**	**7407**
Upregulated	2679	2792
Downregulated	4632	4615

Unique entries for GO and KEGG	5328	5417

Table 4. Identified pathways of cancer cells compared to normal gland DE genes considered for functional enrichment analysis

	# genes*		***p value*** **	
	M5	**M25**	**M5**	**M25**
Cell adhesion molecules (CAMs)	69	70	8.67^{-17}	4.13^{-17}
Cytokine-cytokine receptor interaction	91	93	3.18^{-15}	1.11^{-15}
Focal adhesion	95	94	3.54^{-16}	2.68^{-15}
Metabolic pathways	329	325	3.13^{-12}	1.30^{-12}
Pathways in cancer	121	124	5.60^{-12}	1.50^{-12}
MAPK signaling	103	104	4.90^{-11}	7.35^{-11}
Calcium signaling pathway	80	77	3.72^{-12}	2.05^{-10}
Leukocyte transendothelial migration	58	-	4.86^{-10}	-
Chemokine signaling pathway	74	-	2.37^{-10}	-
Axon guidance	64	-	5.60^{-12}	-
ECM-receptor interaction	-	43	-	2.64^{-10}
Regulation of actin cytoskeleton	-	87	-	2.64^{-10}
Phagosome	-	65	-	3.77^{-10}

DISCUSSION

In this study, we report the successful establishment and characterization of two new cell lines from canine mammary malignant neoplasms where one cell line was distinctly more malignant than the other. Transcriptome analysis by RNA-seq corroborated this result and showed the main altered pathways in both cell lines which can now be used for testing new target molecules for anticancer therapy.

Two out of forty-nine primary cell cultures were successfully established in this work. This low number could be explained by the difficulty of expanding new cell lineages from solid neoplasms due to the number and viability of malignant tumor cells capable of surviving in vitro, the contamination with and overgrowth of stromal cells such as fibroblasts, and the heterogeneity of cell populations of the various subtypes of mammary tumors found in dogs (HOLLIDAY; SPEIRS, 2011). Even so, the established cell cultures presented here had similar features to previous studies involving canine mammary cancer cell cultures, in terms of growth, morphology and phenotype (ELSE; NORVAL; NEILL, 1982; HELLMÉN, 1992; UYAMA et al., 2006; CHANG et al., 2010). The M5 and M25 cells presented comparable spindle-shape morphology and growth pattern in two-dimension cell culture. However, M5 cells did not produce tumors in mice in our conditions, and were less invasive in vitro than M25 cells. A successful tumorigenic in vivo assay depends on several aspects: the site of injection, cell concentration or the need of additional hormonal supplementation (PRICE et al., 1990; MOLLARD et al., 2011). Also, nude mice present T lymphocyte deficiency, but still have an immune response led by B cells and cytokines, as interferons and perforins, which may interfere in tumor development (SHANKARAN et al., 2001).

Canine and human mammary glands consist basically of two major epithelial groups, luminal and myoepithelial cells. In this study, we analyzed the expression of cytokeratins (in this case identified by A1/A3 clone which covers 14 subtypes used to identify epithelial cells), vimentin and smooth muscle actin (α-SMA), normally found in myoepithelial cells. The M5 and M25 cultures showed simultaneous expression of cytokeratin and vimentin, where vimentin was strongly expressed in all cells and cytokeratin had a heterogeneous patterning in M5 cells. Similarly, α-SMA was not detected in all cells in M5 culture, but such presentation can still suggest a myoepithelial origin. Until recently, it was believed that carcinoma cells would only express cytokeratins, whereas mesenchymal neoplasms would express vimentin (HENDRIX et al., 1997). However, despite this expression pattern still be a tendency, it is now known that a given tumor can co-express two or more types of intermediate filaments simultaneously, and frequently, vimentin is present in most cases, although the reasons still remain unclear (BROERS et al., 1988). Some hypotheses were proposed to explain vimentin expression, such as myoepithelial or even progenitor cell origin (PETERSEN et al., 2001), but so far, the expression of vimentin in human and canine breast cancer is strongly associated to the epithelial-mesenchymal transition (EMT), conferring a higher cell invasiveness and consequent metastatic potential, acting like a valuable prognostic marker (SATELLI; LI, 2011).

The global gene expression of cultured cells advances the knowledge of cancer development, progression and guide further studies for future target therapies. In this context, we performed M5 and M25 transcriptome profiling to identify the main biological processes and their related genes. More than ten thousand genes were expressed in both cell cultures. Moreover, DE analysis between both cell lines showed interesting features of M25 cells, like overexpression of genes related to extracellular matrix modifications, metabolism of xenobiotics and genes involved in cell replication. The prediction of protein-protein interaction of genes overexpressed and involved in focal adhesion showed three potential genes mediating the invasion process: FN1, THBS2 and ITGA8 (adjusted p value ≈ 1.51-53, 0, 4.64-197 and LogFC = 1.347, 3.867 and 2.852, respectively). In fact, some studies have already demonstrated overexpression of these genes in metastatic cells and in solid tumors that recurred or colonized to distant sites (KIM et al., 2010; WAALKES et al., 2010; RYU et al., 2016; ZHUO et al., 2016). ITGA8 have already been speculated as a prognostic factor and potential therapeutic target in human multiple myeloma (RYU et al., 2016), and THBS2 is a potential multi-cancer target focusing in metastasis inhibition (KIM et al., 2010; ZHUO et al., 2016). These results corroborate with our findings, which suggests that M25 cells are in fact more malignant than M5 cells, findings also observed in vitro and in vivo through matrigel and tumorigenicity assays, respectively.

From GO and KEGG analyses, cancer pathways were downregulated in M5 and M25 cells compared to normal mammary gland tissue. As an example, tumor suppressor genes TP53 (M5 adjusted p value = 1.75-71, LogFC = -2.095; M25 adjusted p value = 2.53-97, LogFC = -2.158) and MYCT1 (M5 adjusted p value = 4.72-183, LogFC = -12.373; M25 adjusted p value = 1.02-138, LogFC = -12.453) were found downregulated in both cell lines. Lower TP53 expression can lead not only to the inactivation of antiproliferative mechanisms, but can also enhance the metastatic potential due to a gain of function activity (VAN LEEUWEN et al., 1996; WEISSMUELLER et al., 2014). Losses in TP53 had already been described as responsible for inducing CDH2 and PDGFRB transcription and for activating WNT signaling cascade (HAN et al., 2014; WEISSMUELLER et al., 2014), while down-regulation in MYCT1 gene contributes to cancer progression by apoptosis induction, inhibition of cell proliferation and invasiveness, corroborating with expression analysis of canine mammary carcinomas cell lines established in this study (FU et al., 2011; YANG et al., 2012).

One interesting finding in our transcriptome profile was the overexpression of microRNAs precursor genes such as cf-mir-374b, cf-mir-145 and cf-mir-23b. Indeed, cfa-mir-145 had already been described in a primary culture of canine mammary cancer, where it was

found 993.4-fold over normal mammary gland tissue expression (OSAKI et al., 2016). The mir-374b was associated to malignant behavior in human gastric cancer and was suggested as a potential prognostic marker in cervical cancer (LUI et al., 2007; XIE et al., 2014), while mir-23b was found downregulated in human colon cancer maybe acting as a modulator suppressor of metastasis (ZHANG et al., 2011). Although, one should be aware that poly-A enriched mRNA libraries for RNA-seq technology are not be the best approach for mapping global miRNAs expression. In some cases, it is possible to detect only miRNA precursors which are more than the length of the size selection used in the sequencing library preparation step, and appropriate precautions need to be taken when filtering before data alignment (MORTAZAVI et al., 2008).

In summary, we have established and characterized two primary cell lines from canine mammary carcinomas and despite the similarity in morphological features as cell shape, cytogenetic alterations and immunocytochemistry findings, there were differences regarding tumorigenicity which were reflected by the RNA-seq analysis. The identification of specific molecular signatures such as FN1, THBS2 and ITGA8 that may be regulating the invasion process will allow their use in the development of new therapeutic targets for malignant mammary tumors in the near future.

REFERENCES

ANDERS, S.; PYL, P. T.; HUBER, W. HTSeq—a Python framework to work with high-throughput sequencing data. **Bioinformatics**, v. 31, n. 2, p. 166–169, 15 jan. 2015. Disponível em: <http://www.ncbi.nlm.nih.gov/pmc/articles/PMC4287950/>.

ANDREW, S. **FASTQC: A quality control tool for high throughput sequence data.** Disponível em: <http://www.bioinformatics.babraham.ac.uk/projects/fastqc/>.

BAEK, S. J.; MCENTEE, M. F.; LEGENDRE, A. M. Review Paper: Cancer Chemopreventive Compounds and Canine Cancer. **Veterinary pathology**, v. 46, n. 4, p. 576–588, jul. 2009.

BARRETT, T. et al. NCBI GEO: Archive for Functional Genomics Data Sets--Update. **Nucleic acids research**, v. 41, n. Database issue, p. D991-5, jan. 2013.

BROERS, J. L. V. et al. Spontaneous change in intermediate filament proteins expression patterns in lung cancer cell. **Journal of Cell Science**, v. 91, p. 91–108, 1988.

CHANG, C.-Y. et al. Assessment of the Tumorigenesis and Drug Susceptibility of Three New Canine Mammary Tumor Cell Lines. **Research in veterinary science**, v. 88, n. 2, p. 285–293, abr. 2010.

ELSE, R. W.; NORVAL, M.; NEILL, W. A. The Characteristics of a Canine Mammary Carcinoma Cell Line, REM 134. **British journal of cancer**, v. 46, n. 4, p. 675–681, out. 1982. Disponível em: <https://www.ncbi.nlm.nih.gov/pubmed/7138772>.

FU, S. et al. MYCT1-TV, A Novel MYCT1 Transcript, Is Regulated by c-Myc and May Participate in Laryngeal Carcinogenesis. **PLOS ONE**, v. 6, n. 10, p. e25648, 5 out. 2011. Disponível em: <https://doi.org/10.1371/journal.pone.0025648>.

GOLDSCHMIDT, M. et al. Classification and grading of canine mammary tumors. **Veterinary pathology**, v. 48, n. 1, p. 117–31, jan. 2011. Disponível em: <http://www.ncbi.nlm.nih.gov/pubmed/21266722>. Acesso em: 4 dez. 2014.

HAN, K. et al. MicroRNA-194 Suppresses Osteosarcoma Cell Proliferation and Metastasis in Vitro and in Vivo by Targeting CDH2 and IGF1R. **International journal of oncology**, v. 45, n. 4, p. 1437–1449, out. 2014.

HELLMÉN, E. Characterization of four in vitro established canine mammary carcinoma and one atypical benign mixed tumor cell lines. **In Vitro Cellular & Developmental Biology - Animal**, v. 28, n. 5, p. 309–319, 1992. Disponível em: <https://doi.org/10.1007/BF02877054>.

HELLMÉN, E. Complex mammary tumours in the female dog: a review. **Journal of Dairy Research**, v. 72, n. S1, p. 90, 14 jul. 2005. Disponível em: <http://www.journals.cambridge.org/abstract_S002202990500124X>. Acesso em: 31 dez. 2014.

HENDRIX, M. J. et al. Experimental Co-Expression of Vimentin and Keratin Intermediate Filaments in Human Breast Cancer Cells Results in Phenotypic Interconversion and Increased Invasive Behavior. **The American journal of pathology**, v. 150, n. 2, p. 483–495, fev. 1997. Disponível em: <https://www.ncbi.nlm.nih.gov/pubmed/9033265>.

KANEHISA, M.; GOTO, S. KEGG: Kyoto Encyclopedia of Genes and Genomes. **Nucleic Acids Research**, v. 28, n. 1, p. 27–30, 1 jan. 2000. Disponível em: <http://www.ncbi.nlm.nih.gov/pmc/articles/PMC102409/>.

KIM, H. et al. Multi-cancer computational analysis reveals invasion-associated variant of desmoplastic reaction involving INHBA, THBS2 and COL11A1. **BMC Medical Genomics**, v. 3, n. 1, p. 51, 2010. Disponível em: <https://doi.org/10.1186/1755-8794-3-51>.

LI, H. et al. The Sequence Alignment/Map Format and SAMtools. **Bioinformatics (Oxford, England)**, v. 25, n. 16, p. 2078–2079, ago. 2009.

LIU, D. et al. Molecular Homology and Difference between Spontaneous Canine Mammary Cancer and Human Breast Cancer. **Cancer Research**, v. 74, n. 18, p. 5045–5056, 2014. Disponível em: <http://cancerres.aacrjournals.org/cgi/doi/10.1158/0008-5472.CAN-14-0392>.

LUI, W.-O. et al. Patterns of Known and Novel Small RNAs in Human Cervical Cancer. **Cancer research**, v. 67, n. 13, p. 6031–6043, jul. 2007.

MOLLARD, S. et al. How Can Grafted Breast Cancer Models Be Optimized? **Cancer biology & therapy**, v. 12, n. 10, p. 855–864, 15 nov. 2011. Disponível em: <https://www.ncbi.nlm.nih.gov/pubmed/22057217>.

MORTAZAVI, A. et al. Mapping and Quantifying Mammalian Transcriptomes by RNA-Seq. **Nature methods**, v. 5, n. 7, p. 621–628, jul. 2008.

NAKAMURA, Y. et al. The International Nucleotide Sequence Database Collaboration. **Nucleic acids research**, v. 41, n. Database issue, p. D21–D24, jan. 2013. Disponível em: <https://www.ncbi.nlm.nih.gov/pubmed/23180798>.

OSAKI, T. et al. Establishment of a Canine Mammary Gland Tumor Cell Line and Characterization of Its MiRNA Expression. **Journal of veterinary science**, v. 17, n. 3, p. 385–390, 30 set. 2016. Disponível em: <https://www.ncbi.nlm.nih.gov/pubmed/26726024>.

PAOLONI, M.; KHANNA, C. Translation of new cancer treatments from pet dogs to humans. **Nature Reviews Cancer**, v. 2946, n. 2000, p. 2943–2946, 2008. Disponível em: <http://www.nature.com/nrc/journal/v8/n2/abs/nrc2273.html>. Acesso em: 31 dez. 2014.

PETERSEN, O. W. et al. The Plasticity of Human Breast Carcinoma Cells Is More than Epithelial to Mesenchymal Conversion. **Breast cancer research : BCR**, v. 3, n. 4, p. 213–217, 2001. Disponível

em: <https://www.ncbi.nlm.nih.gov/pubmed/11434871>.

PRICE, J. E. et al. Tumorigenicity and Metastasis of Human Breast Carcinoma Cell Lines in Nude Mice. **Cancer research**, v. 50, n. 3, p. 717–721, fev. 1990.

QUEIROGA, F.; LOPES, C. Tumores mamários caninos, pesquisa de novos factores de prognóstico Canine mammary tumours , research on new prognostic factors. **REVISTA PORTUGUESA DE CIÊNCIAS VETERINÁRIAS**, v. 97, n. 543, p. 119–127, 2002.

ROBINSON, M. D.; MCCARTHY, D. J.; SMYTH, G. K. EdgeR: A Bioconductor Package for Differential Expression Analysis of Digital Gene Expression Data. **Bioinformatics (Oxford, England)**, v. 26, n. 1, p. 139–140, jan. 2010.

ROTH, V. **No Title**. Disponível em: <https://www.doubling-time.com/>.

RYU, J. et al. Highly Expressed Integrin-Alpha8 Induces Epithelial to Mesenchymal Transition-Like Features in Multiple Myeloma with Early Relapse. **Molecules and cells**, v. 39, n. 12, p. 898–908, dez. 2016.

SATELLI, A.; LI, S. Vimentin in Cancer and Its Potential as a Molecular Target for Cancer Therapy. **Cellular and molecular life sciences : CMLS**, v. 68, n. 18, p. 3033–3046, set. 2011.

SHANKARAN, V. et al. IFNgamma and Lymphocytes Prevent Primary Tumour Development and Shape Tumour Immunogenicity. **Nature**, v. 410, n. 6832, p. 1107–1111, abr. 2001.

SHOEMAKER, R. H. **The NCI60 human tumour cell line anticancer drug screen.Nature reviews. Cancer**England, out. 2006. .

SZKLARCZYK, D. et al. STRING V10: Protein-Protein Interaction Networks, Integrated over the Tree of Life. **Nucleic acids research**, v. 43, n. Database issue, p. D447-52, jan. 2015.

TRAPNELL, C. et al. Differential gene and transcript expression analysis of RNA-seq experiments with TopHat and Cufflinks. **Nature Protocols**, v. 7, n. 3, p. 562–578, 1 mar. 2012. Disponível em: <http://www.ncbi.nlm.nih.gov/pmc/articles/PMC3334321/>.

UYAMA, R. et al. Establishment of Four Pairs of Canine Mammary Tumour Cell Lines Derived from Primary and Metastatic Origin and Their E-Cadherin Expression. **Veterinary and comparative oncology**, v. 4, n. 2, p. 104–113, jun. 2006.

VAN LEEUWEN, I. S. et al. p53 mutations in mammary tumor cell lines and corresponding tumor tissues in the dog. **Anticancer Research**, v. 16, n. 6 B, p. 3737–3744, 1996.

VAN STAVEREN, W. C. G. et al. Human Cancer Cell Lines: Experimental Models for Cancer Cells in Situ? For Cancer Stem Cells? **Biochimica et biophysica acta**, v. 1795, n. 2, p. 92–103, abr. 2009.

WAALKES, S. et al. Fibronectin 1 MRNA Expression Correlates with Advanced Disease in Renal Cancer. **BMC cancer**, v. 10, p. 503, set. 2010.

WANG, J. et al. WEB-Based GEne SeT AnaLysis Toolkit (WebGestalt): Update 2013. **Nucleic acids research**, v. 41, n. Web Server issue, p. W77–W83, jul. 2013. Disponível em: <https://www.ncbi.nlm.nih.gov/pubmed/23703215>.

WEISSMUELLER, S. et al. Mutant P53 Drives Pancreatic Cancer Metastasis through Cell-Autonomous PDGF Receptor Beta Signaling. **Cell**, v. 157, n. 2, p. 382–394, abr. 2014.

XIE, J. et al. MiR-374b-5p Suppresses RECK Expression and Promotes Gastric Cancer Cell Invasion and Metastasis. **World journal of gastroenterology**, v. 20, n. 46, p. 17439–17447, dez. 2014.

YATES, A. et al. Ensembl 2016. **Nucleic acids research**, v. 44, n. D1, p. D710–D716, 4 jan. 2016. Disponível em: <https://www.ncbi.nlm.nih.gov/pubmed/26687719>.

ZHANG, H. et al. Genome-Wide Functional Screening of MiR-23b as a Pleiotropic Modulator

Suppressing Cancer Metastasis. **Nature communications**, v. 2, p. 554, nov. 2011.

ZHUO, C. et al. **Elevated thbs2, col1a2, and spp1 expression levels as predictors of gastric cancer prognosis**. Cellular physiology and biochemistry : international journal of experimental cellular physiology, biochemistry, and pharmacology, **v. 40, n. 6, p. 1316–1324, 2016.**

CAPÍTULO 2 - MASS SPECTROMETRY IMAGING IDENTIFIES RETICULAR STRESS AND PROTEIN MISFOLDING ASSOCIATED TO TUMOR PROGRESSION IN CANINE MAMMARY CANCER

CORDEIRO, Y.G[1], HEIJS, B.P.A.M.[2], MULDER, L.M.[2], VAN ZEIJL, R.J.[2], VAN VEELEN.[2], P., RU, A.[2], STREFEZZI, R.F.[1], FUKUMASU, H[1].

[1] Laboratory of Comparative and Translational Oncology, Department of Veterinary Medicine, School of Animal Science and Food Engineering, University of São Paulo, Pirassununga, Brazil
[2] Center of Proteomics and Metabolomics, Leiden University Medical Center, Leiden University, Leiden, the Netherlands.

ABSTRACT

Mammary tumors are one of the most frequent tumors in dogs (canine mammary tumors, CMT), which can be classified in many different subtypes showing a high degree of tumoral heterogeneity. Therefore, the multifocal and complex nature of CMT makes it a great model to study the underlying cancer biology, since dogs share the same environment as humans and present many similarities regarding anatomic, histological, molecular and clinical features. It is well-known that cancer cells gradually lose their morphological and specialized functions acquiring a high oncogenic dedifferentiated phenotype. By performing an in-depth and spatially correlated characterization of CMT tissues, we aimed to identify relevant cancer pathways associated to tumor progression, by comparing peptide expression in neoplastic cell populations with two distinct levels of differentiation: well differentiated (WD) and poorly differentiated (PD), focusing on new early-stage cancer biomarkers. Mass spectrometry imaging (MSI) followed by LC/MS-MS was used in order to simultaneously detect morphological and molecular alterations whilst preserving tissue integrity. Discriminative peaks between conditions were identified, resulting in 45 protein IDs, all downregulated in PD compared to WD regions. Functional enrichment analysis showed an association to pathways such as the endoplasmic reticulum response to stress and cell adhesion, in which the loss of important tumor suppressor proteins as TUBB4B, APOA1, CANX, HSPA5, PDIA3 and others, may had contributed to canine mammary cancer progression. In addition, protein interaction network analysis revealed TPM1, also downregulated in PD, as a key factor to dedifferentiation phenotype and malignancy. Thus, we demonstrated that the malignant phenotype may had arisen as a consequence of endoplasmic reticulum stress, in which the downregulation of key proteins involved in pathways as cell adhesion and post-translational processes can contribute to tumor progression and metastasis.

Key words: breast cancer, comparative oncology, ER stress, MALDI imaging, veterinary oncology

BACKGROUND

Breast cancer incidence and mortality rates have still been growing worldwide. In 2018, breast cancer represented 11.6% of new cases, and occupied the fifth position among the most lethal types of cancer, responsible for 6.6% of all deaths by the disease (BRAY et al., 2018). Even with a proper histopathological evaluation and the use of widely accepted gene expression profiles for molecular subtyping (PARKER et al., 2009), it is known that an accurate classification for clinical prognosis assessment and treatment decision-making can be challenging, therefore, a deeper molecular characterization is necessary for a better understanding of the disease. A reliable animal model that captures the key features of human cancer is essential to bring new insights regarding tumor development. In this context, spontaneously occurring canine mammary cancers are an excellent model of the complex biology behind heterogeneous cancer progression, for several reasons; domesticated dogs not only share the same environment and risk factors as humans, but also present more similarities regarding anatomic, histological and clinical features, as well as DNA and protein sequences content than those of rodents (LINDBLAD-TOH et al., 2005; PAOLONI; KHANNA, 2008; ROWELL; MCCARTHY; ALVAREZ, 2011; LIU et al., 2014). Moreover, the large population of dogs and the increasing dog-owner relationship care created a unique partnership that simultaneously can benefit both sides by helping researchers to improve the assessment of novel treatments for humans by treating pet animals with cancer.

Cellular differentiation can be defined as the capacity of cells to progressively acquire a more specialized function in a tissue, emerging from a stem-cell until reaching a mature phenotype (KUPIEC, 1997). While in normal tissue the differentiation process is frequently unidirectional, cancerous tissues can present a reverse flow and dedifferentiate. During tumor progression and dedifferentiation, transformed cells are subjected to an environment pressure which causes cytotoxic stress and reduce cell survival (GABBERT et al., 1985). The increased proliferation, for example, leads to hypoxia and nutrient deprivation, inducing stress in the endoplasmic reticulum (ER) and activation of a protective unfolded protein response (UPR) (CHIPURUPALLI et al., 2019). ER stress and UPR activation have been documented in the development of many cancer types, and evidence suggests that they have important roles in every aspect of cancer progression and metastasis (WANG; KAUFMAN, 2014).

To our knowledge, this is the first work using mass spectrometry imaging in mammary canine cancers that have demonstrated important events associated to cancer progression as the ER stress linked to morphological changes. Here, we identified alterations in protein expression

and network interaction between populations in distinct degrees of differentiation, which may lead to potential early-stage tumor biomarkers.

MATERIAL AND METHODS

Tissue Samples and TMA construction

Samples from five patients submitted to elective mastectomies were obtained from the Veterinary Hospital of the School of Animal Science and Food Engineering (FZEA/USP) in Pirassununga, Brazil, and the Veterinary Hospital of the Octávio Bastos Teaching Foundation (UNIFEOB) in São João da Boa Vista, Brazil. All procedures were approved by FZEA/USP Ethics Committee (CEUA nº 8632101017). After surgical removal, all tumors were fractionated into smaller fragments of ±1 cm^3. Each fragment was identified and fixed separately in a 10% buffered formalin solution, processed according to standard histological protocol and embedded in paraffin. Mammary cancer diagnosis was confirmed by conventional histopathological evaluation following the classification of Goldschmidt et. al. (GOLDSCHMIDT et al., 2011). For tissue microarray (TMA) construction, paraffin blocks were cut into 4 μm thick sections, stained with hematoxylin and eosin (HE) and comparable regions were marked, in order to have a better representation of intratumor heterogeneity across the entire solid mass. Representative areas of epithelial and myoepithelial cell populations, as well as stromal portions containing blood vessels, inflammatory cells and connective tissues were selected.

Matrix-assisted laser desorption ionization mass spectrometry imaging (MALDI-MSI)

MALDI-MSI was carried in the Department of Proteomics and Metabolomics of Leiden University Medical Center – LUMC (Netherlands). Paraffin-embedded tissue microarrays were sectioned into 4 μm thick slices and placed on indium tin oxide (Bruker Daltonics, Bremen, Germany) coated glass slides pre-treated with 1:1 poly-L-lysine (Sigma Aldrich, St. Louis, USA) and 0,1% Nonidet P-40 (Sigma Aldrich, St. Louis, USA). Sections were incubated on a heated plate for one hour at 60°C, dewaxed in xylene, rehydrated and washed with ultra-filtered water. Antigen retrieval was performed in heated citrate buffer using a steamer at 92°C for 20 minutes, followed by cooling at room temperature for 120 minutes. A specific trypsin solution for mass spectrometry (0.02μg/ml, Trypsin Gold, Promega Corporation, Wisconsin, USA) was sprayed using the SunCollect equipment (SunChrom, Friedrichsdorf, Germany) and slides were then incubated for 18h at 37°C and 95% of relative humidity. Matrix used for ion extraction (25 mg/mL of dihydroxybenzoic acid in 50% aqueous acetonitrile and 0.1% trifluoroacetic acid) was also applied using SunCollect. MALDI-FT-ICR data acquisition was performed in

positive ion mode (Bruker Daltonics, Bremen, Germany), in a range of *m/z* 500-5000 Da and lateral resolution of 100 μm.

Tissue annotation and data processing

After MALDI-MSI, matrix was removed with 70% ethanol, and ITO slides were routinely stained with HE solution and later scanned (Philips Slide Scanner, USA) on 5, 10, 20 and 40x magnification. On FlexImaging Software (Bruker Scientific Instrument, MA, USA), scanned images were co-registered with MALDI-FT-ICR-MSI data allowing the annotation of Regions of Interest (ROIs), mainly containing cancer epithelial populations. Necrotic and desmoplastic areas, as well large vessels and ducts were avoided during annotation procedure in order to reduce the interference that could be caused by other cells intermingled in the region, or the influence of matrix components accumulating inside empty spaces. Tumor ROIs were categorized in two groups: well differentiated tumor populations (WD) and poorly differentiated tumor populations (PD). Morphological criteria for WD and PD classification were adapted from the well-established canine mammary cancer grading system (GOLDSCHMIDT et al., 2011), which was based on the Nottingham Grading System used for human breast cancer classification (IARC, 2012). Details are shown in Table 1.

Table 1. Histopathological criteria for the classification of canine mammary tumor populations used in this study. Adapted from Goldschimdt et. al., 2011.

	Mitotic index	**Cell/nuclear pleomorphism**	**Tubular Differentiation**
1 point	0-3 mitosis/population	Uniform cells and nuclei. Occasional nucleoli	Differentiated tubules in > 75%
2 points	4-6 mitosis/population	Low / moderate degree of pleomorphism, occasional hyperchromatic nuclei, presence of nucleoli	Differentiated tubules in > 25% and < 75%
3 points	> 7 mitosis/population	High degree of pleomorphism, hyperchromatic nuclei, presence of prominent nucleoli and / or multiple	Differentiated tubules < 25% of the region, assuming areas of solid growth

Score	
3-5 points	Well differentiated
6-9 points	Poorly differentiated

Next, selected ROIs were imported into SCiLS Lab Software (2016b, Bruker Daltonics, Bremen, Germany), and raw data exported as an imzML file for preprocessing and peak picking. On R environment (www.r-project.org), spectra were normalized by RMS method, and

peak picking was conducted using the rMSI package (DEL CASTILLO et al., 2017), setting a signal to noise ratio (S/N) = 7, maximum permissible error for alignment of 50 ppm and bin tolerance of 12 scans. Peaklist was also filtered for mass defects.

Liquid chromatrography/tandem mass spectrometry (LC-MS/MS)

For LC-MS/MS analysis, on-tissue tryptic digestion was performed as described in MALDI-MSI method section. Lyophilized peptides were dissolved in 95/3/0.1 v/v/v water/acetonitrile/formic acid and subsequently analyzed by on-line C18 nano HPLC MS/MS with a system consisting of an Easy-nLC 1200 gradient HPLC system (Thermo, Bremen, Germany), and an Orbitrap Fusion Lumos mass spectrometer (Thermo). Samples were injected onto a homemade precolumn (100 µm × 15 mm, C18 Reprosil-Pur C18-AQ, 3 um, 120 A, and eluted via a homemade analytical nano-HPLC column (50 cm × 75 µm; Reprosil-Pur C18-AQ 1.9 um, 120 A (Dr. Maisch, Ammerbuch, Germany). The gradient was run from 2% to 36% solvent B (20/80/0.1 water/acetonitrile/formic acid (FA) v/v/v) in 120 min. The nano-HPLC column was drawn to a tip of ∼10 µm and acted as the electrospray needle of the MS source. The mass spectrometer was operated in data-dependent MS/MS mode for a cycle time of 3 seconds, with a HCD collision energy at 32 V and recording of the MS2 spectrum in the orbitrap, with a quadrupole isolation width of 1.2 Da. In the master scan (MS1) the resolution was 120,000, the scan range 400-1500, at an AGC target of 4,000,000 @maximum fill time of 50ms. Precursors were dynamically excluded after n=1 with an exclusion duration of 60s, and with a precursor range of 20 ppm. Charge states 2-4were included. For MS2 the first mass was set to 110 Da, and the MS2 scan resolution was 30,000 at an AGC target of 40,000 @maximum fill time of 60ms. In a post-analysis process, raw data were first converted to peak lists using Proteome Discoverer version 2.2 (Thermo Electron), and then submitted to the Canis2019 database (24669 entries), using Mascot v. 2.2.04 (www.matrixscience.com) for protein identification. Mascot searches were done with 10 ppm and 0.02 Da deviation for precursor and fragment mass, respectively, and trypsin was specified as the enzyme. Methionine oxidation and the main formaldehyde reaction product on Lysine (+12.000) were set as a variable modification. Carbamidomethyl (C) was set as fixed modification. Peptides with an FDR<1% in combination with a mascot ion score >25 were accepted.

Discriminative m/z signals

In order to identify significant differences regarding *m/z* values intensity among annotated regions, discriminative peaks between WD and PD tumor regions were explored

using Receiving Operator Curve method and later tested using the Mann Whitney Wilcoxon Test, followed by the Benjamini-Hochberg (BH) post-test correction. For this method, the mean intensity of every *m/z* signal in each ROI was calculated and tested. Only *m/z* signals presenting AUC > 0.70 and FDR < 0.05 were considered significant.

Functional enrichment analysis

Gene ontology (GO) was assessed using the online Webgestalt - WEB-based Gene SeT AnaLysis Toolkit (WANG et al., 2017a) platform, while pathway enrichment analysis was performed using the analysis tool from REACTOME database (FABREGAT et al., 2018). Protein symbols were used as inputs, and BH used as a correction method. Both GO and pathway enrichment analyzes were performed using the human genome-coding database as a reference set, for a more comprehensive knowledgebase regarding protein function. Enriched sets were considered significant if FDR < 0.05.

Network Interaction Analysis

MALDI-FT-ICR-MSI is an analytic technique that detects, in a high-resolution manner, the most abundant molecules on a tissue. In order to evaluate the interaction among the relevant molecules extracted from mammary carcinomas, we created the networks using only the peptides which protein identity could be retrieved from LC/MS-MS data. The mean intensity was calculated for every *m/z* signal, for each ROI in each group (well and poorly differentiated). For protein network inference, two networks were created, one for each condition. Proteins were used as nodes, and significant connections between them were identified using the Partial Correlation and Information Theory – PCIT (REVERTER; CHAN, 2008), where the significance between nodes is determined after accounting for all other nodes in the network. Connections were accepted when the partial correlation was greater than two standard deviations from the mean ($p < 0.01$), and significant correlations above |0.7| and their respective proteins were used for visualization in Cytoscape 2.8.3 (SHANNON et al., 2003).

RESULTS

Patients and samples

The study included 17 primary mammary gland tumors which were surgically removed from 5 unspayed female dogs with no previous history of either surgical or chemotherapy treatments. All five patients were diagnosed with metastatic disease, confirmed by anti-cytokeratin immunostaining in lymph nodes and other metastatic sites. Patient information and

histopathological classification of tumors are detailed in Table 1. Areas of epithelial and myoepithelial cell populations, as well as stroma, consisting of connective tissue areas including blood vessels and peritumoral inflammatory cell infiltration, metastatic sites and non-neoplastic glands were selected and resulted in 10 TMA blocks.

Table 1. Patients and sample information.

	Age (years)	**Breed**	**Status**	**Sample**	**Tumor**	**Histopathological classification**
PA1249	9	Labrador Retriever	Death*	58/17	1	Anaplastic carcinoma
					-	Carcinoma e malignant myoepithelioma***
					-	Anaplastic carcinoma***
3255/ 8448	12	Daschund	Death by tumor	61/17	2	Complex carcinoma
					3	Complex carcinoma
					4	Mixed-type carcinoma
					-	Simple adenoma***
					5	Complex carcinoma
					6	Complex carcinoma
					7	Mixed-type carcinoma
					8	Mixed-type carcinoma
					9	Complex carcinoma
3528/ 8432	12	Poodle	Alive**	63/17	10	Mixed-type carcinoma
					11	Simple carcinoma
					12	Mixed-type carcinoma
					13	Simple carcinoma tubular type
					14	Benign mixed-type
066/18	12	Brazilian Mastiff	Death by tumor	66/18	15	Invasive Micropapillar carcinoma
					16	Invasive Micropapillar carcinoma
PA1796	13	Mixed Breed	Death by tumor	71/18	17	Simple carcinoma tubular type

* Unknown cause of death
** Until last contact with the owner > 400 days after surgery.
*** Tumor not included in the study due to tissue processing issues

Mass spectrometry imaging dataset and tissue annotation

Whole imaging data set acquired by MALDI-FT-ICR spectrometer consisting in 48,070 pixels was subjected to RMS normalization procedure and peak picking. Overall, after data pre-processing and filtering, a peak list containing 1,087 individual signals within the mass range of *m/z* 900 to 3500 could be resolved on examined tissue. Average spectra and data set overview image are shown in Supplementary Figure S1.

After MS imaging data acquisition, ITO slides were HE stained and co-registered with MALDI-FT-ICR data set. For those slides which tissue quality was not considered adequate for annotation, consecutive sections from TMA blocks were used for this purpose. Cores that were lost or damaged by MSI tissue processing and/or staining were excluded from the analyses, and therefore, a total of 320 viable cores were subjected to pathological classification and annotation. From annotated regions, a total of 282 tumor ROIs were selected and further categorized as well differentiated (WD) and poorly differentiated (PD) tumor regions according to morphological criteria described in methods section (Figure 1), resulting in 70 and 212 ROIs belonging to each group, respectively. In addition, 108 stroma-only regions were also annotated as ROIs, but not included in any statistical analysis.

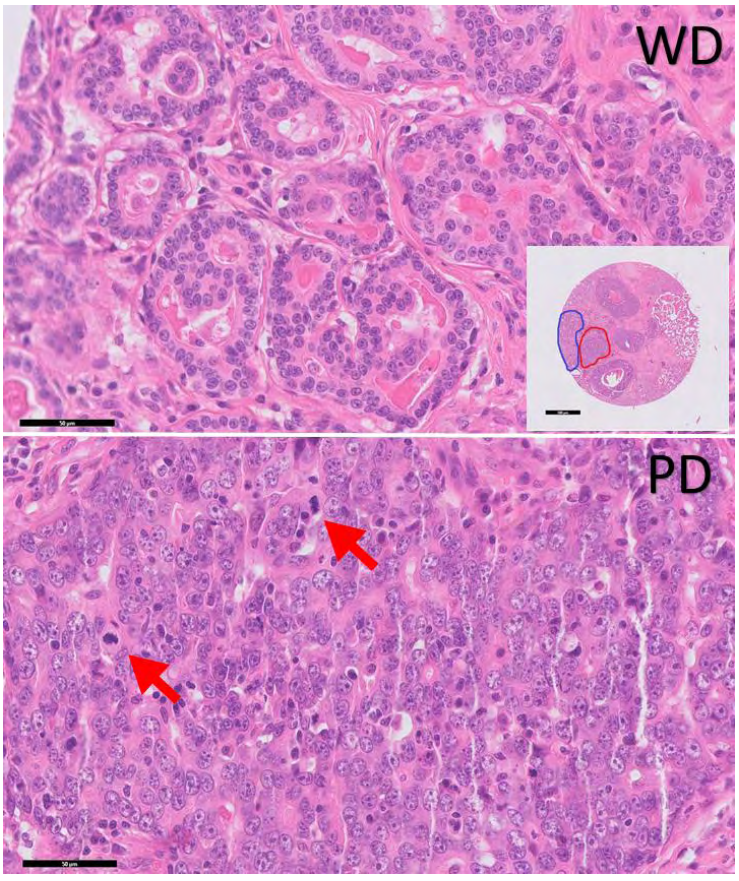

Figure 1 – Well differentiated (WD) and poorly differentiated (PD) tumor populations defined by morphological criteria such as tubule differentiation, mitotic index and nuclei and nucleoli pleomorphism. A total of 282 tumor regions in distinct stages of differentiation annotated from 17 tumors were evaluated for protein expression and network interaction by MSI and LC/MS-MS, in order to detect disease-state markers. Small picture: tissue core showing the annotation of a WD (blue) and a PD (red) region detailed in the higher magnification pictures. Red arrows point to atypical mitosis inside a PD tumor population. HE staining. Scale bar lower magnification: 500 µm. Scale bar higher magnification: 50 µm

Determination of discriminative m/z signals between mammary tumor populations of distinct degrees of differentiation

Our next approach was to determine molecular dissimilarities between WD and PD subpopulations that could be contributing to tumor progression. Therefore, an equal number of spectra of each condition (n = 3,000) were used for the receiver operating characteristic (ROC) curve and later tested using the Wilcoxon rank-sum method, to detect ions that could be able to discriminate between annotated WD and PD tumor ROIs. We observed 254 significant *m/z* signals with AUC > 0.70 discriminating between conditions (Supplementary Table S1), where all ions were found more intensely expressed in WD tumor regions (heatmap can be visualized in Supplementary Figure S2). In addition, some signals were also expressed across stromal areas (Figure 2).

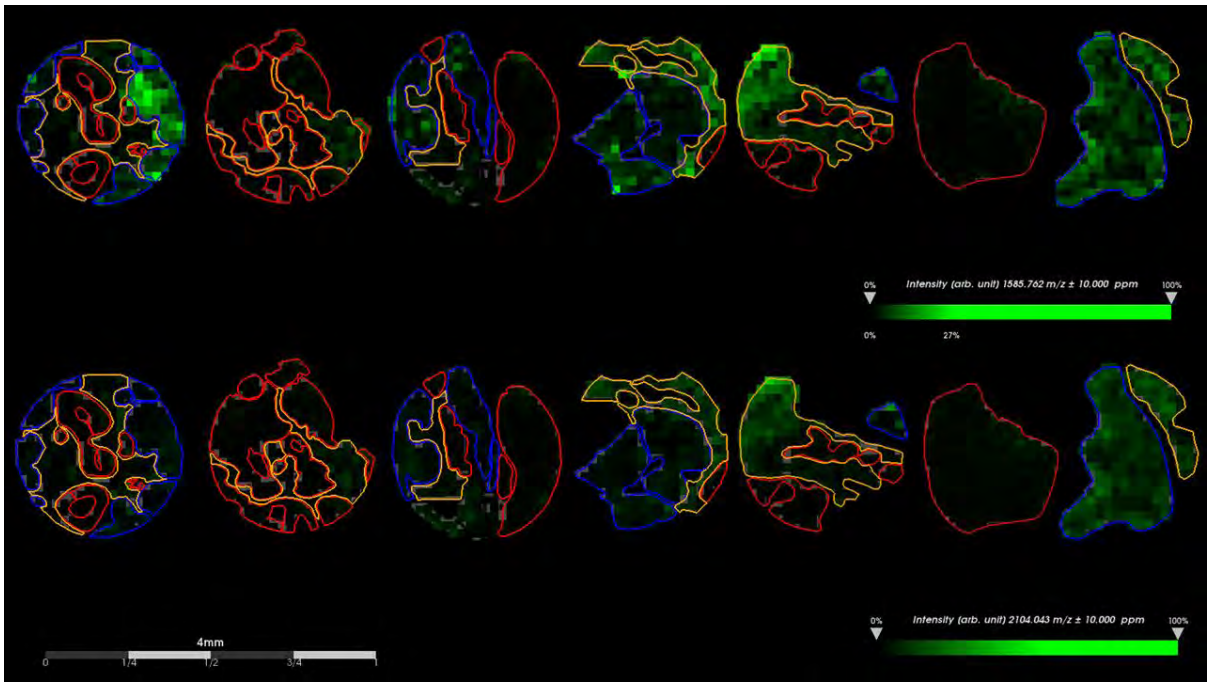

Figure 2 – Tissue distribution of signals at *m/z* 1585.762 (above, AUC = 0.75, FDR = 2.43E-14) and *m/z* 2104.043 (below, AUC = 0.75, FDR = 2.02E-12). Ions intensity is lower in PD (red line) than in WD (blue lines). Both ions were also expressed by stromal areas (yellow line). Note that *m/z* signals are heterogeneously expressed especially in stroma regions and WD tumor populations,

demonstrating the great advantage of MSI for the study of cancer populations as a complex system.

Protein identification and functional enrichment of differentially expressed peptides between well and poorly differentiated tumor populations

To increase our understanding in what types of peptides were detected in WD and PD populations, TMAs belonging to the same case were pooled together, and LC/MS-MS of tryptic peptides was used for protein identity assignment based on mass matching to a canine database. Significant discriminative *m/z* values between WD and PD regions resulted in 45 proteins IDs (Supplementary Table S2) used for gene ontology and pathway functional enrichment analyzes. Gene ontology of differentially expressed proteins significantly enriched for terms such as extracellular matrix structural organization, supramolecular fiber organization and cell adhesion. In addition, proteins calnexin (CANX), heat-shock protein family A member 5 (HSPA5) and protein disulfide isomerase family A member 3 (PDIA3) enriched for protein folding in endoplasmic reticulum. (Table 2).

Table 2 – Biological processes and molecular function terms enriched in GO analysis using the 45 proteins IDs retrieved from LC/MS-MS data.

	Symbol	**Description**	**UniProt ID**
Protein folding in endoplasmic reticulum (FDR = 0.04)	CANX	calnexin	P27824
	HSPA5	heat shock protein Family A member 5	P11021
	PDIA3	protein disulfide isomerase Family A member 3	P30101
Extracellular matrix structure and organization (FDR = 0.045)	ABI3BP	ABI Family member 3 binding protein	Q7Z7G0
	COL12A1	collagen type XII alpha 1 chain	Q99715
	COL1A1	collagen type I alpha 1 chain	P02452
	COL1A2	collagen type I alpha 2 chain	P08123
	COL6A3	collagen type VI alpha 3 chain	P12111
	LAMB2	laminin subunit beta 2	P11047
	VCAN	versican	P13611
Supramolecular fiber organization (FDR = 0.045)	APOA1	apolipoprotein 1	P02647
	COL12A1	collagen type XII alpha 1 chain	Q99715
	COL1A1	collagen type I alpha 1 chain	P02452
	COL1A2	collagen type I alpha 2 chain	P08123
	CTNNA1	catenin alpha 1	P35221
	EZR	ezrin	P15311
	LIMA1	LIM domain and actin binding 1	Q9UHB6
	SPTAN1	spectrin alpha, non-erytrocytic 1	Q13813
	TPM1	Tropomyosin 1	P09493

Cell adhesion (FDR = 0.04)	ABI3BP	ABI Family member 3 binding protein	Q7Z7G0
	APOA1	apolipoprotein 1	P02647
	ARHGDIA	Rho GDP dissociation inhibitor alpha	P52565
	COL12A1	collagen type XII alpha 1 chain	Q99715
	COL1A1	collagen type I alpha 1 chain	P02452
	COL6A3	collagen type VI alpha 3 chain	P12111
	CTNNA1	catenin alpha 1	P35221
	EMILIN2	elastin microfibril interface 2	Q9BXX0
	EZR	ezrin	P15311
	LAMB2	laminin subunit beta 2	P11047

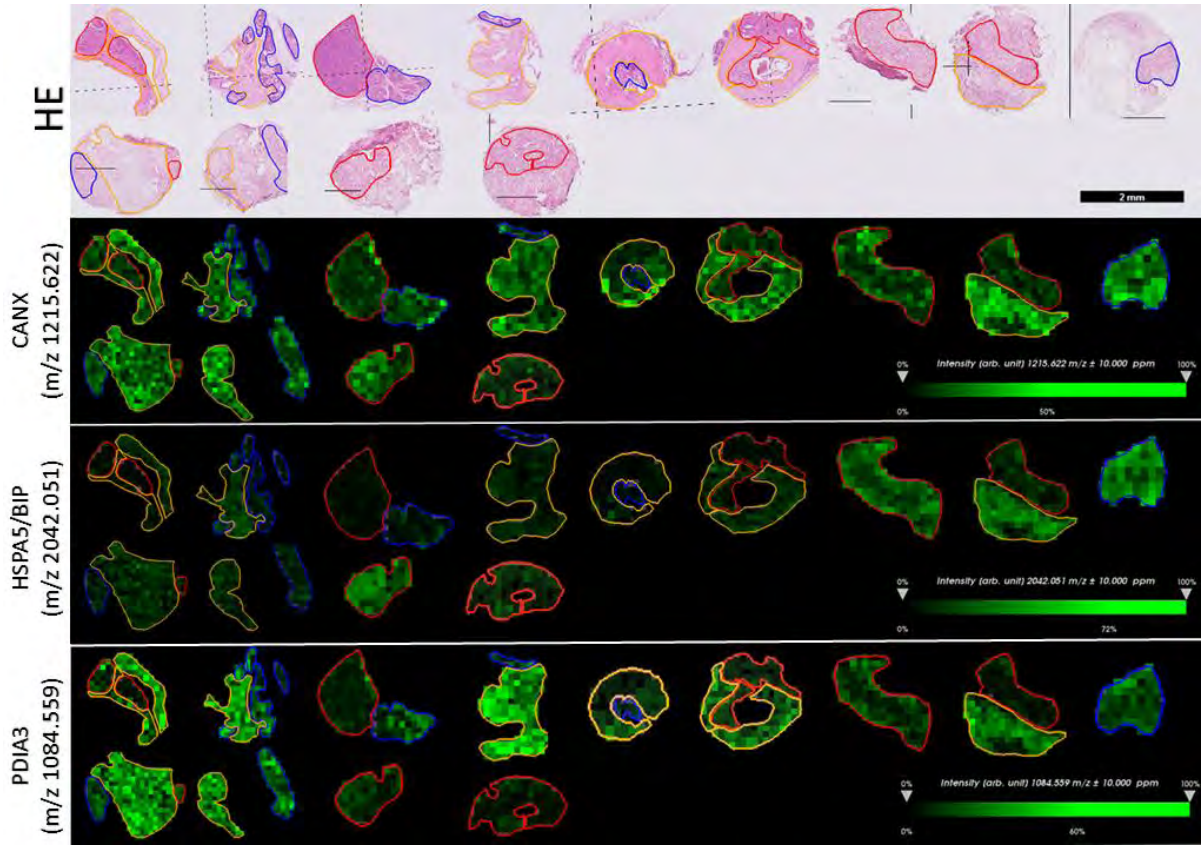

Figure 3 – Tissue distribution of *m/z* signals assigned to proteins enriched in protein folding in endoplasmic reticulum: calnexin (*m/z* 1215.622), heat-shock protein family A member 5 (*m/z* 2042.051) and protein disulfide isomerase family A member 3 (*m/z* 1084.559). WD tumor regions (blue line), PD tumor regions (red line) and stroma (yellow line). A heterogeneous distribution can be observed, especially for HSPA5 protein across tumor ROIs, suggesting microscopically indistinct tumor subpopulations.

Besides a general overview of GO biological and molecular processes, we also performed a functional pathway enrichment of differentially expressed proteins upregulated in WD populations using the open-access and peer-reviewed REACTOME database, which

describes possible reactions if all annotated proteins were present and active simultaneously in a cell. Among the six pathways significantly enriched in the analysis (Table 3), two were directly involved in protein processing in endoplasmic reticulum: the post-translational protein phosphorylation, represented by apolipoprotein 1 (APOA1), laminin subunit beta 2 (LAMB2), insulin-like growth factor binding protein 5 (IGFBP5) and versican (VCAN); and the prefoldin mediated transfer of substrate to CCT/TriC, comprising the T-complex protein 1 subunit gamma (CCT3) and tubulin beta 4B (TUBB4B).

Table 3 – Significant REACTOME enriched pathways sorted by FDR*

PATHWAY NAME	**ENTITIES**			
	found**	**ratio**	**p-value**	**FDR**
ECM proteoglycans	6/118	0.006	9.88E-6	0.008
Collagen chain trimerization	4/44	0.002	3.52R-5	0.015
Post-translational protein phosphorylation	5/109	0.005	7.11E-5	0.025
Prefoldin mediated transfer of substrate to CCT/TriC	3/29	0.001	2.45E-4	0.045
Collagen degradation	5/76	0.004	2.84E-4	0.045
Assembly of collagen fibrils and other multimeric structures	4/79	0.004	3.29E-4	0.045

*FDR: false discovery rate
** number of input proteins/total number of proteins in the pathway

Network analysis of molecules detected in heterogeneous tumor populations

Interaction networks are a useful tool to decrypt the molecular basis of phenotypes. Therefore, to further explore protein functions and interaction in each condition, networks were created for well and poorly differentiated regions using all identified proteins across the MSI dataset. Two measures were taking into consideration for network analysis: the betweenness centrality value, which is a way of detecting the amount of influence a node has over the flow of information based on shortest paths; and the degree value, that is the number of connections a certain node has. Both networks were composed of 147 proteins and 10,737 connections, in which 1,448 were considered significant in WD and 1,986 were found significant in PD tumor regions (correlations > |0.7|), with a mean of 20 and 29 connections per node, respectively. From those, 32% in WD and 33% in PD were connections between two differentially expressed proteins. Tropomyosin 1 (TPM1) and BCL-2 associated athanogene (BAG3) were found highly connected and with a high betweenness in WD network, while caldesmon 1 (CALD1) and

cathenin alpha 1 (CTNNA1) were among the top 15 most connected and with a higher betweenness centrality in the PD network (Figure 4). CALD1 presented the highest number of connections in both WD (50 connections) and PD (65 connections) populations. Interestingly, TPM1 protein, which showed the highest betweenness in WD condition, was also significantly more expressed in this group in discriminative *m/z* analyses. Measurement results for all proteins in both networks are described in Supplementary Table S3 and S4.

DISCUSSION

In the present study, we studied the inter and intratumor heterogeneity of canine mammary cancers using mass spectrometry imaging and LC-MS/MS associated to bioinformatic analyses. We assessed and compared 280 subpopulations extracted within 17 tumors from 5 patients, reducing the effect of genetic background and the influence of macro and microenvironment. The degree of differentiation is an important feature to generate relevant information regarding clinical behavior, and even in the molecular era, it has still been widely employed by human and veterinary pathologists having a direct impact to determine patient diagnosis and prognosis (ELSTON; ELLIS, 1991; RAKHA et al., 2010; CANADAS et al., 2018; KUPPUSAMY et al., 2019). It is well-known that the dedifferentiation degree is positively associated to malignancy (KUPIEC, 1997). Therefore, we used a well-established histological grading system to divide cancer populations into two distinct groups based on their level of differentiation: well and poorly differentiated tumor regions (WD and PD). Since all five patients had already developed to the metastatic form of the disease, a higher number of PD regions were observed in our samples.

Cells undergoing malignant progression and dedifferentiation have an increased proliferation and ability of adapting under adverse environments, which require a large demand for protein synthesis inevitably leading to ER stress resulting in protein misfolding, reduced ER processing and UPR activation (ARENSDORF; DIEDRICHS; RUTKOWSKI, 2013; CLARKE et al., 2014). In our study, we found five proteins involved in UPR and protein folding processes to be upregulated in WD compared to PD tumor populations: CCT3, TUBB4B, CANX, HSPA5 and PDIA3, demonstrating that ER stress possibly contribute to morphological changes and malignancy in canine cancer. This finding corroborates with a study by Ulianish et. al., which has demonstrated that thyroid cells execute a dedifferentiation programming with loss of epithelial organization as a response mechanism to ER stress, as part of an adaptive way

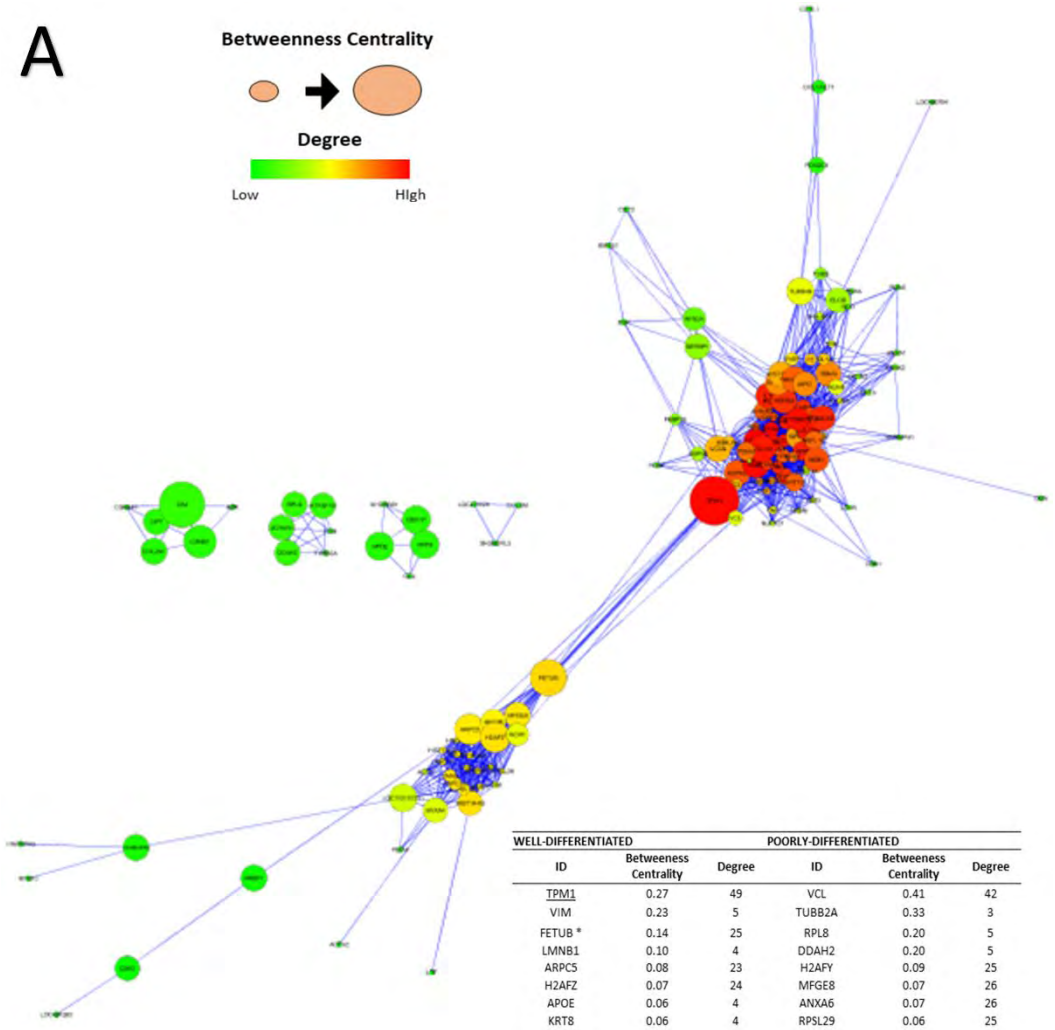

WELL-DIFFERENTIATED			POORLY-DIFFERENTIATED		
ID	Betweeness Centrality	Degree	ID	Betweeness Centrality	Degree
TPM1	0.27	49	VCL	0.41	42
VIM	0.23	5	TUBB2A	0.33	3
FETUB *	0.14	25	RPL8	0.20	5
LMNB1	0.10	4	DDAH2	0.20	5
ARPC5	0.08	23	H2AFY	0.09	25
H2AFZ	0.07	24	MFGE8	0.07	26
APOE	0.06	4	ANXA6	0.07	26
KRT8	0.06	4	RPSL29	0.06	25
DDX17	0.06	4	FETUB *	0.06	25
LOC102157231	0.05	17	CALD1	0.05	65
TUBB4B *	0.05	19	TNKS1BP1	0.05	35
BAG3	0.04	49	TUBB4B *	0.04	30
HNRNPM	0.03	3	CTNNA1	0.03	59
RRBP1	0.03	2	ANXA4	0.03	15

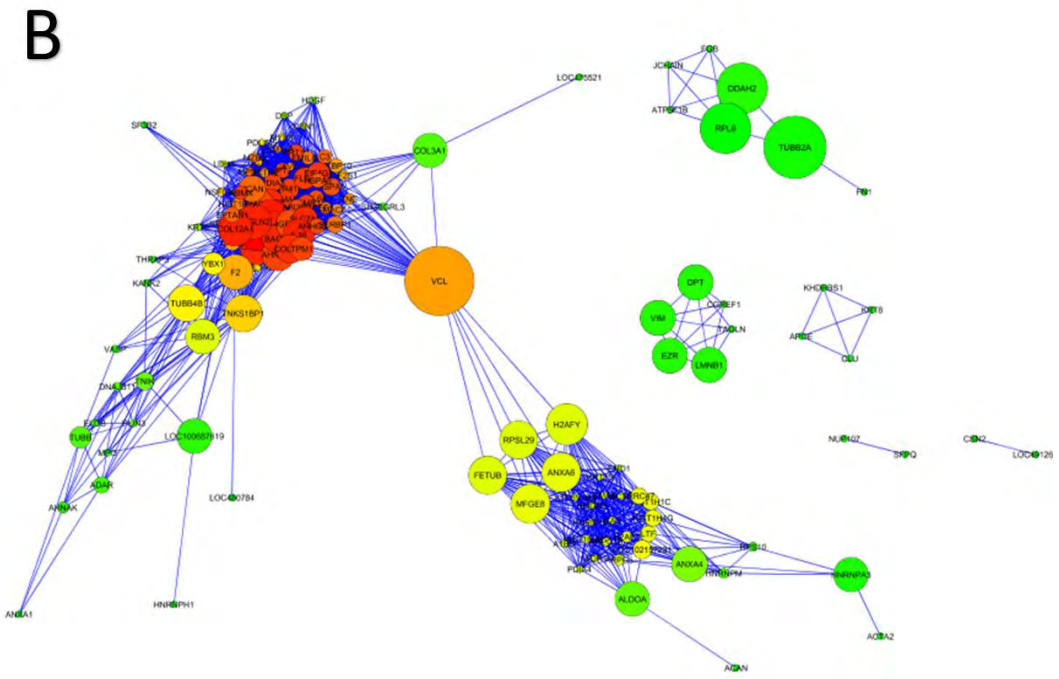

Figure 4 –Well differentiated (A) and poorly differentiated (B) networks created from significant correlations > |0.7| calculated by PCIT algorithm with all proteins detected in MSI data set (n = 147). Molecules in networks always have the structures in which molecules are more closely connected. Table shows the top proteins sorted by betweenness centrality value, where underlined symbols are differentially expressed proteins found in discriminative analysis, and asterisk represents proteins with a high betweenness in both conditions. Both WD and PD showed smaller modules containing connections between three or more proteins. Node size is positively correlated with betweenness, while color bar represents number of connections.

that facilitated cell survival (ULIANICH et al., 2008). In addition, for canine mammary cancer, immunostaining for Derlin-1 showed that metastatic cells, the later stage of tumor progression, presented an increased stress-associated unfolded protein response (KLOPFLEISCH et al., 2010a) compared to non-metastatic samples.

PDIA3 interacts with lectin chaperones calreticulin and calnexin to modulate folding of newly synthesized glycoproteins (ZHANG; BAIG; WILLIAMS, 2006). The low expression of PDIA3 have been associated to a poor overall survival for non-small lung cancer and gastric cancer, due to the formation of a complex with MHC class I and the high correlation with the expression of calreticulin, responsible for maintaining adequate calcium levels in organisms and also acting in ER (ZHANG; BAIG; WILLIAMS, 2006; WANG et al., 2017b; SHIMODA et al., 2019). Calnexin is a highly abundant transmembrane chaperone which folds synthesized glycoproteins in the lumen of the endoplasmic reticulum (AEBI et al., 2010; SHIBATA et al., 2010), while the heat shock protein 5 (also known as BIP) is a master regulator of the UPR (MALHOTRA; KAUFMAN, 2007). Higher levels of CANX and BIP were pointed out as markers for a worse prognosis in several types of cancer, indicating their association to tumor progression (LAKKARAJU; VAN DER GOOT, 2013; KOBAYASHI et al., 2015; RYAN et al., 2016). However, our results showed that both proteins were downregulated in PD in comparison to WD, suggesting that the loss of these proteins may also play a role in adaptation of cancer cells to ER stress and malignancy, together with PDIA3. In fact, some studies have demonstrated that, upon induction of ER stress, CANX and BIP proteins were underregulated inside normal and tumor cells, due to proteolytic cleavage of approximate 20% of CANX by caspase-8, and BIP sequestration on the cytoplasm by binding to misfolded or unfolded protein as to prevent the activation of signaling pathways, which could lead to apoptosis (BERTOLOTTI et al., 2000; LAKKARAJU; VAN DER GOOT, 2013; WANG; KAUFMAN, 2014). Those events trigger a compensatory mechanism which induces gene transcription and increase ER capacity by synthesizing more chaperones and UPR proteins, explaining the

transient expression from early to advanced ER stress stages (KOZUTSUMI et al., 1988; DORNER; WASLEY; KAUFMAN, 1989).

Proteins with a significant number of interactions and/or a central role on information flow often can be used as key components to understand cancer-associated pathways and for biomarker discovery. As different expressed molecules are often downstream effects of network disturbing, molecules with high values of degree, and specially betweenness centrality, may be more important for network regulation than the differentially expressed proteins per se (GAMBARDELLA et al., 2013). In this work, TUBB4B protein was found not only downregulated in WD regions, but also with a high betweenness value, enriching for a pathway related to protein folding in ER. In cancer, β-tubulins interact with vimentin, a well-known metastasis marker intermediate filament, regulating the polarity of cell cytoskeleton with influence on EMT and cell migratory processes (GAN et al., 2016; CIRILLO; GOTTA; MERALDI, 2017). An intrinsic link between ER homeostasis, the initiation of ER stress response and the microtubule network has already been observed, but the mechanisms co-regulating these processes still remain unclear (PARKER; KAVALLARIS; MCCARROLL, 2014). TUBB4B downregulation has been shown to be critical for increasing migration of metastatic cells in colon cancer, where TUBB4B decrease was followed by changes in cell morphology and an increased number of matured focal adhesion sites, corroborating with our results (SOBIERAJSKA et al., 2019). Although TUBB4B did not enrich for this specific biological process, cell adhesion was also a significant term found in our GO analysis.

Besides microtubules, tropomyosins also have an increased functional complexity in non-muscle cells acting as microfilaments which stabilize the cytoskeleton (GUNNING et al., 2015). In this study, protein network interaction showed TPM1 as an important regulator protein in WD regions, as it presented the higher betweenness value and was also found significantly upregulated in this condition, therefore losing its expression during dedifferentiation. In 2010, Klopfleisch and collaborators showed that TPM1 was downregulated in canine metastatic mammary carcinomas compared to non-metastatic samples, but the mechanisms behind it were not evaluated (KLOPFLEISCH et al., 2010b). In human breast cancer, TPM1 was reported as having a tumor suppression gene function (BHARADWAJ; PRASAD, 2002). Recently, studies in different types of cancer have been able to describe how a lower expression of TPM1 was associated to an increase of cell proliferation, metastasis and evasion of apoptosis (LIU et al., 2018; TANG et al., 2018; LIN et al., 2019; WANG et al., 2019). In this work, we also observed that TPM1 might be linked with protein processing alterations due to ER stress, since connections between TPM1 and proteasomal

ubiquitin receptor ADRM1, as well as TPM1 and apolipoprotein-1 (APOA1), were among the connections with the most significant partial correlations (>|0.9|) involving TPM1 protein. Proteasomal ubiquitin receptor ADRM1 is part of a complex which plays a role in the maintenance of protein homeostasis by removing misfolded or damaged proteins, participating in numerous cellular processes, such as cell cycle progression, apoptosis and DNA damage repair (JORGENSEN et al., 2006), while APOA1 is the major protein component of high-density lipoprotein, and it has been suggested as having a protective role against cancer (ZAMANIAN-DARYOUSH; DIDONATO, 2015). Here, enrichment analysis showed APOA1 overlapping with cell adhesion and post-translational protein phosphorylation processes. These results support the theory that reticular stress is a major contributor to cancer dedifferentiation and metastatic progression in canine mammary carcinomas.

In conclusion, through the comparison of the proteomic profile of intratumor populations in different degrees of differentiation, we demonstrated that the malignant phenotype may had arisen as a consequence of alterations in protein processing due to endoplasmic reticulum stress, in which the downregulation of key proteins like TPM1, TUBB4B, CANX, HSPA5, PDIA3 and APOA1 involved in pathways as cell adhesion and post-translational processes can contribute to tumor progression and metastasis. Now, further investigations are necessary to deeply characterize molecular alterations in tumor subpopulations in regard to the way that pathways such as the response of reticular stress evolves with malignancy. Therefore, we expect to identify proteins that may be validated as disease-state markers in canine mammary cancer, and further expand our findings to comparative studies in human oncology research.

REFERENCES

AEBI, M. et al. N-Glycan Structures: Recognition and Processing in the ER. **Trends in biochemical sciences**, v. 35, n. 2, p. 74–82, fev. 2010.

ARENSDORF, A. M.; DIEDRICHS, D.; RUTKOWSKI, D. T. Regulation of the Transcriptome by ER Stress: Non-Canonical Mechanisms and Physiological Consequences. **Frontiers in genetics**, v. 4, p. 256, 2 dez. 2013. Disponível em: <https://www.ncbi.nlm.nih.gov/pubmed/24348511>.

BERTOLOTTI, A. et al. Dynamic Interaction of BiP and ER Stress Transducers in the Unfolded-Protein Response. **Nature cell biology**, v. 2, n. 6, p. 326–332, jun. 2000.

BHARADWAJ, S.; PRASAD, G. L. Tropomyosin-1, a Novel Suppressor of Cellular Transformation Is Downregulated by Promoter Methylation in Cancer Cells. **Cancer letters**, v. 183, n. 2, p. 205–213, set. 2002.

BRAY, F. et al. Global cancer statistics 2018: GLOBOCAN estimates of incidence and mortality worldwide for 36 cancers in 185 countries. **CA: A Cancer Journal for Clinicians**, v. 68, n. 6, p. 394–424, 1 nov. 2018. Disponível em: <https://doi.org/10.3322/caac.21492>.

CANADAS, A. et al. Canine Mammary Tumors: Comparison of Classification and Grading Methods in a Survival Study. **Veterinary Pathology**, v. 56, n. 2, p. 208–219, 31 out. 2018. Disponível em: <https://doi.org/10.1177/0300985818806968>.

CHIPURUPALLI, S. et al. Hypoxia Induced ER Stress Response as an Adaptive Mechanism in Cancer. **International journal of molecular sciences**, v. 20, n. 3, p. 749, 11 fev. 2019. Disponível em: <https://www.ncbi.nlm.nih.gov/pubmed/30754624>.

CIRILLO, L.; GOTTA, M.; MERALDI, P. The Elephant in the Room: The Role of Microtubules in Cancer. **Advances in experimental medicine and biology**, v. 1002, p. 93–124, 2017.

CLARKE, H. J. et al. Endoplasmic Reticulum Stress in Malignancy. **Cancer Cell**, v. 25, n. 5, p. 563–573, 2014. Disponível em: <http://dx.doi.org/10.1016/j.ccr.2014.03.015>.

DEL CASTILLO, E. et al. rMSI: an R package for MS imaging data handling and visualization. **Bioinformatics**, v. 33, n. 15, p. 2427–2428, 30 mar. 2017. Disponível em: <https://doi.org/10.1093/bioinformatics/btx182>.

DORNER, A. J.; WASLEY, L. C.; KAUFMAN, R. J. Increased Synthesis of Secreted Proteins Induces Expression of Glucose-Regulated Proteins in Butyrate-Treated Chinese Hamster Ovary Cells. **The Journal of biological chemistry**, v. 264, n. 34, p. 20602–20607, dez. 1989.

ELSTON, C. W.; ELLIS, I. O. pathological prognostic factors in breast cancer. I. The value of histological grade in breast cancer: experience from a large study with long-term follow-up. **Histopathology**, v. 19, n. 5, p. 403–410, 1 nov. 1991. Disponível em: <https://doi.org/10.1111/j.1365-2559.1991.tb00229.x>.

FABREGAT, A. et al. The Reactome Pathway Knowledgebase. **Nucleic acids research**, v. 46, n. D1, p. D649–D655, 4 jan. 2018. Disponível em: <https://www.ncbi.nlm.nih.gov/pubmed/29145629>.

GABBERT, H. et al. Tumor Dedifferentiation: An Important Step in Tumor Invasion. **Clinical & experimental metastasis**, v. 3, n. 4, p. 257–279, 1985.

GAMBARDELLA, G. et al. Differential Network Analysis for the Identification of Condition-Specific Pathway Activity and Regulation. **Bioinformatics (Oxford, England)**, v. 29, n. 14, p. 1776–1785, 15 jul. 2013. Disponível em: <https://www.ncbi.nlm.nih.gov/pubmed/23749957>.

GAN, Z. et al. Vimentin Intermediate Filaments Template Microtubule Networks to Enhance Persistence in Cell Polarity and Directed Migration. **Cell Systems**, v. 3, n. 3, p. 252- 263.e8, 2016. Disponível em: <http://www.sciencedirect.com/science/article/pii/S2405471216302629>.

GOLDSCHMIDT, M. et al. Classification and grading of canine mammary tumors. **Veterinary pathology**, v. 48, n. 1, p. 117–31, jan. 2011. Disponível em: <http://www.ncbi.nlm.nih.gov/pubmed/21266722>. Acesso em: 4 dez. 2014.

GUNNING, P. W. et al. Tropomyosin – master regulator of actin filament function in the cytoskeleton. **Journal of Cell Science**, v. 128, n. 16, p. 2965 LP – 2974, 15 ago. 2015. Disponível em: <http://jcs.biologists.org/content/128/16/2965.abstract>.

IARC. **WHO Classification of Tumours of the Breast**. 4th. ed. [s.l: s.n.]

JORGENSEN, J. P. et al. Adrm1, a Putative Cell Adhesion Regulating Protein, Is a Novel Proteasome-Associated Factor. **Journal of molecular biology**, v. 360, n. 5, p. 1043–1052, jul. 2006.

KLOPFLEISCH, R. et al. Increased Derlin-1 Expression in Metastases of Canine Mammary Adenocarcinomas. **Journal of Comparative Pathology**, v. 142, n. 1, p. 79–83, 2010a. Disponível em: <http://www.sciencedirect.com/science/article/pii/S0021997509000917>.

KLOPFLEISCH, R. et al. Proteome of Metastatic Canine Mammary Carcinomas : Similarities to and Differences from Human Breast Cancer † research articles. p. 6380–6391, 2010b.

KOBAYASHI, M. et al. Calnexin is a novel sero-diagnostic marker for lung cancer. **Lung Cancer**, v. 90, n. 2, p. 342–345, 2015. Disponível em: <http://www.sciencedirect.com/science/article/pii/S0169500215300398>.

KOZUTSUMI, Y. et al. The Presence of Malfolded Proteins in the Endoplasmic Reticulum Signals the Induction of Glucose-Regulated Proteins. **Nature**, v. 332, n. 6163, p. 462–464, mar. 1988.

KUPIEC, J. J. A Darwinian theory for the origin of cellular differentiation. **Molecular and General Genetics MGG**, v. 255, n. 2, p. 201–208, 1997. Disponível em: <https://doi.org/10.1007/s004380050490>.

KUPPUSAMY, K. et al. **Cytological Grading of Breast Tumors—The Human and Canine Perspective Frontiers in Veterinary Science** , 2019. . Disponível em: <https://www.frontiersin.org/article/10.3389/fvets.2019.00283>.

LAKKARAJU, A. K. K.; VAN DER GOOT, F. G. Calnexin Controls the STAT3-Mediated Transcriptional Response to EGF. **Molecular Cell**, v. 51, n. 3, p. 386–396, 8 ago. 2013. Disponível em: <https://doi.org/10.1016/j.molcel.2013.07.009>.

LIN, J. et al. MiRNA-183-5p.1 promotes the migration and invasion of gastric cancer AGS cells by targeting TPM1. **Oncology Reports**, v. 42, n. 6, p. 2371–2381, 2019.

LINDBLAD-TOH, K. et al. Genome sequence, comparative analysis and haplotype structure of the domestic dog. **Nature**, v. 438, n. 7069, p. 803–19, 8 dez. 2005. Disponível em: <http://www.ncbi.nlm.nih.gov/pubmed/16341006>. Acesso em: 11 jul. 2014.

LIU, D. et al. Molecular Homology and Difference between Spontaneous Canine Mammary Cancer and Human Breast Cancer. **Cancer Research**, v. 74, n. 18, p. 5045–5056, 2014. Disponível em: <http://cancerres.aacrjournals.org/cgi/doi/10.1158/0008-5472.CAN-14-0392>.

LIU, G. et al. Long non-coding RNA MEG3 suppresses the development of bladder urothelial carcinoma by regulating miR-96 and TPM1. **Cancer Biology & Therapy**, v. 19, n. 11, p. 1039–1056, 2 nov. 2018. Disponível em: <https://doi.org/10.1080/15384047.2018.1480279>.

MALHOTRA, J. D.; KAUFMAN, R. J. The Endoplasmic Reticulum and the Unfolded Protein Response. **Seminars in cell & developmental biology**, v. 18, n. 6, p. 716–731, dez. 2007.

PAOLONI, M.; KHANNA, C. Translation of new cancer treatments from pet dogs to humans. **Nature Reviews Cancer**, v. 2946, n. 2000, p. 2943–2946, 2008. Disponível em: <http://www.nature.com/nrc/journal/v8/n2/abs/nrc2273.html>. Acesso em: 31 dez. 2014.

PARKER, A. L.; KAVALLARIS, M.; MCCARROLL, J. A. **Microtubules and Their Role in Cellular Stress in Cancer Frontiers in Oncology** , 2014. . Disponível em: <https://www.frontiersin.org/article/10.3389/fonc.2014.00153>.

PARKER, J. S. et al. Supervised Risk Predictor of Breast Cancer Based on Intrinsic Subtypes. **Journal of Clinical Oncology**, v. 27, n. 8, p. 1160–1167, 9 fev. 2009. Disponível em: <https://doi.org/10.1200/JCO.2008.18.1370>.

RAKHA, E. A. et al. Breast cancer prognostic classification in the molecular era: the role of histological grade. **Breast Cancer Research**, v. 12, n. 4, p. 207, 2010. Disponível em: <https://doi.org/10.1186/bcr2607>.

REVERTER, A.; CHAN, E. K. F. Combining partial correlation and an information theory approach to the reversed engineering of gene co-expression networks. **Bioinformatics**, v. 24, n. 21, p. 2491–2497, 10 set. 2008. Disponível em: <https://doi.org/10.1093/bioinformatics/btn482>.

ROWELL, J. L.; MCCARTHY, D. O.; ALVAREZ, C. E. Dog models of naturally occurring cancer. **Trends in Molecular Medicine**, v. 17, n. 7, p. 380–388, 1 jul. 2011. Disponível em: <https://doi.org/10.1016/j.molmed.2011.02.004>.

RYAN, D. et al. Calnexin, an ER Stress-Induced Protein, Is a Prognostic Marker and Potential Therapeutic Target in Colorectal Cancer. **Journal of translational medicine**, v. 14, n. 1, p. 196, 1 jul. 2016. Disponível em: <https://www.ncbi.nlm.nih.gov/pubmed/27369741>.

SHANNON, P. et al. Cytoscape: A Software Environment for Integrated Models of Biomolecular Interaction Networks. **Genome research**, v. 13, n. 11, p. 2498–2504, nov. 2003. Disponível em: <https://www.ncbi.nlm.nih.gov/pubmed/14597658>.

SHIBATA, Y. et al. Mechanisms Determining the Morphology of the Peripheral ER. **Cell**, v. 143, n. 5, p. 774–788, 24 nov. 2010. Disponível em: <https://www.ncbi.nlm.nih.gov/pubmed/21111237>.

SHIMODA, T. et al. Expression of Protein Disulfide Isomerase A3 and Its Clinicopathological Association in Gastric Cancer. **Oncology reports**, v. 41, n. 4, p. 2265–2272, abr. 2019.

SOBIERAJSKA, K. et al. TUBB4B Downregulation Is Critical for Increasing Migration of Metastatic Colon Cancer Cells. **Cells**, v. 8, n. 8, p. 810, 1 ago. 2019. Disponível em: <https://www.ncbi.nlm.nih.gov/pubmed/31375012>.

TANG, C. et al. Tropomyosin-1 Promotes Cancer Cell Apoptosis via the P53-Mediated Mitochondrial Pathway in Renal Cell Carcinoma. **Oncology letters**, v. 15, n. 5, p. 7060–7068, maio 2018. Disponível em: <https://www.ncbi.nlm.nih.gov/pubmed/29731872>.

ULIANICH, L. et al. ER stress is associated with dedifferentiation and an epithelial-to-mesenchymal transition-like phenotype in PC Cl3 thyroid cells. **Journal of Cell Science**, v. 121, n. 4, p. 477 LP – 486, 15 fev. 2008. Disponível em: <http://jcs.biologists.org/content/121/4/477.abstract>.

WANG, J. et al. WebGestalt 2017: a more comprehensive, powerful, flexible and interactive gene set enrichment analysis toolkit. **Nucleic Acids Research**, v. 45, n. W1, p. W130–W137, 3 maio 2017a. Disponível em: <https://doi.org/10.1093/nar/gkx356>.

WANG, J. et al. Tropomyosin-1 Functions as a Tumor Suppressor with Respect to Cell Proliferation, Angiogenesis and Metastasis in Renal Cell Carcinoma. **Journal of Cancer**, v. 10, n. 10, p. 2220–2228, 2019. Disponível em: <http://www.jcancer.org/v10p2220.htm>.

WANG, K. et al. Combination of CALR and PDIA3 is a potential prognostic biomarker for non-small cell lung cancer. **Oncotarget; Vol 8, No 57**, 2017b. Disponível em: <http://legacy.oncotarget.com/index.php?journal=oncotarget&amp>.

WANG, M.; KAUFMAN, R. J. The impact of the endoplasmic reticulum protein-folding environment on cancer development. **Nature Reviews Cancer**, v. 14, n. 9, p. 581–597, 2014. Disponível em: <https://doi.org/10.1038/nrc3800>.

ZAMANIAN-DARYOUSH, M.; DIDONATO, J. A. Apolipoprotein A-I and Cancer. **Frontiers in pharmacology**, v. 6, p. 265, 12 nov. 2015. Disponível em: <https://www.ncbi.nlm.nih.gov/pubmed/26617517>.

ZHANG, Y.; BAIG, E.; WILLIAMS, D. B. Functions of ERp57 in the Folding and Assembly of Major Histocompatibility Complex Class I Molecules. **Journal of Biological Chemistry** , v. 281, n. 21, p. 14622–14631, 26 maio 2006. Disponível em: <http://www.jbc.org/content/281/21/14622.abstract>.

CAPÍTULO 3 - MALDI-IMAGING GUIDED PROTEOMIC ANALYSIS OF INTRATUMOR HETEROGENEITY: A STUDY IN A CANINE METASTATIC MAMMARY CARCINOMA

CORDEIRO, Y.G[1], HEIJS, B.P.A.M.[2], MULDER, L.M.[2], VAN ZEIJL, R.J.[2], VAN VEELEN.[2], P., RU, A.[2], STREFEZZI, R.F.[1], FUKUMASU, H[1].

[1] Laboratory of Comparative and Translational Oncology, Department of Veterinary Medicine, School of Animal Science and Food Engineering, University of São Paulo, Pirassununga, Brazil

[2] Center of Proteomics and Metabolomics, Leiden University Medical Center, Leiden University, Leiden, the Netherlands.

ABSTRACT

In recent years, it has become evident that cells within a single tumor may differ in morphological, genetic and behavioral phenotypes. Sequential analyzes in several types of cancer showed that intratumor heterogeneity (ITH) evolves during the disease course, with implications for predictive and therapeutic targets. Importantly, tumor subclones influencing patient outcome may evade detection as a consequence of the regional separation from the tumor biopsy site. In this study, we aimed to identify and characterize spatially resolved molecular diversity in various tissue compartments within a unique solid canine mammary tumor mass, in order to detect cancer subpopulations which could be further evaluated as driving malignant progression. MALDI-FT-ICR-MSI spectra acquired from a primary tumor sample were grouped using an unsupervised clustering method in order to obtain segmentation maps of molecularly distinct regions. Then, discriminative analysis was performed in five major tumor clusters using ROC method, for a deeper exploration of differences in peptide expression between clusters. We demonstrated a distinct expression pattern of 44 proteins retrieved from 68 peptides, which enriched for terms such as structural molecule activity, immune system process, gene expression regulation, epigenetic regulation and others. Additionally, peptides corresponding to proteins CSN2, CLU, LOC475521, Histone H2, RPL8, GAPDH and IGHM were found upregulated on metastatic cells inside lymphatic vessels (ILM) compared to those in the regional lymph node (LNM). Also, ILM and LNM regions correlated to distinct primary tumor subpopulations CL3 and CL1, respectively. Further analyzes are needed for new insights into the underlying biological processes related to ITH, which will help in the development of novel and improved targeted therapies.

Key words: Cancer biology, intratumor heterogeneity, MALDI-imaging, mammary cancer

BACKGROUND

Although morphological tumor heterogeneity was first described many decades ago, evidences of molecular intratumor heterogeneity only started to be deeply explored after the advent of next-generation sequencing (NGS) technologies, where cancer subpopulations differing in genetic, epigenetic and microenvironmental components were found to be cooperative and contributing to tumor progression (AXELROD; AXELROD; PIENTA, 2006; TSUJI et al., 2008; CALBO et al., 2011; NEELAKANTAN; DRASIN; FORD, 2015). In veterinary medicine, the perception of tumor heterogeneity as a potential problem has existed for decades (LARUE et al., 1994). However, the lack of genomic information, and the sparse information on molecular mechanisms of carcinogenesis in domestic animals appeared as obstacles for the advance of veterinary oncology, especially regarding therapeutic strategies. Only in recent years, relevant findings from studies involving gene and protein expression patterns have been applied to clinical diagnosis and therapy (HAHN et al., 2008; FRANTZ et al., 2012; DA COSTA et al., 2013; REGAN et al., 2016; FOWLES et al., 2017). Still, intratumor heterogeneity appears as an additional and important problem of how to target cancer in a more efficient manner, since current therapies including immunotherapies, rarely take ITH into account.

Mass spectrometry imaging (MSI) correlates the chemical information collected from multiple molecules using a mass spectrometer with spatial information of histological sections, and therefore is a useful tool for analyzing intratumor heterogeneity in cancer tissues (BALLUFF; HANSELMANN; HEEREN, 2017). Up to date, only a few studies were performed using MSI in canine cancer, which all involved lipidic profiling which identified molecules that could be used to distinguish between tumors, or between tumoral from non-tumoral areas (DILL et al., 2009; JARMUSCH et al., 2015; D'HUE et al., 2018). To our knowledge, this is the first work to address intratumor heterogeneity in a canine mammary carcinoma through an untargeted approach, using a high-resolution MALDI imaging platform to spatially resolve distinct molecular features across the tissue. Although still a preliminary study, it comes as an important starting point for exploring such a complex system, directing the search for specific alterations leading to new tumor biomarkers.

MATERIAL AND METHODS

Tissue sample

Primary tumor and regional lymph nodes were obtained in collaboration with the Veterinary Hospital of the Octávio Bastos Teaching Foundation (UNIFEOB) in São João da Boa Vista, Brazil (procedures were approved by FZEA/USP Ethics Committee, protocol number CEUA 8632101017). The entire tumor mass was fractionated into ±1 cm^3 pieces, and each fragment was fixed separately in a 10% buffered formalin solution, processed according to standard histological protocols and embedded in paraffin. Diagnosis of mammary carcinoma was confirmed by two pathologists (YGC and RFS) following the classification of Goldschmidt et. al. (GOLDSCHMIDT et al., 2011). In order to better assess intratumor heterogeneity, all FFPE blocks (primary tumor fragments and regional lymph nodes) were sectioned and hematoxylin and eosin stained for histopathological evaluation and determination of areas to be assembled for multiplex analysis. Comparable areas of epithelial cancer cells in primary tumors, as well as metastatic populations in the lymph node were marked on histological slides and served as guides for tissue removal. Selected cores were assembled as tissue microarrays (TMAs).

Immunostaining

Pan-cytokeratin immunostaining was performed in the lymph node sample in order to confirm metastatic cell infiltration. Briefly, FFPE blocks were cut into 3 µm thick fragments and mounted into silanized glass slides. Antigen retrieval was performed using a 0,01M Sodium Citrate solution at pH 6 on a steam heating at approximately 96°C for 20 minutes. For blockades, slides were incubated to a 3% hydrogen peroxide solution for 20 minutes at room temperature, followed by a second blockade using a 5% non-fat milk solution at room temperature for one hour. Primary mouse monoclonal antibody (Clone AE1/AE3, Agilent Dako, EUA) was used at 1:200 concentration (diluted in 1% BSA/PBS) at room temperature for 2 hours. Primary antibody was omitted as a negative control, and a canine primary mammary carcinoma used for positive control. Next, slides were incubated for 20 minutes with the polymer system EasyLink One (EasyLink One kit EP-12-20502, EasyPath), visualized with DAB (EP-12-20542, EasyPath) and counterstained with hematoxylin.

Matrix-assisted laser desorption ionization mass spectrometry imaging (MALDI-MSI) and peak picking

MALDI-MSI was carried in the Department of Proteomics and Metabolomics of Leiden University Medical Center – LUMC (Netherlands). Paraffin-embedded tissue microarrays were sectioned into 4 µm thick slices and placed on indium tin oxide (Bruker Daltonics, Bremen, Germany) coated glass slides pre-treated with 1:1 poly-L-lysine (Sigma Aldrich, St. Louis,

USA) and 0,1% Nonidet P-40 (Sigma Aldrich, St. Louis, USA). Sections were incubated on a heated plate for one hour at 60°C, dewaxed in xylene, rehydrated and washed with ultra-filtered water. Antigen retrieval was performed in heated citrate buffer using a steamer at 92°C for 20 minutes, followed by cooling at room temperature for 120 minutes. A specific trypsin solution for mass spectrometry (0.02µg/ml, Trypsin Gold, Promega Corporation, Wisconsin, USA) was sprayed using the SunCollect equipment (SunChrom, Friedrichsdorf, Germany) and slides were then incubated for 18h at 37°C and 95% of relative humidity. Matrix used for ion extraction (25 mg/mL of dihydroxybenzoic acid in 50% aqueous acetonitrile and 0.1% trifluoroacetic acid) was also applied using SunCollect. MALDI-FT-ICR data acquisition was performed in positive ion mode (Bruker Daltonics, Bremen, Germany), in a range of *m/z* 500-5000 Da and lateral resolution of 100 µm. RMS normalized average spectrum was exported to mMass 5.5.0, an open source mass spectrometry tool (STROHALM et al., 2008), and mass spectral processing and peak picking were conducted using skyline projection with the following settings: (i) baseline correction, relative offset 25; (ii) signal to noise ratio (S/N) = 7 and relative intensity threshold of 1%; and (iii) deisotoping with a max charge of 2+ and isotope mass tolerance of 0.02 m/z.

Liquid chromatrography/tandem mass spectrometry (LC-MS/MS)

For LC-MS/MS analysis, on-tissue tryptic digestion was performed as described in MALDI-MSI method section. Lyophilized peptides were dissolved in 95/3/0.1 v/v/v water/acetonitrile/formic acid and subsequently analyzed by on-line C18 nano HPLC MS/MS with a system consisting of an Easy-nLC 1200 gradient HPLC system (Thermo, Bremen, Germany), and an Orbitrap Fusion Lumos mass spectrometer (Thermo). Samples were injected onto a homemade precolumn (100 µm × 15 mm, C18 Reprosil-Pur C18-AQ, 3 um, 120 A, and eluted via a homemade analytical nano-HPLC column (50 cm × 75 µm; Reprosil-Pur C18-AQ 1.9 um, 120 A (Dr. Maisch, Ammerbuch, Germany). The gradient was run from 2% to 36% solvent B (20/80/0.1 water/acetonitrile/formic acid (FA) v/v/v) in 120 min. The nano-HPLC column was drawn to a tip of ~10 µm and acted as the electrospray needle of the MS source. The mass spectrometer was operated in data-dependent MS/MS mode for a cycle time of 3 seconds, with a HCD collision energy at 32 V and recording of the MS2 spectrum in the orbitrap, with a quadrupole isolation width of 1.2 Da. In the master scan (MS1) the resolution was 120,000, the scan range 400-1500, at an AGC target of 4,000,000 @maximum fill time of 50ms. Precursors were dynamically excluded after n=1 with an exclusion duration of 60s, and with a precursor range of 20 ppm. Charge states 2-4were included. For MS2 the first mass was

set to 110 Da, and the MS2 scan resolution was 30,000 at an AGC target of 40,000 @maximum fill time of 60ms. In a post-analysis process, raw data were first converted to peak lists using Proteome Discoverer version 2.2 (Thermo Electron), and then submitted to the Canis2019 database (24669 entries), using Mascot v. 2.2.04 (www.matrixscience.com) for protein identification. Mascot searches were done with 10 ppm and 0.02 Da deviation for precursor and fragment mass, respectively, and trypsin was specified as the enzyme. Methionine oxidation and the main formaldehyde reaction product on Lysine (+12.000) were set as a variable modification. Carbamidomethyl (C) was set as fixed modification. Peptides with an FDR<1% in combination with a mascot ion score >25 were accepted.

Statistical analysis

Unsupervised clustering and principal component analysis (PCA)

For the assessment of detailed molecular patterns across tissue samples, spectra from primary tumor and metastasis ROIs were imported into SCiLS Lab software (2016b, Bruker Daltonics, Bremen, Germany) and pre-processed by RMS normalization. In order to identify primary intratumor subclones, a multivariate partitioning algorithm was applied, where tumor spectra were clustered using bisecting *k-means* method and Euclidean distance metrics, with a minimum interval width of 10 ppm and weak denoising. Common spatial identities of molecular patterns in the sample were visualized by colored pixels accordingly to dendrogram nodes. Hierarchical clustering using Euclidean distance, row normalization and Ward's linkage method and principal component analysis with unit variance scaling were performed to determine the variability among primary intratumor clusters assessed by image segmentation, and metastasis regions of interest.

Discriminative m/z values

In order to identify significant differences regarding *m/z* values among tumor subclones, discriminative peaks were at first evaluated using Receiving Operator Curve method, with adjusted number of spectra per group, and later tested for statistical significance using multiple *t-tests* followed by Benjamini-Hochberg (BH) correction on GraphPad Prism 6.01 for Windows (GraphPad Software, La Jolla, California, USA, www.graphpad.com). Only *m/z* signals presenting AUC > 0.70 and Q-value < 1% were considered significant. For the assessment of differential peptide expression between intra-lymphatic and regional lymph node metastasis, *m/z* signals were tested using Wilcoxon Rank Sum Test followed by BH correction, and only *m/z* values with FDR < 0.01 were considered significant.

Pathway enrichment analysis

Enrichment analysis was performed through the overrepresentation test on PANTHER classification system (www.pantherdb.org), using the Reactome version 65 as annotation version and the human genome-coding database for a more comprehensive knowledgebase regarding protein function. Protein symbols were used as input lists and were analyzed by Fisher's exact test followed by FDR correction. Enriched pathways were considered significant if FDR < 0.05.

RESULTS

Tissue annotation and proteomics

Nine mammary tumors were surgically removed from the 12 years old unspayed female Dachshund with no previous history of either surgical or chemotherapy treatments. However, in this study, only the one tumor diagnosed as a complex carcinoma was used (Figure 1A and 1B). Metastatic cell groups were detected in a regional lymph node by histopathological examination and immunostaining, also included in the analysis (Figure 1C and 1D). In total, primary tumor and lymph node samples resulted in 37 viable cores used for histopathological annotation (Figure 1E). HE stained tissue scanned image was co-registered with MALDI-FT-ICR-MSI data, and cancer areas in primary tumor (n = 115) and synchronous metastasis inside lymphatic vessels (n = 3) and in regional lymph node (n = 3) were annotated and defined as regions of interest (ROIs). Spectra generated by imaging of tryptic peptides (n = 4,131) were exported from all 121 ROIs, where the participation of spectra of each group was as follows: primary tumor – 94%; metastasis inside lymphatics – 0.7%; metastasis in regional lymph node – 5.1%. Overall, after data processing and peak picking, 1,535 individual signals within the mass range of *m/z* 900 to 3500 could be resolved on examined tissue. Tryptic peptides were also extracted from a consecutive TMA section, analyzed by LC-MS/MS and compared to a canine database, from which 530 protein IDs could be retrieved. The comparison between 1,535 MSI *m/z* signals to LC/MS-MS data resulted in the identification of 108 peptides, assuming a mass tolerance of ±10 ppm. Several peptides were assigned to the same proteins, and therefore, 62 proteins could be identified in MSI dataset (complete list of proteins with respective *m/z* signals can be find in Supplementary Table S1).

Differential expression between intra-lymphatic metastatic cells and regional lymph node metastasis

Cancer cells spreading to regional lymph nodes has been established as an important prognostic factor in many types of cancer, whilst no treatment strategies specifically target lymph metastasis. Our first step was to verify significant molecular differences between intra-lymphatic metastatic cancer cells (ILM) and cancer populations in the regional lymph node (LNM). Considering data structure and large disparity of number of spectra across ILM and LNM groups (n = 27 and 212, respectively), 108 *m/z* signals were tested using Wilcoxon Rank

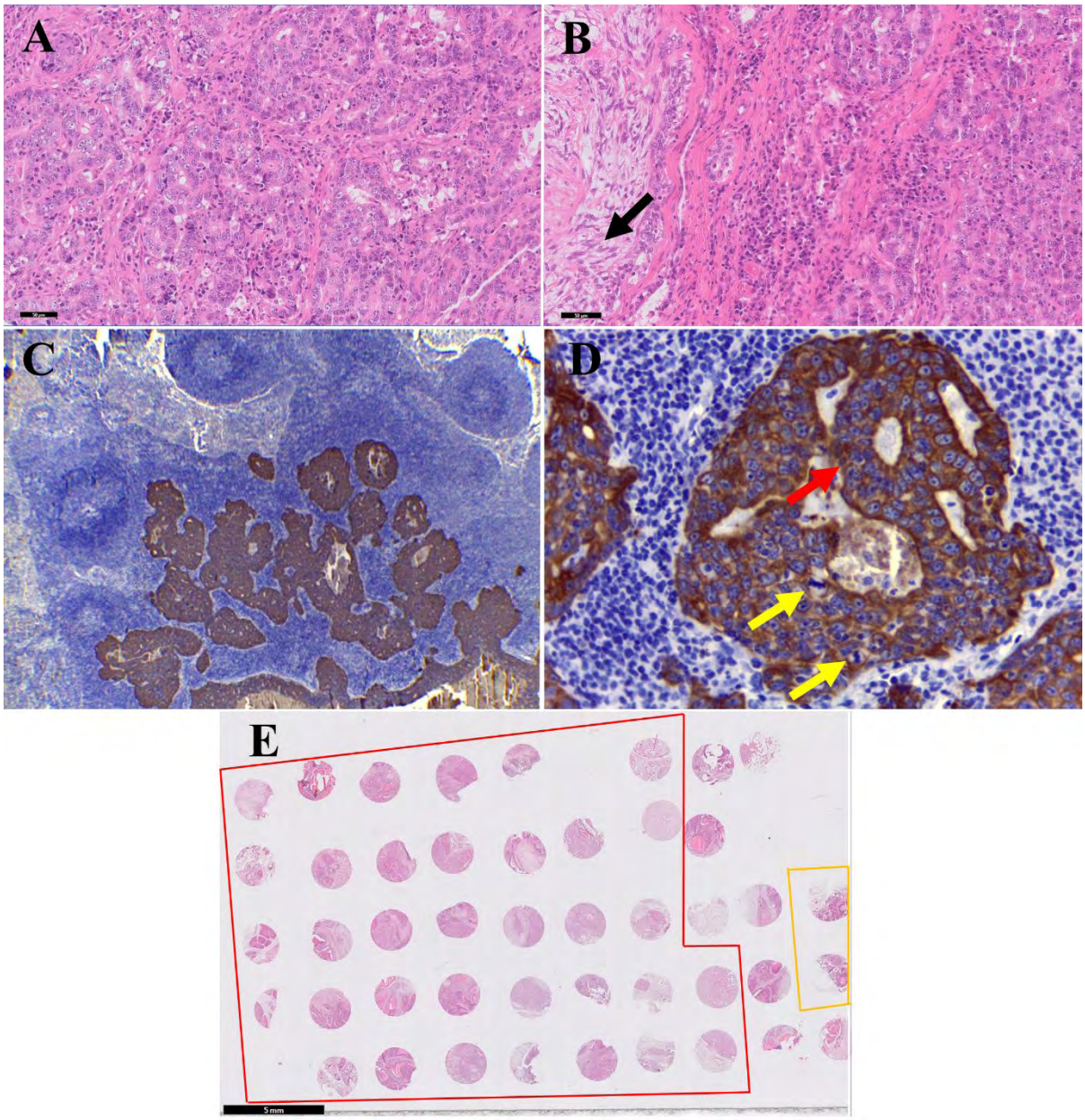

Figure 1 – Canine samples used in the study. (A, B) Mammary gland carcinoma, complex-type, showing areas of malignant epithelial proliferation and spindle-shaped myoepithelial cells (black arrow), supported by a fibrovascular stroma. Epithelial cells were arranged in irregular tubules, presenting moderate to marked anisokaryosis and anisocytosis, and variable number of mitoses were present. Scale: 50 µm (C, D) Pan-cytokeratin immunostaining of mammary cancer cells in the regional lymph node. Areas of tubule differentiation (red arrow) and mitotic figures (yellow arrows) could be evidenced. (E) Tissue microarray comprising 35 cores removed from primary tumor tissue (red line area) and two cores collected from the regional lymph node (yellow line area). Scale bar: 5 mm.

Sum method, a more robust method for unequal sample sizes (MANN; WHITNEY, 1947). We found 37 significant *m/z* signals differentially expressed between groups (FDR < 0.01), from which 31 proteins IDs could be retrieved. Clusterin (CLU, at *m/z* 1232.610 and *m/z* 1427.639), beta-casein (CSN2, at *m/z* 1585.775), LOC475521 (at *m/z* 1045.565), histone H2 (HIST1H2BB, at *m/z* 1751.059), ribosomal protein L8 (RPL8, at *m/z* 1749.091), glyceraldehyde-3-phospate dehydrogenase (GAPDH, at *m/z* 1697,895) and immunoglobulin heavy chain mu (IGHM, at *m/z* 1635.862) were found significantly upregulated in metastatic cells inside lymphatic vessels compared to regional lymph node cell populations (Figure 2).

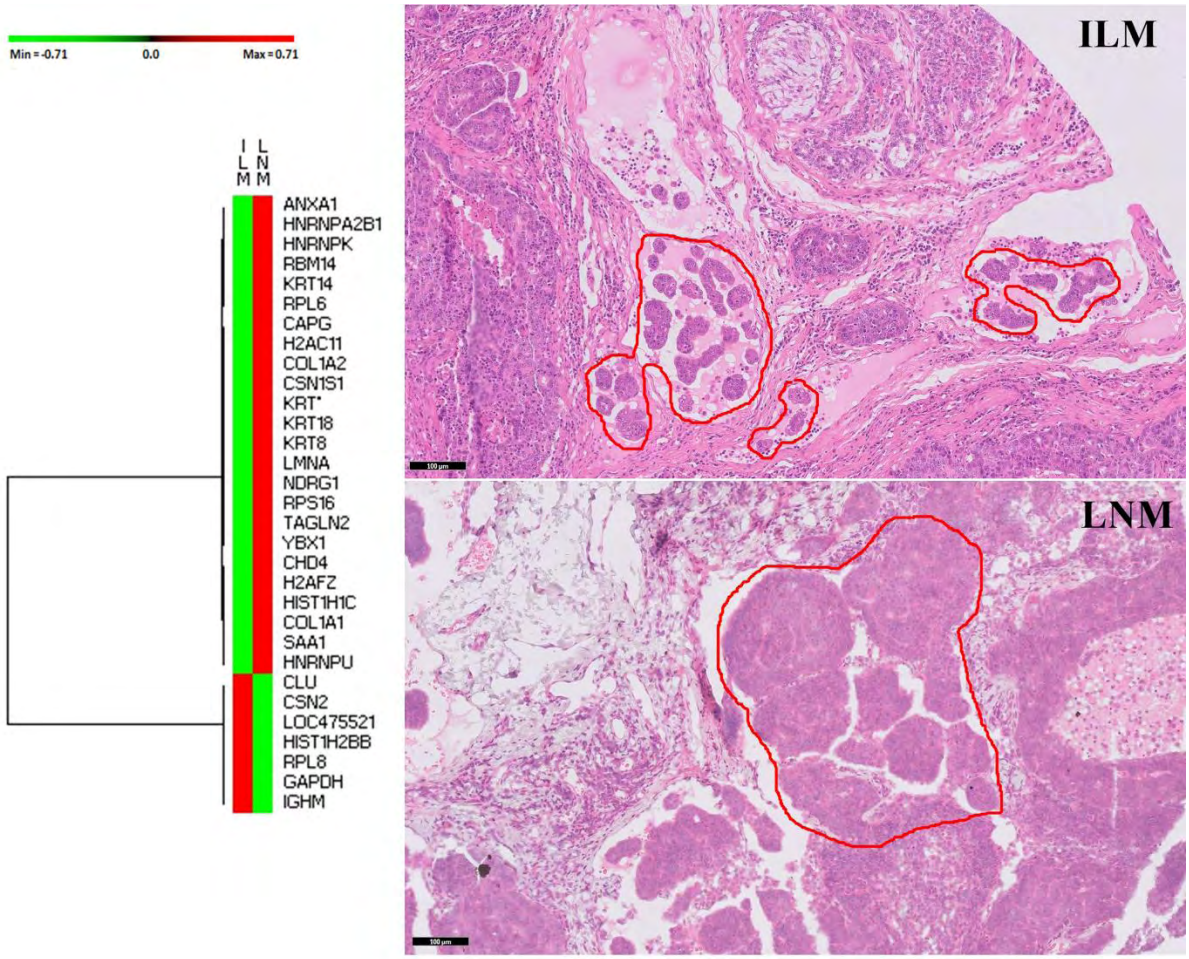

Figure 2 – Heatmap showing protein expression patterns between intra-lymphatic metastatic cells (ILM) and metastasis in the regional lymph node (LNM) after testing 108 *m/z* values for differential expression. CLU, CSN2, LOC475521, HIST1H2BB, RPL8, GAPDH and IGHM were found to be upregulated in ILM compared to LNM regions. *KRT represents unique peptides which were assigned to two different types of keratin, but were not excluded from the analysis.

Molecular clustering for the identification of primary intratumor subpopulations

Intratumor heterogeneity influences cancer progression and disease outcome, where the identification of tumor subclones with greater clinical relevance is fundamental for patient management. Thus, our next step was to assess molecular distinct tumor subclones regardless morphological phenotype, by means of a *top-down* unsupervised method that works without a pre-defined number of clusters. *M/z* values of the 108 peptides were used for image segmentation of primary tumor, and spectral features (n = 3,892), represented by a dendrogram, were colored allowing on-tissue identification of different clusters with distinct peptide expression patterns across the sample (Figure 3A). Morphologically similar clusters with a distinct peptide expression pattern could be identified (Figure 3B), demonstrating that malignant tumor behavior may be driven by microscopically indistinct subpopulations.

Discriminative m/z signals between intratumor subpopulations

For an in-depth characterization of intratumor subpopulations, a univariate biomarker analysis was used to evaluate the ability of *m/z* values to distinguish between clusters, in order to identify differences that could be relevant for tumor progression. Therefore, area under the curve was calculated for each one of the 108 peptides by comparisons between five major clusters - CL1, CL2, CL3, CL4 and CL5 – where *m/z* signals presenting AUC > 0.70 were later tested for statistical significance (Figure 4). A total of 68 peptides resulted from ten comparisons, (average of 26 ± 9.5 significant *m/z* value per comparison) with several *m/z* values distinguishing two or more clusters (Table 1). Interestingly, peptides identified by LC/MS-MS corresponding to alpha-casein s1 (CSN1S1, at *m/z* 1375.618) beta-casein (CSN2, at *m/z* 1585.776 and *m/z* 1002.573), and basal keratin 5 (KRT5, at *m/z* 1824.910) presented AUC ≥ 0.90 and FDR < 0.01 between CL5 and every other cluster, demonstrating that the combination of such signals have a strong accuracy to distinguish this specific subclone from all others (highlighted in Table 1).

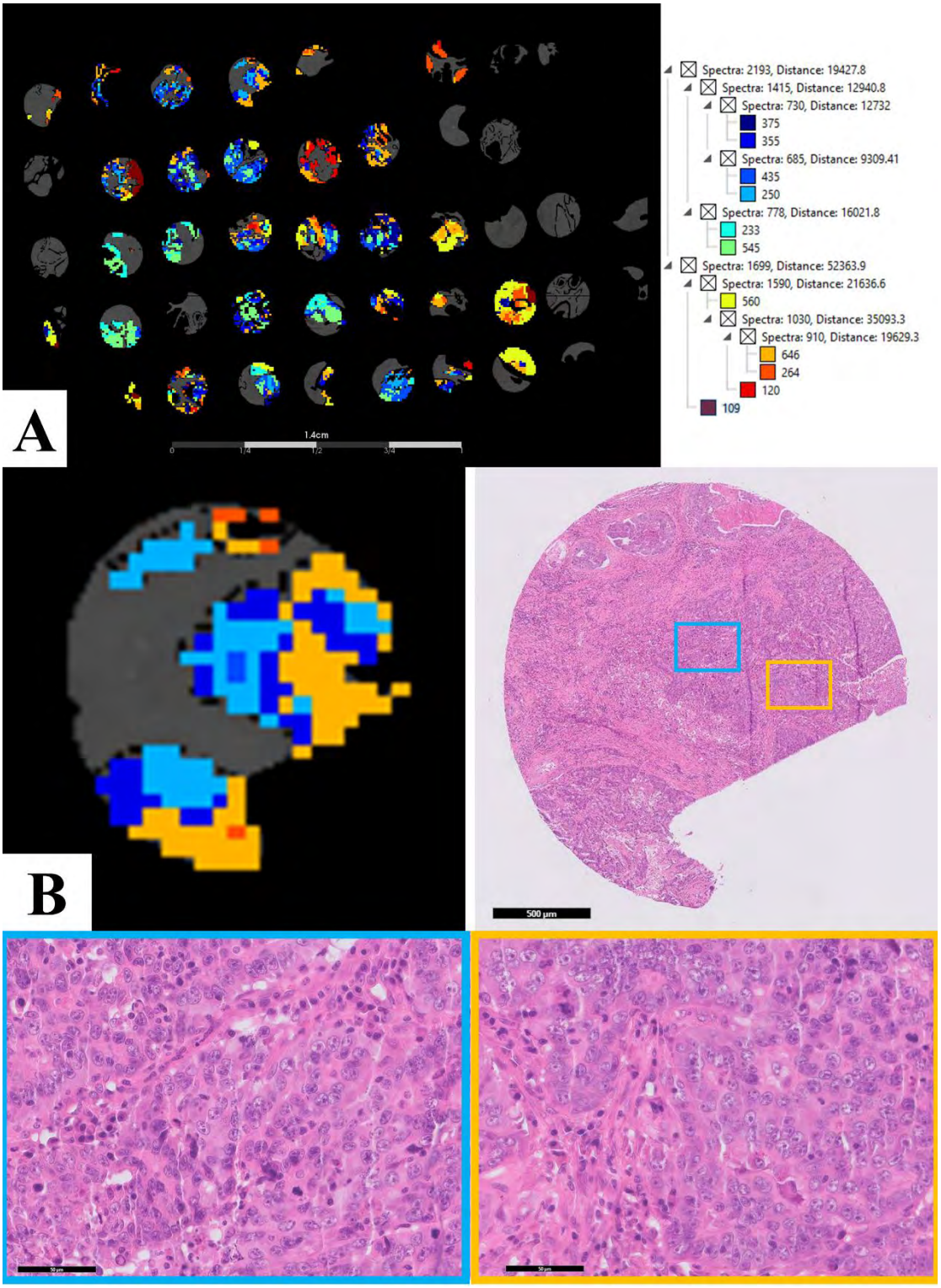

Figure 3 – Image segmentation of MSI dataset using *m/z* values from 108 peptides. (A) Unsupervised molecular clustering of primary tumor spectra using bisecting k-means method aiming to the identification of distinct subpopulations. Dendrogram shows spatial localization of each cluster. Numbers beside colored boxes represent the number of spectra per cluster. (B) Representation of microscopically identical primary tumor areas within the same tissue core in which two distinct clusters (light blue and gold) could be evidenced. Scale bar: 500 µm (upper right HE tissue core) and 50 µm (bottom).

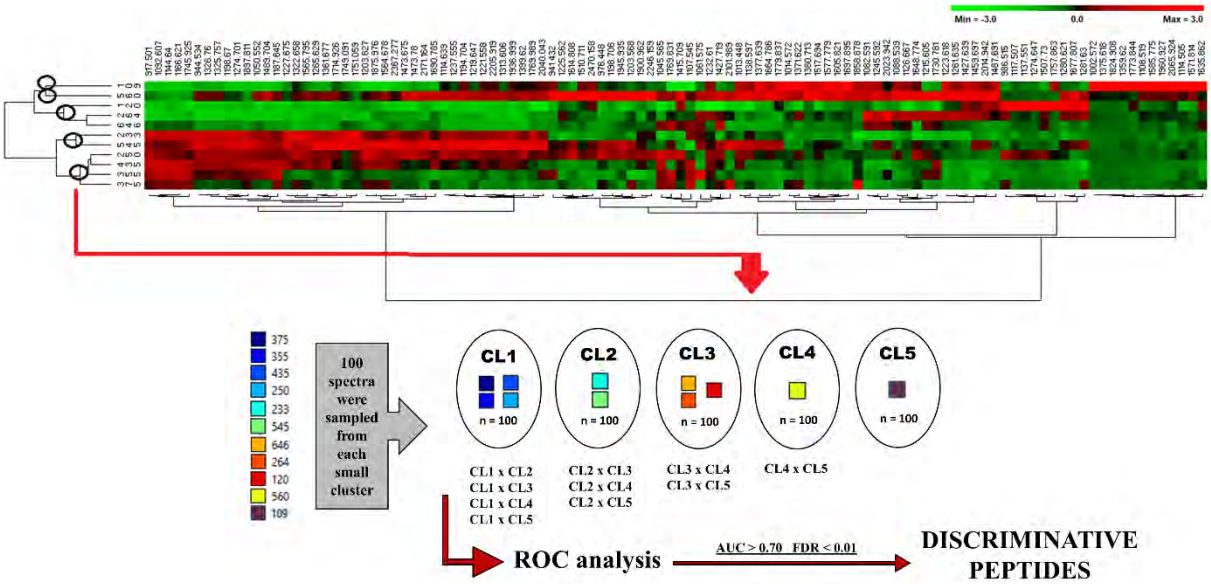

Figure 4 – Five major clusters (CL1, CL2, CL3, CL4 and CL5) were selected for discriminative analysis after molecular clustering of imaging dataset using 108 *m/z* values. First, groups were formed by picking 100 random spectra of each small cluster. Then, test sample size was adjusted to 100 spectra per group, also randomly assigned. Ten ROC analyzes were performed in order to identify the most relevant peptides/proteins which could be influencing in tumor progression: (i) CL1 *vs*. CL2; (ii) CL1 *vs*. CL3; (iii) CL1 *vs*. CL4; (iv) CL1 *vs*. CL5 (v) CL2 *vs*. CL3; (vi) CL2 *vs*. CL4; and (vii) CL2 *vs*. CL5; (viii) CL3 *vs*. CL4; (ix) CL3 *vs*. CL5; and (x) CL4 *vs*. CL5. *M/z* values presenting AUC > 0.70 were later tested for statistical significance, and those with FDR < 0.01 were considered as discriminative peptides.

Table 1 – AUC of discriminative peptides between clusters (FDR < 0.01).

Peptide *m/z*	Protein ID	CL1 vs. CL2	CL1 vs. CL3	CL1 vs. CL4	CL1 vs. CL5	CL2 vs. CL3	CL2 vs. CL4	CL2 vs. CL5	CL3 vs. CL4	CL3 vs. CL5	CL4 vs. CL5
976.4490	**ACTB**								0.72		
1198.7064	**ACTB**		0.72				0.72		0.81		0.76
1427.6390	**CLU**			0.75			0.71				
1223.6181	**COL1A2**						0.74				
1261.6359	**COL1A2**			0.72			0.72				
1114.5050	**COL4A3**				0.79			0.75		0.77	0.7
1359.6201	**CSN1S1**				0.86			0.87		0.88	0.80
1375.6181	**CSN1S1**			0.72	**0.96**			**0.92**		**0.95**	**0.90**
1773.8443	**CSN1S1**				0.84			0.85		0.82	0.82
2065.9241	**CSN1S1**				0.81			0.78		0.79	0.72
1002.5725	**CSN2**			0.82	**0.98**		0.73	**0.98**	0.71	**0.97**	**0.94**
1014.5720	**CSN2**				0.73			0.72		0.74	
1585.7756	**CSN2**			0.85	**0.99**		0.84	**0.99**	0.73	**0.97**	**0.90**
1564.6783	**DTD1**		0.74		0.77			0.72			0.71

1225.5624	**FLNA**			0.75							0.72
1697.8958	**GAPDH**			0.76	0.86		0.76	0.85	0.73	0.83	
1274.7013	**H2AC11**	0.74	**0.94**	0.80	**0.95**	0.82		0.86			
944.5340	**H2AFZ**	0.73	**0.94**	0.71	0.89	0.82		0.76	0.79		0.74
1325.7572	**H4C1**	0.79	**0.94**	0.74	**0.90**	0.77		0.73	0.77		0.73
1166.6212	**HIST1H1C**		0.79	0.82	**0.91**	0.80	0.83	**0.91**			
1198.6701	**HIST1H1C**		0.89	0.78	**0.93**	0.76		0.82			0.73
1326.7608	**HIST1H1C**	0.75	**0.91**	0.75	**0.90**	0.78		0.75	0.75		0.73
1092.6077	**HIST1H2BB**		0.76	0.74	0.82	0.79	0.77	0.84			
1137.5513	**HIST1H2BB**		0.71			0.71				0.74	
1751.0592	**HIST1H2BB**	0.77	**0.92**	0.86	**0.95**	0.71		0.75			
1227.6750	**HIST1H2BB**		0.84	0.70	0.77						
1221.5584	**HNRNPA2B1**	0.71	0.86		0.71	0.70			0.75		
1313.6062	**HNRNPA2B1**	0.72	**0.90**		0.77	0.76			0.77		
1377.6394	**HNRNPA2B1**		0.74								
1664.7863	**HNRNPA2B1**						0.72		0.73		
2205.9200	**HNRNPA2B1**	0.74	**0.90**		0.75	0.74			0.80		
1194.7048	**HNRNPK**		0.76								
1114.6393	**HNRNPM**		0.76					**0.91**	0.75		
1459.6979	**HNRNPM**						0.76				
1714.9268	**HNRNPU**	0.80	**0.91**	0.72	0.80	0.72			0.76		
2171.1641	**HNRNPU**	0.71	0.81		0.83				0.75		0.76
917.5012	**HSPB1**		0.82	0.73	0.85	0.80		0.83			
1960.9278	**IGHM**							0.75		0.72	
1415.7094	**IGLL5**							0.72		0.75	0.77
1050.5524	**KRT***				0.71						
1203.6275	**KRT***		0.87	0.76	**0.95**	0.73		0.84			0.76
1361.6779	**KRT***		0.80		0.73	0.75			0.74		
1265.6293	**KRT1**	0.75	**0.91**	0.75	0.88	0.72					
2367.2775	**KRT10**	0.71	0.79		0.85			0.73			0.71
1936.9996	**KRT18**		0.87		0.75	0.73			0.70		
1380.7139	**KRT5**			0.77			0.83		0.77		
1824.9089	**KRT5**			0.77	**0.99**		0.73	**0.99**	0.73	**0.98**	**0.92**
1126.6675	**KRT7**								0.70		
1473.7804	**KRT8**		0.71								
1489.7047	**KRT8**		0.74		0.77	0.71		0.74			
1473.6759	**LASP1**			0.77			0.79				
1507.7304	**LMNA**									0.78	
1108.5195	**LOC491263**			0.85	**0.99**		0.79	**0.99**	0.70	**0.95**	0.88
1745.9258	**LRRFIP1**				0.73						
1571.8141	**MAP4**				0.72			0.74		0.74	
1322.6586	**NDRG1**		0.73								
1757.8635	**PRRC2A**				0.73	0.72		0.74			
1237.5552	**RBM14**	0.70	0.82		0.74						
1144.6405	**RPL6**		0.85	0.85	**0.92**	0.84	0.84				
1769.9900	**RPL6**		0.78								
1749.0916	**RPL8**	0.70	0.72		0.73						
1187.6457	**RPS16**		0.74		0.72	0.72		0.71			

1219.6474	**RPS8**		0.76		0.70						
1117.5070	**SAA1**		0.72								
1274.6473	**SAA1**								0.74	0.74	0.75
1399.6201	**TAGLN2**	0.71	0.85		0.74						
1510.7110	**VIM**			0.75			0.79		0.75		0.74
1897.8114	**YBX1**		**0.91**	0.88	**0.94**	0.81	0.76	0.85			

* KRT: unique peptides which were assigned to two different types of keratin, but were not excluded from the analysis.

Protein identification and pathway enrichment analysis

Our next step was to verify whether discriminative peptides between clusters could be related to proteins involved in cancer development and progression pathways, where the identification of specific alterations could lead to the determination of clusters in different levels of malignancy and/or disease-state markers. Thus, protein IDs were retrieved for the 68 *m/z* values resulting from discriminative analysis, and the expression pattern of the 44 resulting proteins are demonstrated in Figure 5. For those proteins which presented two or more peptides, mean expression was used for a better visual representation. Protein IDs served as input for gene ontology, and significantly enriched for terms involved in molecular binding, regulation, cellular organization, metabolic processes and others (Figure 5). Next, the same protein ID input list was used for pathway enrichment analysis using the REACTOME database on PANTHER overrepresentation test, where 32 pathways presenting a fold enrichment higher than 20 were found to be significant (Table 2).

Molecular clustering for the identification of primary intratumor subpopulations with a similar ILM and LNM molecular signature

Finally, we aimed to identify, among primary tumor clusters, in which peptide expression pattern resembled ILM and LNM regions, in order to characterize a molecular signature that could be further explored and validated as predictive of metastasis. Thus, hierarchical clustering and principal component analysis were performed using the average *m/z* intensity of the 68 peptides resulting from previous discriminative analysis. Both analyzes showed ILM and LNM regions closely related to different tumor subpopulations, respectively CL3 and CL1, as demonstrated in Figure 6.

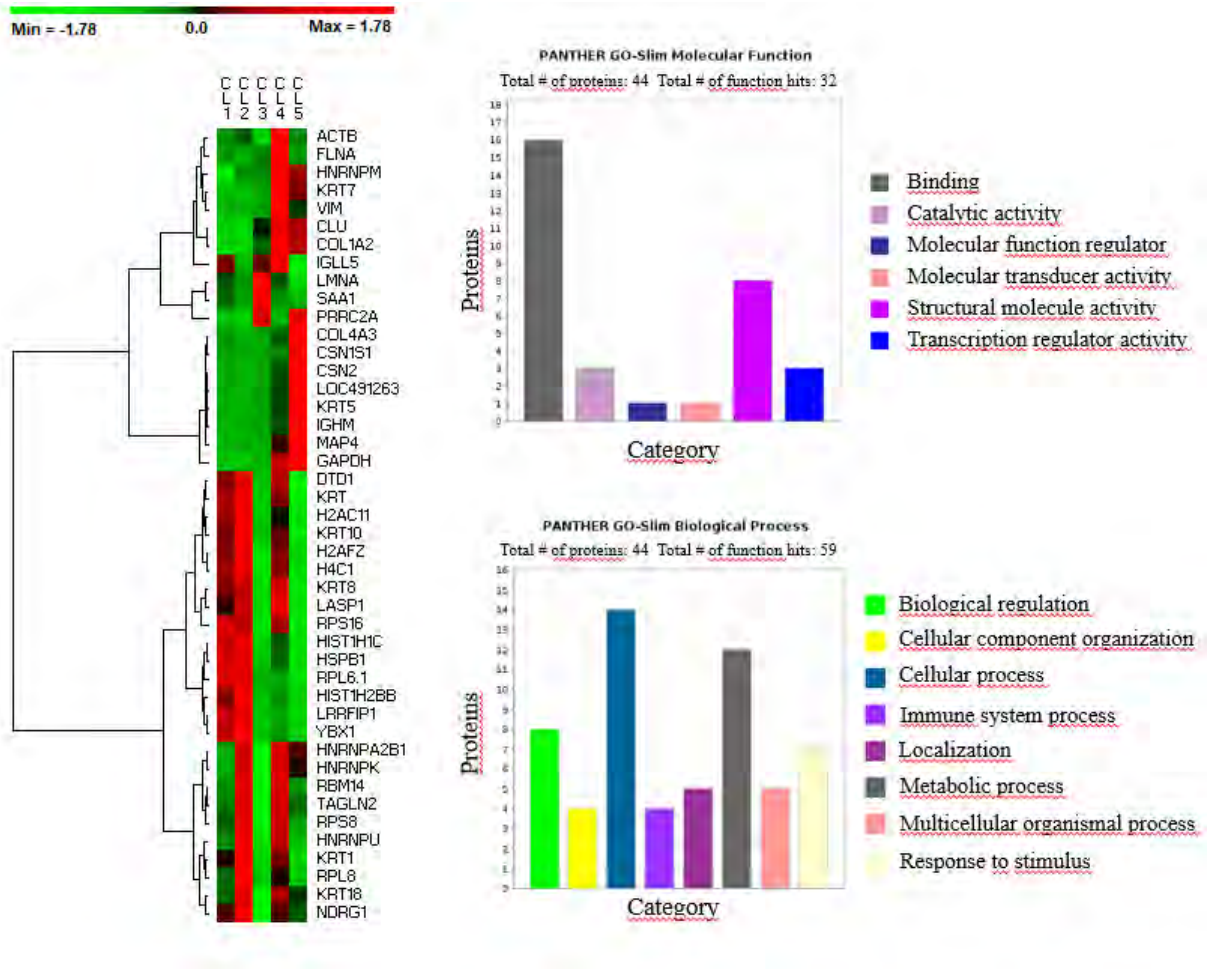

Figure 5 – Protein expression pattern of 44 proteins in five major tumor clusters selected after unsupervised image segmentation. Proteins such as collagen IV (COL4A3), caseins (CSN1S1, CSN2), basal keratin 5 (KRT 5), immunoglobulin heavy chain mu (IGHM) and microtubule-associated protein (MAP4) were upregulated in CL5 compared to other clusters. A list comprised by the 44 protein IDs were used for gene ontology regarding their molecular function and related biological processes, in which binding and structural molecule activity, as well as cellular and metabolic processes were the functions with a higher number of hits.

Table 2 – Pathway enrichment analysis using a human protein-coding reference database for a better comprehension of protein functions. Significant pathways are sorted by fold enrichment value.

Pathways (reference number)	Reference List (20996)	Input List* (42)	Expected**	Fold Enrichment	FDR
GP1b-IX-V activation signalling (R-HSA-430116)	11	2	0.02	90.89	2.19E-02
Anchoring fibril formation (R-HSA-2214320)	15	2	0.03	66.65	3.25E-02
Cell-extracellular matrix interactions (R-HSA-446353)	18	2	0.04	55.54	4.28E-02
Crosslinking of collagen fibrils (R-HSA-2243919)	18	2	0.04	55.54	4.17E-02

B-WICH complex positively regulates rRNA expression (R-HSA-5250924)	59	3	0.12	25.42	2.02E-02
DNA Damage/Telomere Stress Induced Senescence (R-HSA-2559586)	61	3	0.12	24.59	2.14E-02
Formation of the cornified envelope (R-HSA-6809371)	129	6	0.26	23.25	2.97E-04
Viral mRNA Translation (R-HSA-192823)	89	4	0.18	22.47	1.10E-02
Peptide chain elongation (R-HSA-156902)	89	4	0.18	22.47	9.65E-03
Selenocysteine synthesis (R-HSA-2408557)	93	4	0.19	21.5	9.10E-03
Eukaryotic Translation Termination (R-HSA-72764)	93	4	0.19	21.5	8.28E-03
Amyloid fiber formation (R-HSA-977225)	70	3	0.14	21.42	2.86E-02
Eukaryotic Translation Elongation (R-HSA-156842)	94	4	0.19	21.27	7.90E-03
Nonsense Mediated Decay (NMD) independent of the Exon Junction Complex (EJC) (R-HSA-975956)	95	4	0.19	21.05	7.59E-03
Positive epigenetic regulation of rRNA expression (R-HSA-5250913)	74	3	0.15	20.27	3.24E-02

* Total number of proteins on input list: 44; uniquely mapped IDs: 42; multiple mapping information: 2
** Expected value corresponds to the number of proteins you would expect on the input list for each category, based on the reference list

DISCUSSION

One of the major clinical challenges in cancer treatment is the different outcome of cancer patients under conventional therapies. An important determinant for this phenomenon has been identified as intratumor heterogeneity (ITH), defined as the coexistence of tumor subpopulations that differ in their (epi)genetic, phenotypic or behavioral characteristics within a primary tumor, or between the primary tumor and its metastasis (MARUSYK; POLYAK, 2010). In human breast cancer, evidences show that cancer cells subclones may exist across different geographical regions of a tumor, and may evolve over time (GEYER et al., 2010; NAVIN et al., 2010). Therefore, investigation of ITH requires an untargeted molecular analysis technique that accounts for the spatial and temporal dynamics of the tumor. In this context, mass spectrometry imaging comes as a powerful tool for spatially resolved molecular analysis of biological tissues. In this pilot study, we described for the first time the application of MSI in canine mammary carcinomas for the assessment of intratumor heterogeneity, which can be used for veterinary and comparative oncology studies. Using 121 different intratumor populations and synchronous metastatic regions from the same patient, which nearly eliminates genetic and experimental biases, we demonstrated molecular alterations that may indicate areas

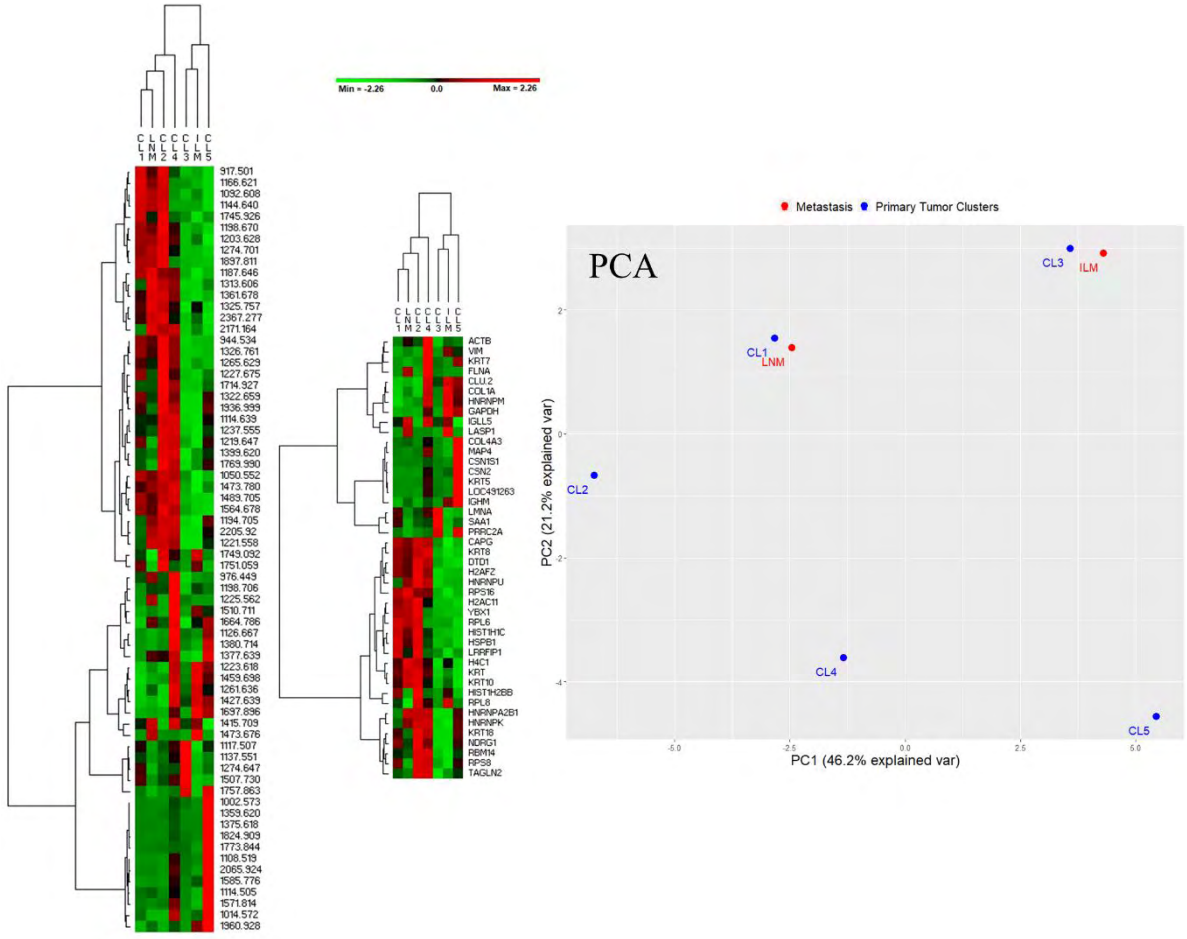

Figure 6 – Heatmap in both peptide (left, represented by *m/z* values) and protein levels (right, represented by protein symbols), and principal component analysis showing the proximity of ILM and LNM regions with clusters CL3 and CL1, respectively. PCA was performed in protein level, and for proteins with two or more assigned peptides, mean expression was used.

in different stages of tumor progression and can be further explored for new predictive and therapeutic targets.

The first scientific description of MALDI-MSI to evaluate intratumoral heterogeneity have demonstrated that regions within the same tumor could be grouped and related to one another by spectrum similarity, through unsupervised methods such as the hierarchical clustering approach (DEININGER et al., 2008). Since then, positive associations between clinical prognosis, malignancy characteristics, and ITH analyzed by the MALDI-MSI technique have been reported in gastric, mammary, intestinal, prostatic, and renal tumors, in which statistical strategies were efficient to separate samples with similar molecular profiles, revealing different tumor subpopulations (BALLUFF et al., 2015; BUCK et al., 2015; PANDERI et al., 2017). For example, among three ovarian tumors primarily classified as noninvasive, post-MSI

reclassification have shown that these tumors in fact presented features associated with the development of malignant progression (SANS et al., 2017). In another study using formalin-fixed specimens, MALDI-MSI evaluation associated to principal component analysis was able to distinguish prostate neoplasms from healthy tissues more efficiently than the conventional histopathological method (PANDERI et al., 2017).

Approximately 90% of cancer related deaths occur due to metastatic dissemination (MEHLEN; PUISIEUX, 2006). In breast cancer, lymph metastasis is the earliest sign of metastatic spread and the one of the most powerful independent prognostic factors, where the detection of vascular invasion has a close relationship with recurrence and overall survival (PINDER et al., 1994; WEIGELT; PETERSE; VAN'T VEER, 2005). However, metastasis is considered to be an inefficient process, with only a small percentage of the cells within the primary tumor having the potential to colonize and survive in a secondary site (CHAMBERS; GROOM; MACDONALD, 2002). In addition, evidences show that metastatic cells in secondary sites present a distinct molecular spectrum from those in the primary tumor cells, which could be addressed mainly to the fact that disseminated cells undergo rounds of mutation and selection, and also to the fact that current studies simply missed the area in the primary tumor from which cancer cells had disseminated (KLEIN, 2009; STOECKLEIN; KLEIN, 2010). Here, we were able to access not only differences between metastatic emboli within vessels (ILM) and a secondary site (LNM), but also differences in tumor subclones that may lead to a more accurate indication of the population that originated these metastases.

Among differentially expressed proteins between ILM and LNM regions, ILM upregulated clusterin, GAPDH and CSN2, stand out for their reported association with cells exhibiting a higher metastatic potential (LAU et al., 2006; FLANAGAN et al., 2010; ZHOU et al., 2017; SIROVER, 2018; ZHU et al., 2018). For example, GAPHD function has always been consistently regarded as the main housekeeping gene/protein for expression quantification in tumors, but experimental evidences have been shown that up and downregulation of GAPDH in several types of cancer may have a strong influence in cancer cell growth and tumor formation (SIROVER, 2018). GAPDH over-expression was found to be correlated with cell motility and metastatic potential in rat prostatic adenocarcinoma (EPNER et al., 1993), and may functionalize in tumor metastasis through the interaction of dimerized GAPDH with the putative metastasis supressor Nm23-H1 (ENGEL et al., 1998). Still, although a few mechanisms and pathways involved in GAPDH regulations and its different roles in cancer cells have been already described (GUO; LIU; SUN, 2013; ZHANG et al., 2015), the possible relevance of its activity in metastasis needs to be further investigated. In addition, in this pilot

study, IGHM was also found upregulated in ILM compared to LNM annotated regions. Although IGHM encodes an immunoglobulin heavy chain rather than any specific cancer cell protein, a few studies have already observed a deregulation in IGHM mRNA and protein levels in breast and liver cancer (QIN et al., 2013; HSU et al., 2019). IGHM was also found as part of a dispositive developed for the detection, determination and/or prediction of esophageal lymph node metastasis (patent number US20090270267A1).

In summary, using bottom-up proteomics associated to mass spectrometry imaging, we were able to identify different tumor subpopulations within a unique solid tumor mass, as well as access differentially expressed proteins between metastatic populations at different stages of dissemination. It is evident that the method, as well as the results obtained in here still need to be deeply explored through novel experiments and data analysis, besides to be validated in a larger number of samples. However, even at an early stage, this study demonstrates the importance of investigating intratumoral heterogeneity for a better understanding of canine mammary carcinoma development and behavior, directing future investigations that can be used for comparative and translational oncology research.

REFERENCES

AXELROD, R.; AXELROD, D. E.; PIENTA, K. J. Evolution of cooperation among tumor cells. **Proceedings of the National Academy of Sciences**, v. 103, n. 36, p. 13474 LP – 13479, 5 set. 2006. Disponível em: <http://www.pnas.org/content/103/36/13474.abstract>.

BALLUFF, B. et al. De novo discovery of phenotypic intratumour heterogeneity using imaging mass spectrometry. **Journal of Pathology**, v. 235, n. 1, p. 3–13, 2015.

BALLUFF, B.; HANSELMANN, M.; HEEREN, R. M. A. **Mass Spectrometry Imaging for the Investigation of Intratumor Heterogeneity**. 1. ed. [s.l.] Elsevier Inc., 2017. v. 134

BUCK, A. et al. High-resolution MALDI-FT-ICR MS imaging for the analysis of metabolites from formalin-fixed, paraffin-embedded clinical tissue samples. **Journal of Pathology**, v. 237, n. 1, p. 123–132, 2015.

CALBO, J. et al. A Functional Role for Tumor Cell Heterogeneity in a Mouse Model of Small Cell Lung Cancer. **Cancer Cell**, v. 19, n. 2, p. 244–256, 2011. Disponível em: <http://www.sciencedirect.com/science/article/pii/S1535610810005301>.

CHAMBERS, A. F.; GROOM, A. C.; MACDONALD, I. C. Dissemination and growth of cancer cells in metastatic sites. **Nature Reviews Cancer**, v. 2, n. 8, p. 563–572, 2002.

D'HUE, C. A. et al. Fatty Acid Patterns Detected By Ambient Ionization Mass Spectrometry in Canine Invasive Urothelial Carcinoma From Dogs of Different Breeds. **Bladder cancer (Amsterdam, Netherlands)**, v. 4, n. 3, p. 283–291, 30 jul. 2018. Disponível em: <https://www.ncbi.nlm.nih.gov/pubmed/30112439>.

DA COSTA, A. et al. Multiple RT-PCR markers for the detection of circulating tumour cells of metastatic canine mammary tumours. **The Veterinary Journal**, v. 196, n. 1, p. 34–39, 2013. Disponível em:

<http://www.sciencedirect.com/science/article/pii/S109002331200370X>.

DEININGER, S.-O. et al. MALDI Imaging Combined with Hierarchical Clustering as a New Tool for the Interpretation of Complex Human Cancers. **Journal of Proteome Research**, v. 7, n. 12, p. 5230–5236, 5 dez. 2008. Disponível em: <http://dx.doi.org/10.1021/pr8005777>.

DILL, A. L. et al. Lipid Profiles of Canine Invasive Transitional Cell Carcinoma of the Urinary Bladder and Adjacent Normal Tissue by Desorption Electrospray Ionization Imaging Mass Spectrometry. **Analytical chemistry**, v. 81, n. 21, p. 8758–8764, 2009. Disponível em: <http://europepmc.org/abstract/MED/19810710>.

ENGEL, M. et al. Glyceraldehyde-3-phosphate Dehydrogenase and Nm23-H1/Nucleoside Diphosphate Kinase A: two old enzymes combine for the novel nm23 protein phosphotransferase function . **Journal of Biological Chemistry** , v. 273, n. 32, p. 20058–20065, 7 ago. 1998. Disponível em: <http://www.jbc.org/content/273/32/20058.abstract>.

EPNER, D. E. et al. Association of Glyceraldehyde-3-Phosphate Dehydrogenase Expression with Cell Motility and Metastatic Potential of Rat Prostatic Adenocarcinoma. **Cancer research**, v. 53, n. 9, p. 1995–1997, maio 1993.

FLANAGAN, L. et al. Effects of clusterin over-expression on metastatic progression and therapy in breast cancer. **BMC Cancer**, v. 10, n. 1, p. 107, 2010. Disponível em: <https://doi.org/10.1186/1471-2407-10-107>.

FOWLES, J. S. et al. The Flint Animal Cancer Center (FACC) Canine Tumour Cell Line Panel: a resource for veterinary drug discovery, comparative oncology and translational medicine. **Veterinary and Comparative Oncology**, v. 15, n. 2, p. 481–492, 1 jun. 2017. Disponível em: <https://doi.org/10.1111/vco.12192>.

FRANTZ, A. M. et al. Molecular Profiling Reveals Prognostically Significant Subtypes of Canine Lymphoma. **Veterinary Pathology**, v. 50, n. 4, p. 693–703, 2 nov. 2012. Disponível em: <https://doi.org/10.1177/0300985812465325>.

GEYER, F. C. et al. Molecular analysis reveals a genetic basis for the phenotypic diversity of metaplastic breast carcinomas. **The Journal of Pathology**, v. 220, n. 5, p. 562–573, 1 abr. 2010. Disponível em: <https://doi.org/10.1002/path.2675>.

GOLDSCHMIDT, M. et al. Classification and grading of canine mammary tumors. **Veterinary pathology**, v. 48, n. 1, p. 117–31, jan. 2011. Disponível em: <http://www.ncbi.nlm.nih.gov/pubmed/21266722>. Acesso em: 4 dez. 2014.

GUO, C.; LIU, S.; SUN, M. Z. Novel insight into the role of GAPDH playing in tumor**. Clinical and Translational Oncology**, 2013. .

HAHN, K. A. et al. Masitinib is Safe and Effective for the Treatment of Canine Mast Cell Tumors. **Journal of Veterinary Internal Medicine**, v. 22, n. 6, p. 1301–1309, 1 nov. 2008. Disponível em: <https://doi.org/10.1111/j.1939-1676.2008.0190.x>.

HSU, H.-M. et al. Six novel immunoglobulin genes as biomarkers for better prognosis in triple-negative breast cancer by gene co-expression network analysis. **Scientific Reports**, v. 9, n. 1, p. 4484, 2019. Disponível em: <https://doi.org/10.1038/s41598-019-40826-w>.

JARMUSCH, A. K. et al. Characteristic lipid profiles of canine non-Hodgkin's lymphoma from surgical biopsy tissue sections and fine needle aspirate smears by desorption electrospray ionization-mass spectrometry. **Analyst**, v. 140, n. 18, p. 6321–6329, 2015.

KLEIN, C. A. Parallel progression of primary tumours and metastases. **Nature Reviews Cancer**, v. 9, n. 4, p. 302–312, 2009. Disponível em: <https://doi.org/10.1038/nrc2627>.

LARUE, S. M. et al. Impact of Heterogeneity in the Predictive Value of Kinetic Parameters in Canine Osteosarcoma. **Cancer Research**, v. 54, n. 14, p. 3916 LP – 3921, 15 jul. 1994. Disponível em: <http://cancerres.aacrjournals.org/content/54/14/3916.abstract>.

LAU, S. H. et al. Clusterin plays an important role in hepatocellular carcinoma metastasis. **Oncogene**, v. 25, n. 8, p. 1242–1250, 2006. Disponível em: <https://doi.org/10.1038/sj.onc.1209141>.

MANN, H. B.; WHITNEY, D. R. On a Test of Whether one of Two Random Variables is Stochastically Larger than the Other. **The Annals of Mathematical Statistics**, v. 18, n. 1, p. 50–60, 1947.

MARUSYK, A.; POLYAK, K. Tumor heterogeneity: Causes and consequences. **Biochimica et Biophysica Acta (BBA) - Reviews on Cancer**, v. 1805, n. 1, p. 105–117, 2010. Disponível em: <http://www.sciencedirect.com/science/article/pii/S0304419X09000742>.

MEHLEN, P.; PUISIEUX, A. Metastasis: A question of life or death. **Nature Reviews Cancer**, v. 6, n. 6, p. 449–458, 2006.

NAVIN, N. et al. Inferring tumor progression from genomic heterogeneity. **Genome Research** , v. 20, n. 1, p. 68–80, 1 jan. 2010. Disponível em: <http://genome.cshlp.org/content/20/1/68.abstract>.

NEELAKANTAN, D.; DRASIN, D. J.; FORD, H. L. Intratumoral heterogeneity: Clonal cooperation in epithelial-to-mesenchymal transition and metastasis. **Cell Adhesion and Migration**, v. 9, n. 4, p. 265–276, 2015.

PANDERI, I. et al. Differentiating tumor heterogeneity in formalin-fixed paraffin-embedded (FFPE) prostate adenocarcinoma tissues using principal component analysis of matrix-assisted laser desorption/ionization imaging mass spectral data. **Rapid Communications in Mass Spectrometry**, v. 31, n. 2, p. 160–170, 30 jan. 2017. Disponível em: <https://doi.org/10.1002/rcm.7776>.

PINDER, S. E. et al. Pathological prognostic factors in breast cancer. III. Vascular invasion: relationship with recurrence and survival in a large study with long-term follow-up. **Histopathology**, v. 24, n. 1, p. 41–47, 1 jan. 1994. Disponível em: <https://doi.org/10.1111/j.1365-2559.1994.tb01269.x>.

QIN, X. et al. High-throughput screening of tumor metastatic-related differential glycoprotein in hepatocellular carcinoma by iTRAQ combines lectin-related techniques. **Medical Oncology**, v. 30, n. 1, p. 420, 2013. Disponível em: <https://doi.org/10.1007/s12032-012-0420-8>.

REGAN, D. et al. Cancer immunotherapy in veterinary medicine: Current options and new developments. **The Veterinary Journal**, v. 207, p. 20–28, 2016. Disponível em: <http://www.sciencedirect.com/science/article/pii/S1090023315004050>.

SANS, M. et al. Metabolic markers and statistical prediction of serous ovarian cancer aggressiveness by ambient ionization mass spectrometry imaging. **Cancer Research**, v. 77, n. 11, p. 2903–2913, 2017.

SIROVER, M. A. Pleiotropic effects of moonlighting glyceraldehyde-3-phosphate dehydrogenase (GAPDH) in cancer progression, invasiveness, and metastases. **Cancer and Metastasis Reviews**, v. 37, n. 4, p. 665–676, 2018. Disponível em: <https://doi.org/10.1007/s10555-018-9764-7>.

STOECKLEIN, N. H.; KLEIN, C. A. Genetic disparity between primary tumours, disseminated tumour cells, and manifest metastasis. **International Journal of Cancer**, v.

126, n. 3, p. 589–598, 2010.

STROHALM, M. et al. mMass data miner: an open source alternative for mass spectrometric data analysis. **Rapid Communications in Mass Spectrometry**, v. 22, n. 6, p. 905–908, 30 mar. 2008. Disponível em: <https://doi.org/10.1002/rcm.3444>.

TSUJI, T. et al. Epithelial-Mesenchymal Transition Induced by Growth Suppressor p12^{CDK2-AP1} Promotes Tumor Cell Local Invasion but Suppresses Distant Colony Growth. **Cancer Research**, v. 68, n. 24, p. 10377 LP – 10386, 15 dez. 2008. Disponível em: <http://cancerres.aacrjournals.org/content/68/24/10377.abstract>.

WEIGELT, B.; PETERSE, J. L.; VAN'T VEER, L. J. Breast cancer metastasis: markers and models. **Nature Reviews Cancer**, v. 5, n. 8, p. 591–602, 2005. Disponível em: <https://doi.org/10.1038/nrc1670>.

ZHANG, J. et al. Critical protein GAPDH and its regulatory mechanisms in cancer cells. p. 10–22, 2015.

ZHOU, W. et al. RMP promotes epithelial-mesenchymal transition through NF-κB/CSN2/Snail pathway in hepatocellular carcinoma. **Oncotarget**, v. 8, n. 25, p. 40373–40388, 2017.

ZHU, B. et al. Prognostic Significance of CSN2, CD8, and MMR Status-Associated Nomograms in Patients with Colorectal Cancer. **Translational Oncology**, v. 11, n. 5, p. 1202–1212, 2018. Disponível em: <http://www.sciencedirect.com/science/article/pii/S1936523318301074>.

CONCLUSÃO

Através de análises *in vitro* e *in situ*, exploramos a heterogeneidade tumoral das neoplasias mamárias em cadelas através da caracterização morfológica e molecular de linhagens celulares primárias e populações tumorais em tecidos parafinados. Demonstramos que células com maior expressão de genes como ITGA8, THBS2 e FN1 apresentam maior agressividade tumoral e potencial metastático. Também, observamos que populações pouco diferenciadas e, portanto, mais malignas, podem ter surgido como consequência de alterações no processamento de proteínas devido ao estresse do retículo endoplasmático liso, causados pela diminuição na expressão de proteínas como TPM1, TUBB4B, CANX, HSPA5, PDIA3 e APOA1. Ainda, utilizando uma abordagem não-direcionada por espectrometria de massas por imagem, identificamos peptídeos diferencialmente expressos entre grupos de células metastáticas em diferentes estágios de disseminação, além de correlacionar este perfil de expressão à subpopulações intratumorais que não seriam distinguíveis apenas por métodos histopatológicos convencionais.

Desta forma, ao longo dos três capítulos desta tese de doutorado, identificamos e apresentamos moléculas que podem e devem ser futuramente validadas como potenciais marcadores diagnósticos, prognósticos e preditivos em carcinomas mamários em cadelas. Também, reforçamos a importância destas neoplasias como modelos para novas pesquisas em oncologia comparada e translacional.

APÊNDICE A – MATERIAL SUPLEMENTAR CAPÍTULO 1

Table S1: alignment rates of M5 and M25 cells.

Sample	Sequenced PE reads	Aligned pairs	% alignment	Multiple alignments	Multiple alignments (%)	Discordant alignments	Discordant alignments (%)	Concordant alignments (%)
M5.1	17605245	14794559	86,4	840021	5,7	374060	2,5	81,9
M5.2	15865311	13313857	86,3	831164	6,2	306422	2,3	82,0
M5.3	15586596	12459555	82,4	914089	7,3	273252	2,2	78,2
M25.1	16791374	14088582	86,3	873563	6,2	315023	2,2	82,0
M25.2	17000811	14135480	85,2	834349	5,9	247752	1,8	81,7
M25.3	14351658	11984821	86,0	743413	6,2	365970	3,1	81,0

Table S2: differentially expressed genes between M5 and M25 cell cultures.

Ensembl Gene	external_ gene_name	logFC	logCPM	FDR (adjusted p value)
ENSCAFG00000011117	FABP3	-4.377151924	6.809114329	0
ENSCAFG00000023449	KRT13	-3.63771758	6.041609447	0
ENSCAFG00000012963		3.319176151	6.013225013	0
ENSCAFG00000010058	SYT8	3.617748233	6.052245816	0
ENSCAFG00000015360	GLDN	3.85011139	5.743444141	0
ENSCAFG00000000874	THBS2	3.866467927	8.510389175	0
ENSCAFG00000011534	ACAN	4.230630965	5.717972042	0
ENSCAFG00000018560	MYH11	3.874678201	8.485594307	2.87E-301
ENSCAFG00000023855	IGFL3	-3.31084531	6.575511395	2.00E-274
ENSCAFG00000006142	DCN	4.411516544	4.723116458	9.94E-265
ENSCAFG00000010068	TNNI2	3.700973302	4.85250639	3.03E-259
ENSCAFG00000018012	TRPV2	-3.102096358	5.11295044	1.19E-256
ENSCAFG00000017018	COL1A1	2.847089635	9.81029451	1.42E-255
ENSCAFG00000014582	SERPINI1	2.918458039	6.755852524	3.31E-249
ENSCAFG00000009569	SPP1	-3.007003012	5.557200561	9.83E-241
ENSCAFG00000014322	PCOLCE	2.270024952	6.310193274	1.77E-237
ENSCAFG00000009506	ABI3BP	-4.170634733	4.297079341	1.28E-216
ENSCAFG00000020290	DAB2IP	2.375430847	5.817002799	1.21E-211
ENSCAFG00000004656	ITGA8	2.852208319	4.853145945	4.64E-197
ENSCAFG00000005843	LTBP1	2.501507099	7.499765163	7.07E-194
ENSCAFG00000014923	FGF7	2.093465175	6.448031136	2.57E-187
ENSCAFG00000011769	ANK2	-3.772896346	4.13757529	4.06E-185
ENSCAFG00000007047	MAL	2.581912879	7.325970761	7.82E-184
ENSCAFG00000015818	ACLY	-2.467307974	9.984483383	5.80E-181
ENSCAFG00000009334	OLFML3	2.795353709	4.906616443	3.43E-179
ENSCAFG00000015282	GGT6	2.49594907	4.901614475	8.06E-175
ENSCAFG00000012619	MGST1	2.833887634	5.339509708	1.43E-174
ENSCAFG00000000656	CTHRC1	-3.901535976	4.180780697	2.37E-163
ENSCAFG00000009051	SLC26A7	-2.310980433	8.328007471	5.29E-161
ENSCAFG00000024647	SERPINB5	-1.827933056	6.091774043	7.73E-156
ENSCAFG00000031999	SLC30A1	-1.835978989	6.20456488	2.65E-154
ENSCAFG00000013243	LAMC2	-1.92134984	6.178707942	4.27E-154
ENSCAFG00000007475	SORBS2	3.570393474	3.918904511	2.72E-153
ENSCAFG00000031675	COL8A1	2.449488607	8.149399705	1.17E-152
ENSCAFG00000008617	GLRB	-4.166161961	4.169869241	5.22E-152
ENSCAFG00000014474	IGFBP5	-2.968358508	8.68425632	5.72E-152
ENSCAFG00000029034	PDLIM3	2.201320471	8.195624645	1.19E-149
ENSCAFG00000006138	LUM	2.242886233	7.943808361	3.70E-147
ENSCAFG00000018405	FST	1.961926716	5.756613706	2.16E-145
ENSCAFG00000016755	CRABP2	-1.940408586	5.622769158	7.32E-144
ENSCAFG00000019809	GSTM3	-1.881414931	5.441767489	1.69E-140
ENSCAFG00000019807		-1.930990642	5.384295864	1.85E-136
ENSCAFG00000013617	IDH1	-1.569270159	6.318718221	1.90E-134
ENSCAFG00000011251		2.649501008	4.816972059	9.98E-134
ENSCAFG00000031938	GEM	1.97395201	5.186499177	1.15E-133
ENSCAFG00000002653	EPCAM	-2.780197872	4.313977655	4.55E-131
ENSCAFG00000006388	NTN4	2.059459302	6.547689061	4.63E-131
ENSCAFG00000024758	ADAMTS5	3.059406272	5.925837296	1.87E-130
ENSCAFG00000008756	ACTG2	2.190556888	11.10470715	1.79E-129
ENSCAFG00000010292	DOCK10	-1.655746288	6.276620697	2.37E-129
ENSCAFG00000008273		4.181412906	3.579076062	5.04E-127
ENSCAFG00000007903	ROBO1	1.981691723	8.279093986	3.77E-122
ENSCAFG00000013985	P3H2	-1.810812128	6.40221345	5.48E-119
ENSCAFG00000012969	INPP5J	-2.808521673	4.348132186	5.63E-119
ENSCAFG00000031894	FAM46A	1.95969756	6.622522527	3.69E-118
ENSCAFG00000013466	LRRC15	-2.084796479	5.605303326	4.29E-116
ENSCAFG00000009519	WISP2	2.622753395	4.897033428	1.05E-115
ENSCAFG00000000399		2.00998396	5.078644055	1.17E-113
ENSCAFG00000001232	SLC45A4	-1.843296344	5.44440524	7.86E-113
ENSCAFG00000002928	SVEP1	1.944184044	9.530403281	1.76E-112
ENSCAFG00000018589	OXCT1	-2.839956582	4.049491302	2.67E-112
ENSCAFG00000001091	TGFBI	-2.27363393	4.77125124	1.33E-111
ENSCAFG00000031706		-3.653465155	4.107883266	8.60E-111
ENSCAFG00000010991	ACACB	-3.72477939	3.383773036	1.35E-109
ENSCAFG00000006054	SLC16A3	1.812973462	6.783988526	2.22E-109
ENSCAFG00000032089		-2.444968027	4.259842437	5.81E-108
ENSCAFG00000014370		-1.804509038	7.038785583	9.19E-107
ENSCAFG00000012981	PLA2G3	-2.60836626	4.036268823	1.23E-106
ENSCAFG00000001106	LAMA2	2.774155655	4.149866276	3.22E-106
ENSCAFG00000010936	NPNT	-1.845857886	10.39799989	1.19E-104
ENSCAFG00000019002	TTC4	1.538713971	6.164339106	4.45E-104
ENSCAFG00000000296	ADGRG6	-1.690517229	7.690891088	6.30E-102
ENSCAFG00000013983	COL13A1	-1.91718882	5.396081807	1.97E-101
ENSCAFG00000014034		-2.285741828	4.523645853	4.06E-101
ENSCAFG00000015246	PLD1	2.020220983	5.208341922	4.98E-99
ENSCAFG00000011196	NID1	1.870669324	6.938460909	1.64E-98
ENSCAFG00000030102		1.526967011	5.413499954	5.18E-98
ENSCAFG00000011817		3.243111629	4.72130927	2.64E-96
ENSCAFG00000031368	SPINK6	-1.688097643	5.626244165	4.97E-95
ENSCAFG00000007251	KRT5	-1.901968326	4.926328081	3.22E-94
ENSCAFG00000009482	CPQ	2.193512025	5.098409336	3.76E-94
ENSCAFG00000002627	EPAS1	-1.765286422	5.145715334	7.12E-94
ENSCAFG00000016538	NPPB	2.664581898	4.173364709	1.38E-93
ENSCAFG00000009005	CYP26B1	1.792806481	5.156093827	9.64E-93
ENSCAFG00000011335	GNB4	1.808512484	4.774739347	4.17E-92
ENSCAFG00000001855	SRI	1.493123043	6.373110286	2.20E-91
ENSCAFG00000008478	MOGS	-1.340110669	6.248365613	1.13E-89
ENSCAFG00000011417		2.201520382	4.362731587	1.46E-89
ENSCAFG00000012875	FBXW12	-1.906210445	5.419747857	7.18E-88
ENSCAFG00000029966		-1.483399344	5.362505691	1.44E-87
ENSCAFG00000029053	TRIB2	-1.500242587	5.719587196	3.42E-87
ENSCAFG00000031288		2.036693755	7.452214129	8.77E-86
ENSCAFG00000009365	SPINT1	-1.548936315	6.269062505	9.29E-86
ENSCAFG00000014546	HTRA3	1.538832247	5.166097833	2.59E-85
ENSCAFG00000001911	ALDH1L2	-1.620305312	6.961730223	1.22E-84
ENSCAFG00000018115	CDH2	1.443964028	6.446222686	3.12E-84
ENSCAFG00000013863	CEMIP	1.497746186	5.365331944	4.31E-84
ENSCAFG00000017026	XYLT2	-1.360382527	5.746900296	6.22E-83
ENSCAFG00000015788	B4GALNT3	-1.718778928	5.479180729	1.04E-82

ENSCAFG00000007637	ACSS2	-1.536619312	7.352421554	2.17E-82
ENSCAFG00000013205	DHX9	1.312310768	6.06937258	6.56E-82
ENSCAFG00000008981		1.189703747	6.170788314	9.97E-81
ENSCAFG00000017973	MPI	1.795689289	4.898968807	1.22E-80
ENSCAFG00000011835	IGSF9	-2.40265779	4.794066459	4.85E-80
ENSCAFG00000023249	CILP2	2.225525205	9.627781667	7.01E-80
ENSCAFG00000003180	SLC1A4	1.31633716	6.152267562	2.15E-78
ENSCAFG00000024988		1.479410714	6.057678442	7.15E-78
ENSCAFG00000007870	DCLK2	2.866630636	3.91979176	2.35E-77
ENSCAFG00000031727	STC2	1.675064408	9.034200203	2.42E-77
ENSCAFG00000000123	ATP8B1	1.2782724	6.219496121	3.94E-77
ENSCAFG00000013909	SERPINE1	1.609597333	11.29091386	1.96E-76
ENSCAFG00000032756	FAM198B	2.816866446	3.889881939	2.86E-76
ENSCAFG00000013159	FZD9	2.107017679	5.171398256	7.80E-76
ENSCAFG00000022730	COX3	-1.44376724	11.92001242	1.13E-74
ENSCAFG00000007052	MALL	1.475414227	5.606167628	1.81E-74
ENSCAFG00000007683	AADAT	2.190507668	3.844568774	2.15E-74
ENSCAFG00000002266	WNK2	-1.378681197	5.736186052	2.37E-74
ENSCAFG00000011607	MSMO1	-1.353158015	6.368123317	9.51E-74
ENSCAFG00000009497	ACCS	1.450268307	5.123159151	1.04E-73
ENSCAFG00000004556	GPRC5C	-1.680577452	5.556416724	5.42E-72
ENSCAFG00000031382	PMEPA1	1.87114809	7.101742708	1.40E-71
ENSCAFG00000015625		-1.856224114	4.515121337	4.05E-71
ENSCAFG00000011184	SIAE	1.300619343	5.286197216	1.93E-70
ENSCAFG00000018572		-1.668806623	7.43901853	6.79E-70
ENSCAFG00000022709		-1.73032725	8.290973931	1.72E-69
ENSCAFG00000030838	PTGES	1.42191476	6.001324385	2.42E-69
ENSCAFG00000024310	FBXO27	1.268912562	5.906437797	5.02E-69
ENSCAFG00000029937	EFHD1	1.444723811	8.226524568	1.00E-68
ENSCAFG00000008199	FMN1	-1.542698871	5.105586187	1.43E-68
ENSCAFG00000009317	TMEM45A	-2.776978936	3.391821381	2.74E-68
ENSCAFG00000008600	DNAJC22	-2.642636538	3.348359242	6.24E-68
ENSCAFG00000003307	DOCK4	-2.117485024	4.228671466	1.11E-67
ENSCAFG00000028917	SNX10	-1.191085226	5.783968733	1.21E-67
ENSCAFG00000018081	SPECC1L-ADORA2A	1.404490661	8.152659583	2.20E-67
ENSCAFG00000000413	MTHFD1L	1.167945442	6.17040913	3.78E-67
ENSCAFG00000016956	KCNMB1	1.103549843	6.258828199	3.90E-66
ENSCAFG00000017166	TMEM63C	-2.107858848	3.88717423	9.86E-66
ENSCAFG00000006145	QPCT	-1.927728217	5.095798527	2.67E-65
ENSCAFG00000029346		1.122361802	6.411726981	5.79E-64
ENSCAFG00000000420	CPM	-2.241576557	3.742088995	9.19E-64
ENSCAFG00000015553	DKK1	1.604443827	4.731634786	2.16E-63
ENSCAFG00000014435	MAOA	1.405484595	6.700052642	2.57E-63
ENSCAFG00000018704	GLAST	-1.480331406	7.101014681	2.67E-63
ENSCAFG00000002007	SAMD9L	-1.288469014	5.365904172	3.73E-63
ENSCAFG00000003280	RSPO1	1.834321904	4.793008603	4.72E-63
ENSCAFG00000030307		-1.310403906	7.103008945	5.06E-63
ENSCAFG00000003808	JADE1	1.320568427	7.094585864	5.30E-63
ENSCAFG00000013735	GPIIIa	-1.210087915	5.845861617	6.86E-63
ENSCAFG00000012553		1.185947595	6.498466561	1.80E-62
ENSCAFG00000001450	MEST	-1.145367718	6.474660842	1.35E-61
ENSCAFG00000029798		1.922500005	6.055816845	3.86E-61
ENSCAFG00000012079	MCAM	1.55171856	6.803775612	4.37E-61
ENSCAFG00000023349		3.444867289	3.309516067	1.60E-60
ENSCAFG00000017326		1.374120934	10.04462064	1.91E-60
ENSCAFG00000020062	DPYD	1.608268948	4.272586272	2.51E-60
ENSCAFG00000003621	LPIN1	-1.664367427	4.632751052	2.84E-60
ENSCAFG00000010321	PPFIA4	1.243549745	6.402107217	3.38E-60
ENSCAFG00000001672	LEP	1.527312544	4.867453385	5.38E-60
ENSCAFG00000003570	FBXW2	1.120765762	6.125484965	9.31E-60
ENSCAFG00000001133	WISP1	2.378441842	3.928963093	1.05E-59
ENSCAFG00000011772	EGLN1	1.262907216	6.682093499	1.20E-59
ENSCAFG00000029313	CLDN1	2.263720841	3.577759083	3.00E-59
ENSCAFG00000032473	ISCA2	-1.923791624	3.983429355	8.68E-59
ENSCAFG00000030005		-1.235441816	5.996577072	1.54E-58
ENSCAFG00000018951	CDH6	1.276850412	6.63170705	4.03E-58
ENSCAFG00000029265	THY1	-1.29037682	9.755385958	5.22E-58
ENSCAFG00000006006	FASN	-1.450070408	9.683509727	5.70E-58
ENSCAFG00000020243	ZFHX3	1.232722975	5.938858938	8.29E-58
ENSCAFG00000006577		-1.390392444	5.186794057	1.01E-57
ENSCAFG00000002281	RECK	1.309404025	5.283451716	1.24E-57
ENSCAFG00000020166	ANGPTL2	-1.177537056	6.381636175	1.76E-57
ENSCAFG00000011229	AUTS2	1.661240653	4.851443616	3.08E-57
ENSCAFG00000018117	CHRDL1	1.247226552	7.911348743	1.10E-56
ENSCAFG00000004542	CYP27C1	-1.039021083	6.45812215	3.18E-56
ENSCAFG00000018719	ALDOC	-1.254393459	8.34271528	4.62E-56
ENSCAFG00000010821	TMTC1	1.268107755	6.642576136	1.14E-55
ENSCAFG00000002412	ZNF154	1.62310039	4.372726444	1.50E-55
ENSCAFG00000013006	ITGA6	1.304566363	9.274803378	2.58E-55
ENSCAFG00000000148	RDH16	-1.35267753	5.082450291	2.66E-55
ENSCAFG00000010028	IFITM10	-1.317176407	6.796195615	2.98E-55
ENSCAFG00000010423	COL4A4	-2.600339123	3.162970492	1.14E-54
ENSCAFG00000030132	ELOVL4	1.324247154	5.010195678	2.71E-54
ENSCAFG00000018001	NEIL1	2.94766391	3.137972935	3.12E-54
ENSCAFG00000019949	TLDC1	-2.092396395	3.701043983	3.51E-54
ENSCAFG00000010949	SLC37A2	-1.149638582	6.221701247	5.07E-54
ENSCAFG00000019189	BGN	1.285306947	10.36238867	6.24E-54
ENSCAFG00000007782	MYH7B	-1.450369947	4.596895318	7.98E-54
ENSCAFG00000014345	FN1	1.347340244	11.56561053	1.51E-53
ENSCAFG00000012925	PHKA2	-1.264812159	5.612650103	1.95E-53
ENSCAFG00000032222		-1.224802943	7.832859185	2.22E-53
ENSCAFG00000005073	SPHK1	-1.274395941	5.389694056	5.50E-53
ENSCAFG00000030823	POMGNT2	1.798887624	3.871657318	5.61E-53
ENSCAFG00000013651	UPK3B	1.480139136	4.608684162	5.80E-53
ENSCAFG00000017329	FLRT2	2.591703718	2.782339281	6.43E-53
ENSCAFG00000010729	MRGPRF	-1.846570504	4.285363324	1.41E-52
ENSCAFG00000004524	TTYH2	-1.131096684	5.833730296	2.10E-52
ENSCAFG00000032192		1.979242572	6.790069148	3.08E-52
ENSCAFG00000002008		-1.340740478	6.920738518	4.04E-52
ENSCAFG00000006838	PLPP1	1.277251024	6.925915366	8.08E-52
ENSCAFG00000001069	ECHDC1	1.294386046	6.839818833	9.30E-52
ENSCAFG00000025083	FADS1	-1.072195582	5.864427606	1.44E-51
ENSCAFG00000015116		-1.225665091	7.74831159	4.21E-51
ENSCAFG00000008358	LOXL3	-1.182996667	10.78301302	5.01E-51
ENSCAFG00000014748	MCM7	1.19092931	5.416415911	1.13E-50
ENSCAFG00000010785	RBM20	1.176691537	5.401324466	1.23E-50
ENSCAFG00000012424	SYNPO2	-1.479216261	5.667306733	1.68E-50
ENSCAFG00000018188	TNFAIP2	-2.313701438	3.625760343	3.69E-50
ENSCAFG00000013079	OLFML2B	1.233109295	5.67090794	4.00E-50
ENSCAFG00000017871	FAT2	1.381812829	7.847856647	5.31E-50
ENSCAFG00000001141	NDRG1	1.210632194	5.973183066	8.79E-50
ENSCAFG00000001900	FAM189A2	1.438813006	7.241336289	1.77E-49
ENSCAFG00000007140	ELOVL7	-1.632123598	4.507793629	1.78E-49
ENSCAFG00000017357	ADAM19	-1.190502182	8.770988953	2.79E-49
ENSCAFG00000003399	TES	1.097926432	5.34957957	3.97E-49
ENSCAFG00000014220	C1R	-1.653029218	3.939038488	4.87E-49
ENSCAFG00000010188	LGR4	-1.061527561	5.935927929	5.91E-49
ENSCAFG00000011324	ISCU	1.022845063	6.229101561	6.18E-49
ENSCAFG00000004500	SYTL2	-2.613202376	3.220909752	6.24E-49
ENSCAFG00000004613	PLXND1	-1.31359598	5.27767014	6.28E-49
ENSCAFG00000031250	KRT14	-1.234414967	8.436742022	1.06E-48
ENSCAFG00000017160	IGDCC4	-1.25073236	4.974427866	1.24E-48
ENSCAFG00000030804	RNLS	-1.239477706	4.796837001	1.24E-48
ENSCAFG00000022742	CYTB	1.180240937	8.843087195	1.44E-48
ENSCAFG00000016091	SNCG	2.232873063	3.398395188	1.79E-48
ENSCAFG00000003792		-1.823531707	3.988859821	4.56E-48
ENSCAFG00000014523	ENO2	-2.02684209	3.390800402	4.78E-48
ENSCAFG00000020198	LRRC8C	1.080808572	5.871984276	5.65E-48
ENSCAFG00000001016	TRDN	3.214720998	2.51188025	1.82E-47
ENSCAFG00000005373	SLC24A3	1.156222223	6.825622948	3.42E-47
ENSCAFG00000013958	FAH	1.819210589	3.759684111	5.92E-47
ENSCAFG00000012197	CCDC14	-1.220930333	5.158466698	7.21E-47
ENSCAFG00000005811	FMNL2	-1.04421389	5.540375046	7.76E-47
ENSCAFG00000030337	MYH1	1.167290039	9.002509743	8.44E-47
ENSCAFG00000006058	IRS2	1.495710754	4.82284962	1.03E-46
ENSCAFG00000017390	TRIM25	-1.377804139	5.021746244	1.11E-46
ENSCAFG00000015633	GREM2	-1.700441243	4.059070831	2.23E-46
ENSCAFG00000011171	ALDH3B1	2.606479162	3.330771777	3.02E-46
ENSCAFG00000004713	PLK3	-1.481968317	5.099406193	3.29E-46
ENSCAFG00000020110	TF	-1.246507655	9.0347225	4.51E-46
ENSCAFG00000019142	LRP8	-1.056198758	5.729943097	7.47E-46
ENSCAFG00000031331	OCIAD2	-1.407093378	4.274381801	9.88E-46
ENSCAFG00000011089	ARNTL2	-1.112271375	5.013377713	1.08E-45
ENSCAFG00000018341	TYMS	1.304403573	5.170155555	1.12E-45
ENSCAFG00000013852	MATN2	1.126964669	9.873408749	1.18E-45
ENSCAFG00000012803	RIN1	-1.46059668	4.319108424	1.28E-45
ENSCAFG00000030498		1.994790922	3.48876004	2.41E-45
ENSCAFG00000002919	EFEMP1	1.15082943	10.47053821	4.14E-45
ENSCAFG00000029131	HAPLN1	1.144728793	11.32783051	1.09E-44
ENSCAFG00000012403	COL7A1	-1.762090273	4.130469117	2.64E-44
ENSCAFG00000015627	SIX4	-1.24453708	5.068281679	3.82E-44
ENSCAFG00000002301	ECM2	1.133458734	6.959337076	5.65E-44
ENSCAFG00000008612	PDGFC	1.361697234	4.879880845	1.46E-43
ENSCAFG00000009517	HMGCR	-1.11008457	8.395630332	1.53E-43
ENSCAFG00000014943	CYP27A1	-1.483670817	4.508931038	2.19E-43
ENSCAFG00000020425	CDH11	1.100612125	8.24670026	6.51E-43
ENSCAFG00000002067	SLC1A1	-1.103510416	8.183431846	1.09E-42
ENSCAFG00000013741	SLC30A4	-1.437801317	4.778729789	1.55E-42
ENSCAFG00000000060	ITGA7	-1.051016435	5.197663944	2.57E-42
ENSCAFG00000014040	CDCP1	-1.091740006	6.819159852	4.62E-42
ENSCAFG00000000131	GLS2	-2.428156336	2.9314957	4.69E-42
ENSCAFG00000012390	NYNRIN	-1.238972201	5.085623469	4.73E-42
ENSCAFG00000012295	SYCP2	-1.920328173	3.286206193	5.23E-42
ENSCAFG00000013219	BNC1	-1.845349034	3.76173906	5.79E-42
ENSCAFG00000001371	SUN2	1.073495148	8.087447796	6.42E-42
ENSCAFG00000014812	COL3A1	1.142946355	12.19892092	7.73E-42
ENSCAFG00000001709	MCM5	2.375736683	4.212348491	1.32E-41
ENSCAFG00000030713	BTBD19	-1.381325195	4.811863443	1.52E-41

ENSCAFG00000004052	MCM2	1.71219157	4.101374922	1.52E-41	ENSCAFG00000003910	RASIP1	-2.104536784	3.289040137	3.03E-30
ENSCAFG00000029442	CTGF	1.216381545	11.32900523	1.81E-41	ENSCAFG00000015135	LDB2	-1.302692234	4.020022928	5.18E-30
ENSCAFG00000029153	PEG3	-1.07672872	6.691082135	1.88E-41	ENSCAFG00000017135	APOBR	-2.01759194	2.764954205	7.03E-30
ENSCAFG00000032758		1.227810687	5.274938717	1.89E-41	ENSCAFG00000012759	SLC17A9	-1.151413811	4.856001428	1.23E-29
ENSCAFG00000014570	ACAT1	1.022074166	5.66570481	2.25E-41	ENSCAFG00000015465	KCNMA1	-1.524595801	3.397864396	2.28E-29
ENSCAFG00000010948	PREX1	1.852007673	3.614295582	2.30E-41	ENSCAFG00000000394		1.201082651	4.325146754	3.00E-29
ENSCAFG00000011155	STARD9	1.496216232	5.908335497	2.52E-41	ENSCAFG00000032030	TMEM119	1.64005294	4.537476286	4.66E-29
ENSCAFG00000009773	NEDD9	1.14766684	7.232244205	3.35E-41	ENSCAFG00000004676	CGREF1	-1.076287504	4.557476736	4.70E-29
ENSCAFG00000001367	NPTXR	-1.140082717	4.718554021	4.09E-41	ENSCAFG00000022711		-1.101764303	7.993334712	7.14E-29
ENSCAFG00000007247	ANKRD1	1.363036124	8.5044555	6.42E-41	ENSCAFG00000020369	SLC9A5	-1.181374064	4.115002075	2.43E-28
ENSCAFG00000007893	RBP4	-1.082775998	7.021189365	2.49E-40	ENSCAFG00000032660	LRRTM2	2.421505784	2.010958942	3.14E-28
ENSCAFG00000009324	LOXL4	1.225908881	9.555071688	3.47E-40	ENSCAFG00000000212	SLC2A12	1.00938797	4.807971518	4.34E-28
ENSCAFG00000011383	CMKLR1	1.092233792	4.852860533	7.27E-40	ENSCAFG00000009284	F2R	1.064908538	4.626782657	8.05E-28
ENSCAFG00000004254	FAAH	1.639528016	3.958376797	9.99E-40	ENSCAFG00000011880	GRIK4	1.296721813	3.861097078	1.24E-27
ENSCAFG00000006638	SNAI2	-1.006326719	6.118132976	2.76E-39	ENSCAFG00000019735	PIK3CD	-1.063723407	4.542808758	1.88E-27
ENSCAFG00000029738		-2.336924035	2.774062401	2.97E-39	ENSCAFG00000016428	ARG2	-1.011590609	4.747344558	2.42E-27
ENSCAFG00000002098	C2orf40	1.107735836	7.536756921	5.26E-39	ENSCAFG00000011368		1.248133007	4.316316727	2.73E-27
ENSCAFG00000011742	PLEKHO1	1.019148318	4.990674988	6.66E-39	ENSCAFG00000006576	WDFY4	2.089566813	3.256631556	3.09E-27
ENSCAFG00000000337	PPM1H	1.011741649	5.22559311	7.28E-39	ENSCAFG00000000641	HSP70	1.05831144	4.501067794	3.77E-27
ENSCAFG00000031644	FBXL7	1.221345294	5.709487617	7.65E-39	ENSCAFG00000014083	ADAMTS14	-1.178286685	4.746243048	4.24E-27
ENSCAFG00000003600	BVES	1.083425006	4.873825058	8.41E-39	ENSCAFG00000019181	INPP5K	1.054385974	4.389033119	5.87E-27
ENSCAFG00000005021	EVPL	1.671650937	3.523507649	8.42E-39	ENSCAFG00000029799	RASSF5	-1.9192836	3.724466752	1.67E-26
ENSCAFG00000020354	CARMIL2	-1.324838735	4.341687612	2.29E-38	ENSCAFG00000013112	METRNL	-1.372913157	5.358435608	1.98E-26
ENSCAFG00000012270	SEC23IP	-1.05190217	7.461002092	2.59E-38	ENSCAFG00000016093		-2.317820914	2.089992799	3.90E-26
ENSCAFG00000019734	PLPP2	1.037137889	5.032500425	3.69E-38	ENSCAFG00000017835	HHIPL1	-1.157674045	6.175175483	5.98E-26
ENSCAFG00000011908		-1.185256147	4.700056807	1.25E-37	ENSCAFG00000009254		-1.288278939	3.880915558	5.99E-26
ENSCAFG00000006421	GAS6	1.068087081	7.955750021	1.61E-37	ENSCAFG00000008891	SERINC5	-1.517113559	3.14701319	6.96E-26
ENSCAFG00000007857	SCRG1	2.135344544	3.039685861	1.91E-37	ENSCAFG00000018438	CRIP2	1.00027377	6.367975791	7.69E-26
ENSCAFG00000018089	DSC3	2.133760868	3.081595669	1.97E-37	ENSCAFG00000013255	MKI67	1.160210803	6.089840763	1.13E-25
ENSCAFG00000014346	C1S	-1.370868698	4.215305858	3.41E-37	ENSCAFG00000018339	ADRB2	1.564174974	3.211354289	1.50E-25
ENSCAFG00000016442	RDH11	-1.127188202	4.757612582	7.15E-37	ENSCAFG00000002403	CCDC180	1.102392887	4.897484743	1.92E-25
ENSCAFG00000001077	TRIB1	-1.661410684	5.138236957	7.57E-37	ENSCAFG00000029076	CCDC126	1.301966175	3.638212928	2.38E-25
ENSCAFG00000020432	WLS	1.065116727	8.881833885	8.59E-37	ENSCAFG00000000311	LRIG3	-1.294321128	3.652025662	2.42E-25
ENSCAFG00000001938	VEGFA	-1.059282253	9.662489963	9.76E-37	ENSCAFG00000008286	CETN3	-1.289445142	4.156950307	2.51E-25
ENSCAFG00000009104	STC1	-2.464578871	2.344220659	9.90E-37	ENSCAFG00000031030		1.305446333	3.612748806	3.58E-25
ENSCAFG00000003858	GYS1	1.037093065	5.803138002	9.90E-37	ENSCAFG00000029948	IDNK	2.200350699	2.664133764	4.92E-25
ENSCAFG00000001524	AHCYL2	-1.601828021	3.726416398	1.05E-36	ENSCAFG00000001597	MDFI	-1.174659839	6.305364332	7.77E-25
ENSCAFG00000007092	SCUBE2	-1.53393292	3.892628217	2.00E-36	ENSCAFG00000001957	DOCK8	2.106486854	2.292424071	8.44E-25
ENSCAFG00000008761	CX3CL1	-1.035851962	6.575348359	2.01E-36	ENSCAFG00000001126	KLHL3	-1.451430586	4.621437783	1.11E-24
ENSCAFG00000032262	DHRS1	-1.143961064	5.016924421	5.33E-36	ENSCAFG00000001807	DDX58	-1.415334063	3.742958083	1.18E-24
ENSCAFG00000009033	DYSF	-1.029187	6.529351222	6.14E-36	ENSCAFG00000024645	BNIP3	1.017781159	8.916613657	1.20E-24
ENSCAFG00000017920	ANGPTL6	1.393032896	4.219828232	1.05E-35	ENSCAFG00000024792		-1.727759238	2.928552765	1.33E-24
ENSCAFG00000014581	ARL4D	-1.315385084	4.117088735	1.63E-35	ENSCAFG00000016518	FGFR4	-2.155697376	2.208207093	1.85E-24
ENSCAFG00000009242	FILIP1L	1.072755783	7.362246102	1.72E-35	ENSCAFG00000000907	SCUBE1	1.991778567	2.460812761	2.40E-24
ENSCAFG00000014530	ABLIM2	1.859817735	3.325935841	3.28E-35	ENSCAFG00000005727	RARB	1.550978237	3.130594362	3.24E-24
ENSCAFG00000016293	FAM193B	-1.033215404	5.584957888	4.65E-35	ENSCAFG00000003103	RRAGD	-1.678011195	2.8759499	5.36E-24
ENSCAFG00000006091	KITLG	1.594609025	4.371453022	5.09E-35	ENSCAFG00000018579	GHR	1.770839686	2.637533019	6.50E-24
ENSCAFG00000006991	REM1	-1.139546592	5.726041045	6.99E-35	ENSCAFG00000000784	TTC38	-1.736797541	2.70149525	7.13E-24
ENSCAFG00000003465	EGFR	1.06756517	5.358453451	7.09E-35	ENSCAFG00000013981	RALGPS2	-1.949500501	2.398963351	1.12E-23
ENSCAFG00000016635	MYO1E	1.010992588	8.639917148	9.26E-35	ENSCAFG00000012376	VASH2	-1.380944694	3.599949989	1.33E-23
ENSCAFG00000013370	SERINC4	-1.141604681	4.542347817	1.89E-34	ENSCAFG00000013607	PDE11A	-1.130939451	4.936069754	1.35E-23
ENSCAFG00000009286	SLC38A1	-1.035399459	4.658879614	2.36E-34	ENSCAFG00000005327	TGDS	-1.076013621	4.267637482	1.46E-23
ENSCAFG00000003409	RRM2	1.773508752	4.029818038	2.97E-34	ENSCAFG00000014148	ADAMTS7	-1.992465295	2.581232521	1.78E-23
ENSCAFG00000004905		1.006268536	6.547857425	3.17E-34	ENSCAFG00000015680	MYO5C	2.218450111	2.179732545	2.05E-23
ENSCAFG00000002404	CNNM4	1.205441288	5.035876153	3.62E-34	ENSCAFG00000014104	PCBD1	1.612596625	2.753613622	2.75E-23
ENSCAFG00000017705	ARMCX2	-1.667568669	3.584865397	8.23E-34	ENSCAFG00000015878	UCHL1	-1.17982963	3.790640793	3.20E-23
ENSCAFG00000032422		-1.252994986	4.508337064	1.07E-33	ENSCAFG00000018037	B4GALT6	1.036271423	4.723282559	5.44E-23
ENSCAFG00000009510	EXD1	-1.764956998	3.82654218	1.55E-33	ENSCAFG00000006409	SH3RF2	-1.494888186	3.216165414	6.29E-23
ENSCAFG00000003784	ARMC2	-1.324655365	4.088232898	2.81E-33	ENSCAFG00000019134	PPL	1.301778929	3.970110671	6.34E-23
ENSCAFG00000004861	AAMDC	1.441227956	3.743592399	3.84E-33	ENSCAFG00000005575		1.421978452	3.34825617	7.33E-23
ENSCAFG00000009404	TNNC1	-1.895760397	3.306512193	3.89E-33	ENSCAFG00000019379	ABCA3	1.567667009	2.931526046	1.08E-22
ENSCAFG00000008253	ACTA1	1.368958049	10.53408039	1.01E-32	ENSCAFG00000023132		-1.169279577	3.895071471	1.20E-22
ENSCAFG00000016080	TSPYL2	-1.032610385	4.759769003	1.15E-32	ENSCAFG00000031257	GPR83	-1.628901862	3.018208573	1.61E-22
ENSCAFG00000014245	PDE1A	1.002343	5.050486796	1.58E-32	ENSCAFG00000029557	TRMT61A	1.021840075	4.22699816	2.70E-22
ENSCAFG00000016558	MTHFR	-1.049901819	4.730555095	1.65E-32	ENSCAFG00000023647	KRT19	-1.0343633	4.28250232	2.89E-22
ENSCAFG00000007878		2.05986463	3.157937234	3.59E-32	ENSCAFG00000006030	PCNA	1.018988951	5.044505543	3.76E-22
ENSCAFG00000013740	MAP2	-1.510099778	3.654102272	6.80E-32	ENSCAFG00000005415	ARRB1	1.542988729	3.470027129	3.84E-22
ENSCAFG00000001581	ADAMTSL1	-1.018718184	7.403849588	1.26E-31	ENSCAFG00000020305	CDH1	-1.16141307	4.020547334	4.97E-22
ENSCAFG00000011071	GJA8	-2.262842872	2.827339379	1.67E-31	ENSCAFG00000031805		-1.87573603	2.790323602	5.70E-22
ENSCAFG00000009281	F2RL1	1.367457074	4.06287343	1.76E-31	ENSCAFG00000001152	FAM13B	1.07155164	4.727902374	6.20E-22
ENSCAFG00000003327		1.033277605	6.034137822	2.97E-31	ENSCAFG00000010827	TTC23	-1.008144667	4.107440588	6.99E-22
ENSCAFG00000005746	NAV3	1.021754601	5.946607306	3.20E-31	ENSCAFG00000030441	MGAT3	1.573389465	2.859729465	7.79E-22
ENSCAFG00000019770	LRIF1	-1.087111167	4.767498966	3.39E-31	ENSCAFG00000008445	TLX2	-2.52974043	3.522476171	8.57E-22
ENSCAFG00000001029	TPD52L1	1.864663637	2.889551802	4.11E-31	ENSCAFG00000008318	ASIC1	-1.328219108	3.75840273	9.32E-22
ENSCAFG00000010654	AGPAT3	2.069333961	2.538375076	5.77E-31	ENSCAFG00000002392		1.153106402	3.643044921	1.22E-21
ENSCAFG00000008589	ART3	1.213186899	4.522792709	6.69E-31	ENSCAFG00000020398	PDP2	-1.058103745	4.374794423	2.13E-21
ENSCAFG00000007131	MERTK	1.02335861	4.806885601	1.41E-30	ENSCAFG00000008902	PTX3	-1.135784376	4.456852616	2.67E-21
ENSCAFG00000012806	MPZL2	-2.121306775	2.612983258	1.53E-30	ENSCAFG00000010431	CACNA2D2	-1.115685424	4.249741835	3.00E-21
ENSCAFG00000016596	DISP3	-1.789160536	3.478830908	1.53E-30	ENSCAFG00000007923	MSC	-1.039430878	4.362591034	3.04E-21
ENSCAFG00000014484	ETV4	-1.672479697	3.15574183	1.53E-30	ENSCAFG00000011526	YOD1	-1.616594152	3.161542381	3.52E-21
ENSCAFG00000016097	FAM35A	-1.483727325	3.740619685	1.55E-30	ENSCAFG00000006461	FOXP1	1.44042147	3.784310372	3.55E-21
ENSCAFG00000010350	CYB5R1	1.184274184	4.512815103	2.44E-30	ENSCAFG00000001101	PTPRK	-1.804832648	2.941214078	3.81E-21
ENSCAFG00000009791	HIVEP1	-1.228662867	4.238410002	2.78E-30	ENSCAFG00000008170	JPH1	-1.074721702	4.193272359	4.23E-21
ENSCAFG00000003662	TBC1D9	1.124261468	4.299149949	2.86E-30	ENSCAFG00000012593		1.126651453	4.589806948	4.35E-21

ENSCAFG00000019866	CDT1	1.70820002	2.611351608	7.54E-21	ENSCAFG00000029771	ETFRF1	-1.431187727	2.645212938	1.18E-15
ENSCAFG00000011620	FANCI	1.484585727	3.466464585	7.69E-21	ENSCAFG00000030977	ZNF789	1.609741776	1.981508181	1.47E-15
ENSCAFG00000000199	LVRN	-1.834041683	2.653798128	7.71E-21	ENSCAFG00000028851		-1.691976897	2.083314651	1.71E-15
ENSCAFG00000016677	NCAPG	1.076276034	4.554933494	9.27E-21	ENSCAFG00000004288		-1.5429142	2.372206912	1.76E-15
ENSCAFG00000012643		1.035777798	6.186940086	1.05E-20	ENSCAFG00000005839	SATB1	-1.186530159	3.189489335	1.77E-15
ENSCAFG00000004205	MKNK1	-1.151566033	3.951054633	1.37E-20	ENSCAFG00000031441	WNT9A	1.676402771	2.088235613	2.05E-15
ENSCAFG00000019444	EXD3	-1.244825914	3.332636814	1.55E-20	ENSCAFG00000005254	IL17RE	-1.531235977	2.394969686	2.22E-15
ENSCAFG00000006180	SOCS2	-1.077111563	4.593342978	2.32E-20	ENSCAFG00000019926	AIF1L	-1.651241436	2.423654597	2.28E-15
ENSCAFG00000020320	ESRP2	-1.80985521	2.238230719	2.71E-20	ENSCAFG00000005377	FAM198A	1.64536151	2.228679405	2.46E-15
ENSCAFG00000012293	ADCY4	-1.162704912	3.615099391	2.82E-20	ENSCAFG00000013052	TANC2	-1.051386069	4.069331795	2.65E-15
ENSCAFG00000012903	RUNX3	1.550849926	2.844882235	2.98E-20	ENSCAFG00000000644	SYNJ2	-1.603885911	2.985145565	3.29E-15
ENSCAFG00000011660	MYO18B	1.795331239	2.376076556	3.21E-20	ENSCAFG00000014056	MID1IP1	-1.418272266	4.216739794	3.32E-15
ENSCAFG00000004443	FOSB	-1.751705811	4.013673861	3.49E-20	ENSCAFG00000032077	TIGD7	1.018675937	3.858461669	5.53E-15
ENSCAFG00000013980	CDCA5	1.934837694	1.902604896	3.65E-20	ENSCAFG00000016590	FBXO2	1.022314584	4.837912405	5.59E-15
ENSCAFG00000023594	CSRP2	-1.380672364	3.127035521	3.66E-20	ENSCAFG00000002645	KCNQ5	-1.030255713	4.084062357	6.16E-15
ENSCAFG00000008291		-1.058525025	3.893227206	3.87E-20	ENSCAFG00000020379	HSF4	-1.26414651	3.327667972	6.84E-15
ENSCAFG00000029901	C1QTNF2	-1.676012384	2.541712449	4.88E-20	ENSCAFG00000032632	WNT7A	-1.500084981	3.050179221	1.07E-14
ENSCAFG00000025462	DHRS2	-1.530324828	2.688712824	5.21E-20	ENSCAFG00000011348	AFAP1L2	1.110574472	3.493964755	1.25E-14
ENSCAFG00000002432	TSPAN13	-1.070625428	3.980015781	6.64E-20	ENSCAFG00000016823		1.311882898	2.857881366	1.34E-14
ENSCAFG00000001897	APBA1	1.609703016	2.622032478	9.82E-20	ENSCAFG00000009994	CD40	-1.702368768	3.374576911	1.43E-14
ENSCAFG00000002152	IL1R2	-1.594120516	2.576003044	1.02E-19	ENSCAFG00000003825	MATN3	1.347044656	2.962985519	1.81E-14
ENSCAFG00000014301	TNR	-1.088046409	4.03143698	1.08E-19	ENSCAFG00000002876	TPBG	-1.05870693	4.12079258	2.32E-14
ENSCAFG00000015128	TMCO4	-1.158133962	3.474800564	1.11E-19	ENSCAFG00000019827	AMIGO1	1.57018211	2.10552792	2.60E-14
ENSCAFG00000029593	TMEM35A	1.625125878	2.609010113	1.68E-19	ENSCAFG00000012432	MYOZ2	1.752392929	1.665186281	3.21E-14
ENSCAFG00000003616	FAM131B	1.45770844	3.378577281	1.78E-19	ENSCAFG00000017090	MYCBPAP	-1.565261227	2.470377387	3.24E-14
ENSCAFG00000005489	LIPT2	1.076231741	3.666831	2.55E-19	ENSCAFG00000000626		-1.289211936	2.89663258	4.32E-14
ENSCAFG00000000766	PPT2-EGFL8	-1.054511901	3.745359052	2.57E-19	ENSCAFG00000010754	SLC38A3	-1.680248666	2.395811606	4.75E-14
ENSCAFG00000008088	GATB	1.012574651	3.832680372	2.57E-19	ENSCAFG00000011556	FAM65C	-1.58873589	1.915366258	5.75E-14
ENSCAFG00000006532		-1.00291851	4.109651637	3.30E-19	ENSCAFG00000007042	DNAH10	-1.219705405	3.041332754	6.64E-14
ENSCAFG00000003581	PHF19	1.070106233	4.205122915	4.72E-19	ENSCAFG00000004272	RAD54L	1.781011129	2.135128103	6.66E-14
ENSCAFG00000007280	RNF180	-1.341594103	3.348012971	5.49E-19	ENSCAFG00000003704	SHCBP1	1.062356091	4.39472844	6.82E-14
ENSCAFG00000020416	CMTM3	-1.223972496	3.516729573	8.09E-19	ENSCAFG00000002950	HOXA5	1.327795003	3.297805228	7.40E-14
ENSCAFG00000015333	NPTX2	-1.762945233	2.596816071	1.08E-18	ENSCAFG00000008334	M1AP	-1.358732109	2.339809424	9.35E-14
ENSCAFG00000010160	TPMT	-1.271705321	3.532191514	1.16E-18	ENSCAFG00000009098	KNSTRN	1.414620234	2.491086087	1.04E-13
ENSCAFG00000008613	TROAP	1.299191346	3.937163819	1.26E-18	ENSCAFG00000014469	EFHC2	1.949605511	1.553131031	1.08E-13
ENSCAFG00000013792	STARD5	-1.491047926	2.765977429	1.38E-18	ENSCAFG00000000210	FEM1C	-1.14284979	3.360994481	1.15E-13
ENSCAFG00000029101	NOG	-2.026148009	2.129099815	1.49E-18	ENSCAFG00000028890	ZFP37	1.294033782	2.456674176	1.31E-13
ENSCAFG00000000586	CPT1B	-1.081707323	4.131470766	2.76E-18	ENSCAFG00000030486		1.043565887	3.492138259	1.35E-13
ENSCAFG00000020088	LCN2	1.866183029	1.739229751	2.89E-18	ENSCAFG00000007111	LGI4	-1.020620227	3.987405388	1.47E-13
ENSCAFG00000009190	ST3GAL6	-1.126010965	3.630040758	3.19E-18	ENSCAFG00000014624	IFI35	-1.372547886	2.497516021	1.83E-13
ENSCAFG00000002940	FANCL	1.318941602	3.090179395	3.32E-18	ENSCAFG00000001425	GKAP1	1.192576574	2.808907399	1.91E-13
ENSCAFG00000011572	KCNG1	1.571400429	3.003984729	4.51E-18	ENSCAFG00000028591	POPDC3	-1.694968921	1.77190352	2.23E-13
ENSCAFG00000017277		-1.393943351	3.062631757	4.57E-18	ENSCAFG00000016544		-1.191582567	3.276895208	2.38E-13
ENSCAFG00000004779	CEACAM28	-1.561851559	2.616390348	4.94E-18	ENSCAFG00000029067		1.305194797	3.150736646	2.38E-13
ENSCAFG00000031052		-1.581855929	2.415118508	5.47E-18	ENSCAFG00000001849	TRPM3	-1.304946249	2.649152124	2.83E-13
ENSCAFG00000010588	MARCKSL1	-1.017305607	4.36580477	7.07E-18	ENSCAFG00000029993	DDAH1	-1.053617378	3.316406148	2.96E-13
ENSCAFG00000001622	TAF8	1.102831384	3.74105877	7.45E-18	ENSCAFG00000005610	KIF5C	-1.55021311	2.747970279	3.39E-13
ENSCAFG00000003685	CREM	1.123150364	3.825766342	8.19E-18	ENSCAFG00000001204	KIF20A	1.310147107	4.140059235	3.40E-13
ENSCAFG00000015769	SLC6A13	-1.358454975	3.070704437	8.45E-18	ENSCAFG00000013539	CCNYL1	-1.505096074	2.692833444	3.55E-13
ENSCAFG00000003596	ZMYM1	-1.157742003	3.829406935	9.25E-18	ENSCAFG00000019566	FAM69B	-1.7321924	1.933588624	3.61E-13
ENSCAFG00000024246	LRRC8D	-1.753171138	2.12980984	1.09E-17	ENSCAFG00000000460	LAPTM4B	1.344046958	2.4187008	3.61E-13
ENSCAFG00000017322	LCTL	-1.417505052	3.181521339	1.36E-17	ENSCAFG00000014021		-1.072918541	3.611870306	4.63E-13
ENSCAFG00000008061	ARHGEF3	1.010376684	3.815351299	1.37E-17	ENSCAFG00000032408	TMEM255B	1.453953251	1.98734967	5.39E-13
ENSCAFG00000005855	TMCO6	-1.036152913	3.862018966	1.80E-17	ENSCAFG00000006707	ZNF215	1.399982422	2.330397847	5.89E-13
ENSCAFG00000028513	HOXB3	1.044348676	4.250961379	1.97E-17	ENSCAFG00000015235	SLC19A2	-1.096826988	3.277074663	7.84E-13
ENSCAFG00000005306	SOCS3	-1.906801244	2.180730554	2.36E-17	ENSCAFG00000016997	FBXL22	1.20865339	3.849988296	7.84E-13
ENSCAFG00000014799		-1.637862965	2.295284951	3.34E-17	ENSCAFG00000013843	UPB1	-1.709975124	1.715496534	8.01E-13
ENSCAFG00000019611	CHTF18	1.389770719	3.196934424	3.82E-17	ENSCAFG00000003875	PLK4	1.304512195	2.907859701	9.09E-13
ENSCAFG00000018387	METTL4	-1.260624952	3.265030276	4.17E-17	ENSCAFG00000013833	IL16	1.070436534	3.223217825	9.81E-13
ENSCAFG00000019474	ARHGEF16	-1.537658512	2.700887638	5.59E-17	ENSCAFG00000000548		-1.19513575	3.381973328	1.12E-12
ENSCAFG00000019412	CASKIN1	1.825921113	1.672851049	5.66E-17	ENSCAFG00000019352	PERM1	-1.055647124	3.19655822	1.12E-12
ENSCAFG00000008972		-1.197319075	3.477530881	6.36E-17	ENSCAFG00000014616	COMP	-1.487899099	2.076922802	1.26E-12
ENSCAFG00000014650	CDCA3	1.324251402	3.835127211	7.51E-17	ENSCAFG00000006631	EBF4	-1.933011496	1.619963161	1.40E-12
ENSCAFG00000019995	DPH5	-1.009409498	3.797057129	1.00E-16	ENSCAFG00000013713		1.029319176	3.494438809	1.76E-12
ENSCAFG00000015703	LRRN4CL	-1.18273157	3.379024484	1.01E-16	ENSCAFG00000031571	PRAP1	-1.939114582	2.073760797	1.86E-12
ENSCAFG00000019617	ABCA7	-1.575331024	2.761356151	1.02E-16	ENSCAFG00000014029	IL1RAP	-1.236488867	3.140442385	1.95E-12
ENSCAFG00000020179	TGFBR3	-1.840281612	2.00109331	1.46E-16	ENSCAFG00000002180	SEMA4D	1.607284647	1.596179772	2.19E-12
ENSCAFG00000001565	DAAM2	1.555779393	2.690467012	1.48E-16	ENSCAFG00000003539	CLSPN	1.458358853	2.371748782	2.26E-12
ENSCAFG00000031154	KIAA1161	-1.396091736	3.218112953	1.62E-16	ENSCAFG00000004855	EPB41L5	-1.276152334	2.574000123	2.36E-12
ENSCAFG00000006861	ANGPT4	1.890073005	1.659444511	2.30E-16	ENSCAFG00000017121	SLC51B	1.215375641	2.618157622	3.11E-12
ENSCAFG00000010470	GCA	2.046213191	2.21061752	2.61E-16	ENSCAFG00000020576	cfa-mir-24-1	1.646666903	1.798217712	3.11E-12
ENSCAFG00000012636	METTL8	-1.169679871	3.398691822	2.81E-16	ENSCAFG00000016757	CPLX1	1.228223883	2.765646522	3.19E-12
ENSCAFG00000018934	UHRF1	1.338122994	4.042988857	3.38E-16	ENSCAFG00000005003	NCKAP5	-1.905854409	2.026955481	4.34E-12
ENSCAFG00000015026	DLGAP5	1.276231623	3.726670547	3.99E-16	ENSCAFG00000030694	TMEM38A	1.228700305	3.115215714	4.70E-12
ENSCAFG00000005433	ABCC4	-1.140053882	4.098785926	4.67E-16	ENSCAFG00000013278		-1.224482936	2.502310434	5.01E-12
ENSCAFG00000009649	PLEKHA6	1.348863111	3.21759591	5.33E-16	ENSCAFG00000004856	PROSER2	1.085962306	3.800800012	5.29E-12
ENSCAFG00000018085	DSC2	1.414229916	2.44179602	5.39E-16	ENSCAFG00000007381	BPIFB1	-1.767381691	1.67466196	6.62E-12
ENSCAFG00000016995	PGF	-1.438907651	2.620729865	6.86E-16	ENSCAFG00000009431	E2F8	1.642399757	1.422493936	6.71E-12
ENSCAFG00000004297	CCDC8	-1.469571483	3.009021853	7.00E-16	ENSCAFG00000002816	MPP6	-1.099820404	2.955200335	7.93E-12
ENSCAFG00000003916	KLHL29	1.168694071	3.466418716	8.41E-16	ENSCAFG00000008754	CCL17	-1.53370666	1.89586949	8.64E-12
ENSCAFG00000000318	PLAGL1	1.286029531	3.277117453	9.23E-16	ENSCAFG00000009794	EDN1	1.101896203	5.394160546	8.66E-12
ENSCAFG00000011756	PLXNA2	1.367429956	2.937979356	9.54E-16	ENSCAFG00000009430	IRX6	1.485126424	1.650375289	9.99E-12
ENSCAFG00000002305	LRRC1	-1.932817368	2.811667423	1.01E-15	ENSCAFG00000001882	GTPBP10	-1.115467916	2.675792867	1.03E-11
ENSCAFG00000006695	SLCO2A1	1.897828942	1.402750458	1.16E-15	ENSCAFG00000005122	ST6GALNAC2	-1.319252803	2.705666948	1.17E-11

ENSCAFG00000007460	ZNF341	-1.020444627	3.200705884	1.17E-11	ENSCAFG00000007505		-1.222478234	1.906144056	2.02E-08
ENSCAFG00000010955	PTHLH	1.38870745	2.003173924	1.22E-11	ENSCAFG00000002770	FKTN	1.059797928	2.240653774	2.09E-08
ENSCAFG00000028873		-1.010024775	3.177024865	1.44E-11	ENSCAFG00000018877	NPR3	1.043372724	2.712328562	2.33E-08
ENSCAFG00000006185	RELL2	-1.032413009	3.387344764	1.53E-11	ENSCAFG00000031661		-1.291855232	1.965838201	2.42E-08
ENSCAFG00000020094	FAM102A	-1.086572044	2.980077155	1.66E-11	ENSCAFG00000015414	CREG1	-1.046181284	2.43346722	2.59E-08
ENSCAFG00000001930	PGM5	1.111576877	3.031327437	1.97E-11	ENSCAFG00000024327	NOL3	-1.183569041	3.455509036	2.83E-08
ENSCAFG00000031283	ZNF134	1.154546889	2.812870525	2.17E-11	ENSCAFG00000002727	ABCA1	1.312958161	1.839949181	3.37E-08
ENSCAFG00000003928	DBP	-1.820516972	3.430481062	2.18E-11	ENSCAFG00000003105	ANKRD6	-1.302855642	1.624568805	5.97E-08
ENSCAFG00000011275	MARK1	1.117816215	3.444091634	2.78E-11	ENSCAFG00000030603		1.275891443	1.674873832	6.06E-08
ENSCAFG00000011148	RGS9	1.633724661	1.679311831	2.86E-11	ENSCAFG00000031691	CRADD	-1.282047043	2.881731587	6.70E-08
ENSCAFG00000002477	CORO2A	-1.060036693	3.08271878	3.29E-11	ENSCAFG00000029292		-1.281359496	1.86397644	6.91E-08
ENSCAFG00000005319		-1.01897916	3.578908861	3.59E-11	ENSCAFG00000004490	CCDC17	-1.011035223	2.732867424	7.25E-08
ENSCAFG00000032171		1.268609819	2.409234993	3.76E-11	ENSCAFG00000003988	SPATA5	1.347157068	2.283923393	7.25E-08
ENSCAFG00000030242	HS3ST2	1.434220362	2.660822467	4.13E-11	ENSCAFG00000006676	SYNE4	-1.070877825	2.023801419	7.39E-08
ENSCAFG00000019392	RAB26	1.499123501	1.50000137	4.40E-11	ENSCAFG00000006579	MEDAG	1.228151238	1.431333494	7.48E-08
ENSCAFG00000005667		-1.452833656	2.224020673	4.70E-11	ENSCAFG00000010148	SLC45A3	-1.251202259	1.667387794	9.04E-08
ENSCAFG00000019552	ARHGAP45	-1.472951889	2.769630389	6.28E-11	ENSCAFG00000004147	PIWIL4	-1.105812757	2.557936168	9.24E-08
ENSCAFG00000004133	CCNA2	1.046285107	3.337853554	8.55E-11	ENSCAFG00000024187	DPEP3	-1.303211744	1.350953911	9.26E-08
ENSCAFG00000003568	CPT1C	-1.503988515	2.224685607	9.45E-11	ENSCAFG00000019186	HAUS7	1.379242621	1.555925772	1.13E-07
ENSCAFG00000013001	C10orf90	-1.22873135	2.259905933	1.06E-10	ENSCAFG00000017080	EPN3	-1.048343849	2.367846114	1.30E-07
ENSCAFG00000017511	NPR1	-1.330907533	2.381776729	1.07E-10	ENSCAFG00000004394	SIX5	-1.157398946	3.419642271	1.43E-07
ENSCAFG00000005688		-1.38230909	2.858190191	1.47E-10	ENSCAFG00000006732	PXDNL	-1.086358928	2.366371156	1.50E-07
ENSCAFG00000011953	PARP15	-1.210128595	2.311036934	1.69E-10	ENSCAFG00000017063	KRBA2	1.089934277	2.017303362	1.61E-07
ENSCAFG00000000821	UTP23	-1.027660614	3.070422925	1.96E-10	ENSCAFG00000029908		-1.304875837	1.352335119	1.79E-07
ENSCAFG00000011899	HJURP	1.176450374	3.09398958	2.05E-10	ENSCAFG00000029461	PGLYRP1	-1.094049686	1.787396216	1.81E-07
ENSCAFG00000015971	CLCN5	-1.26822006	2.192466811	2.74E-10	ENSCAFG00000013954	KIF18B	1.321427048	2.241024761	1.82E-07
ENSCAFG00000029080	HRCT1	1.015296365	3.084179985	2.89E-10	ENSCAFG00000016482		1.145851828	2.496699902	2.25E-07
ENSCAFG00000025116	JPH2	1.125865269	3.801859366	3.14E-10	ENSCAFG00000017339		1.408225282	1.199305203	2.31E-07
ENSCAFG00000017895	ZNF396	1.629783572	1.802437649	3.30E-10	ENSCAFG00000016848		1.174250638	2.120886727	2.37E-07
ENSCAFG00000032377	EVA1A	-1.163928542	2.595899297	3.52E-10	ENSCAFG00000031667	ADH4	1.076763857	2.501687509	2.45E-07
ENSCAFG00000015394		1.365095657	2.020296186	4.59E-10	ENSCAFG00000001112	CHADL	1.072382141	2.667954124	2.60E-07
ENSCAFG00000030459		-1.163688129	2.722123057	4.67E-10	ENSCAFG00000006801	HSPB6	-1.388367853	6.528978983	2.80E-07
ENSCAFG00000024175	NHSL2	-1.101441596	2.488972301	7.99E-10	ENSCAFG00000001286	FANCC	-1.061932179	2.569883814	2.90E-07
ENSCAFG00000003005	CREB5	-1.233086959	2.769004136	8.78E-10	ENSCAFG00000014002	H2AFY2	1.176744287	1.934570982	3.23E-07
ENSCAFG00000014866	ZFYVE28	1.213028923	2.747987651	8.91E-10	ENSCAFG00000014232	ARVCF	1.607622908	1.690838751	3.29E-07
ENSCAFG00000003282	ZNF618	-1.154748829	2.411136046	9.08E-10	ENSCAFG00000006655	ADGRD1	1.128747325	2.230178526	3.34E-07
ENSCAFG00000012042	USP2	-1.319151932	2.688776205	1.06E-09	ENSCAFG00000023070	ACYP2	1.118171987	1.667601556	3.39E-07
ENSCAFG00000002615		-1.190931177	2.759100277	1.09E-09	ENSCAFG00000030822		1.081678184	2.212689975	3.74E-07
ENSCAFG00000030766	MSMP	-1.118622708	2.919441987	1.11E-09	ENSCAFG00000007681	MFAP3L	-1.152161961	1.673071878	3.87E-07
ENSCAFG00000000322	STX11	1.464181829	1.707112342	1.33E-09	ENSCAFG00000019072	HSPB11	-1.068224886	1.89653575	4.29E-07
ENSCAFG00000006512	ANO9	1.045172222	2.391823643	1.40E-09	ENSCAFG00000017669	BTK	-1.086746289	2.458963962	4.52E-07
ENSCAFG00000014145	ITGA2B	-1.466734986	1.358740267	1.43E-09	ENSCAFG00000003895	HSD17B14	-1.201510946	2.014460531	4.66E-07
ENSCAFG00000018702	EFCAB7	-1.258312774	2.116542914	1.44E-09	ENSCAFG00000008544	MMP15	-1.101893322	2.402538253	5.09E-07
ENSCAFG00000023455	HAVCR1	-1.749537257	1.390673303	1.50E-09	ENSCAFG00000016965		-1.06868256	2.209113507	5.22E-07
ENSCAFG00000006953	PDGFRL	1.286648393	2.038057056	1.64E-09	ENSCAFG00000009179		-1.193925952	1.47956087	6.44E-07
ENSCAFG00000016869		-1.042221685	3.063416929	1.70E-09	ENSCAFG00000019918	FOXF1	-1.095616773	2.320480017	6.55E-07
ENSCAFG00000008408	TPD52	-1.388108128	2.302607105	1.78E-09	ENSCAFG00000031542	SFR1	-1.009989611	2.404427563	7.26E-07
ENSCAFG00000014161		-1.08840646	3.099582597	2.08E-09	ENSCAFG00000001942	TEC	1.1866348	1.703972583	7.74E-07
ENSCAFG00000002147	IL1R1	-1.610394071	1.797059956	2.20E-09	ENSCAFG00000029520		1.052980117	1.878049973	8.48E-07
ENSCAFG00000007797	MARVELD2	1.038682244	2.87045508	2.23E-09	ENSCAFG00000032633	ZNF283	1.053832212	2.043736685	8.57E-07
ENSCAFG00000002854	IGLON5	-1.253413802	3.186635355	2.29E-09	ENSCAFG00000031828		1.056609663	2.504897784	8.78E-07
ENSCAFG00000014558	ANKRD45	1.481077294	1.379120029	2.75E-09	ENSCAFG00000013237	SH3GL3	-1.301982084	1.408071858	9.65E-07
ENSCAFG00000030141	LONRF1	-1.150695137	2.421854054	2.87E-09	ENSCAFG00000019337	CLDN6	-1.269209608	1.482160425	1.13E-06
ENSCAFG00000017983	PPCDC	-1.043033294	2.783732769	2.98E-09	ENSCAFG00000004704		1.024584778	1.746080325	1.16E-06
ENSCAFG00000002308	VWDE	1.43273832	1.64518539	3.07E-09	ENSCAFG00000013993		-1.064219844	1.599469912	1.22E-06
ENSCAFG00000004396	HDAC11	-1.150828671	2.526602761	3.19E-09	ENSCAFG00000012742	MTFP1	-1.146813482	1.354222579	1.27E-06
ENSCAFG00000032285	HOXA3	-1.193655551	2.400532457	3.21E-09	ENSCAFG00000018248	PRPSAP2	-1.163320387	1.701424939	1.29E-06
ENSCAFG00000002879	UBE3D	1.022477191	2.779122389	3.54E-09	ENSCAFG00000001569	RECQL4	1.368542863	1.417987738	1.35E-06
ENSCAFG00000012193	RNF39	1.017273875	4.770534265	3.78E-09	ENSCAFG00000001985		-1.023796221	3.264397683	1.51E-06
ENSCAFG00000006611	HOXC4	1.348685982	1.921354691	4.08E-09	ENSCAFG00000005213	IL15RA	-1.218696146	1.209070096	1.60E-06
ENSCAFG00000001007	FBXO32	1.663344559	1.198046892	4.40E-09	ENSCAFG00000002722	CHAC2	1.02325707	1.806216446	1.78E-06
ENSCAFG00000028642		-1.302637129	1.9799835	5.25E-09	ENSCAFG00000011298	VWA2	1.506503447	1.282164548	1.87E-06
ENSCAFG00000003059	SNX30	-1.002796283	3.027309305	5.64E-09	ENSCAFG00000017555	GPR68	-1.386514957	1.990408113	1.95E-06
ENSCAFG00000011703		-1.050930032	2.910994527	5.93E-09	ENSCAFG00000008099	CYP2C18	-1.012252186	1.713606538	2.01E-06
ENSCAFG00000019780	SLC2A6	1.219439049	2.667773955	5.94E-09	ENSCAFG00000032382		1.065019785	2.221783053	2.25E-06
ENSCAFG00000003749	SLC7A11	1.300704815	1.596382341	6.25E-09	ENSCAFG00000011861	FANCB	-1.002083607	1.908394794	2.28E-06
ENSCAFG00000017866	ISLR	1.386409556	2.213342946	6.91E-09	ENSCAFG00000004655	BCL3	-1.172448137	2.954216967	2.49E-06
ENSCAFG00000029718	IER5	1.28828336	2.793989733	7.14E-09	ENSCAFG00000011318	ANOS1	1.306545197	1.1336618	2.53E-06
ENSCAFG00000000699	PANX2	-1.070624205	3.48305076	7.74E-09	ENSCAFG00000009113	MT1	1.280587498	1.263485752	2.59E-06
ENSCAFG00000016106	CDC6	1.569253965	2.306468173	7.77E-09	ENSCAFG00000002294	MITD1	-1.258489299	1.850519245	2.61E-06
ENSCAFG00000010874	sulf2	-1.369792648	2.236517013	8.04E-09	ENSCAFG00000002635	RDH13	-1.092486593	2.294628357	3.12E-06
ENSCAFG00000019758		1.03990512	2.870000776	8.60E-09	ENSCAFG00000030657		-1.233387893	1.535309662	3.19E-06
ENSCAFG00000011668	CCDC36	-1.02073936	2.891080656	8.64E-09	ENSCAFG00000003720	NRCAM	1.19282806	1.99886748	3.50E-06
ENSCAFG00000015316	GPR161	-1.419323481	1.348524206	9.04E-09	ENSCAFG00000012551	UBXN11	1.027919544	2.425161582	3.60E-06
ENSCAFG00000001741	GNMT	-1.068892293	2.357454908	9.70E-09	ENSCAFG00000017432	CCDC159	-1.023529947	1.658248951	3.63E-06
ENSCAFG00000001161		-1.311993068	1.721186633	1.02E-08	ENSCAFG00000016268		1.196463497	1.434588176	3.73E-06
ENSCAFG00000000990	TCF7	1.381751528	1.275667874	1.16E-08	ENSCAFG00000017423	PLPPR2	-1.04450711	1.863757568	3.92E-06
ENSCAFG00000010009	DUSP8	1.08703525	2.87917714	1.24E-08	ENSCAFG00000018189		1.135931158	1.407332697	4.45E-06
ENSCAFG00000018779	PROCA1	-1.368071266	1.834251735	1.29E-08	ENSCAFG00000014889	AZGP1	-1.129078164	1.777369607	4.98E-06
ENSCAFG00000024609	CNTN2	1.007930158	2.904724731	1.58E-08	ENSCAFG00000015412	NKX3-2	-1.04086984	1.815915762	6.08E-06
ENSCAFG00000015031		-1.306117288	1.720683356	1.68E-08	ENSCAFG00000006914	STK33	1.142997931	1.370924766	6.15E-06
ENSCAFG00000009973		-1.171061853	2.00288724	1.98E-08	ENSCAFG00000010735	GRAMD1C	-1.076027113	1.732685559	6.59E-06
ENSCAFG00000004664	DNAJC15	1.02534881	2.923939377	2.00E-08	ENSCAFG00000018342	ADSSL1	-1.168664948	1.227341024	8.71E-06
ENSCAFG00000007627	PLEKHF1	-1.5142624	3.007529472	2.02E-08	ENSCAFG00000032530	RGS18	-1.151495649	1.160197721	9.46E-06

ENSCAFG00000029484	METTL21A	-1.018718531	1.501338948	9.55E-06	ENSCAFG00000032618		1.008062439	1.6626742	8.42E-05
ENSCAFG00000002594	KMT5C	-1.038249509	1.805583949	1.01E-05	ENSCAFG00000028754	PLPP3	-1.058529167	1.681335119	9.38E-05
ENSCAFG00000010676	BANK1	-1.031170429	1.593079291	1.02E-05	ENSCAFG00000008305	C21orf91	1.074992788	1.279145203	9.92E-05
ENSCAFG00000001689		1.106299653	1.218269737	1.23E-05	ENSCAFG00000031326	CEBPB	-1.121937819	4.545070766	0.000107049
ENSCAFG00000006442	PURG	-1.334728709	2.016959725	1.28E-05	ENSCAFG00000024052	GGN	-1.106733933	1.938724407	0.00011731
ENSCAFG00000016752	AWAT2	-1.111042707	1.368942053	1.30E-05	ENSCAFG00000005586	AP3M2	-1.070623362	0.977900236	0.000138773
ENSCAFG00000000519		-1.103001808	1.369363934	1.38E-05	ENSCAFG00000032037		1.017536944	1.037694118	0.000169418
ENSCAFG00000002618	TNNI3	-1.022900463	1.495912101	1.47E-05	ENSCAFG00000004465	ZNF467	-1.028040153	1.950392395	0.000184605
ENSCAFG00000008997	FAM105A	1.096883487	1.962615123	1.48E-05	ENSCAFG00000003152	ZNF672	-1.255354768	2.11951837	0.000233738
ENSCAFG00000006595		1.231484662	2.196170593	1.64E-05	ENSCAFG00000019652	ARID3A	-1.139735051	1.264611089	0.00025539
ENSCAFG00000029969	RGS4	1.05380441	1.349438531	1.72E-05	ENSCAFG00000019318	B3GALT6	1.018855369	2.000347008	0.000306841
ENSCAFG00000030707	UBE2U	-1.061402038	1.446133986	1.86E-05	ENSCAFG00000015758	EXO1	1.046306024	1.670113702	0.00033194
ENSCAFG00000016822	NEURL1B	-1.062187263	2.53180066	1.91E-05	ENSCAFG00000003407	ADD2	1.002435342	0.86519613	0.000365261
ENSCAFG00000012720	NTSR1	-1.006344512	1.840467306	2.20E-05	ENSCAFG00000010450	SLC37A1	-1.037511837	1.110132694	0.00048178
ENSCAFG00000010790	SLC9B1	-1.038570006	1.733118102	2.37E-05	ENSCAFG00000028619	C1orf122	-1.01393559	3.682577136	0.000499643
ENSCAFG00000017033	EME1	1.023409575	1.530146136	2.52E-05	ENSCAFG00000019446	TOR4A	-1.056023568	1.706545079	0.000517368
ENSCAFG00000030623	LAYN	-1.16503698	1.410673453	2.91E-05	ENSCAFG00000023690	ERCC6L	1.00305828	1.988921417	0.001465136
ENSCAFG00000008268	MND1	1.002573932	1.477571552	3.10E-05	ENSCAFG00000023035		1.036429777	0.94888688	0.001790146
ENSCAFG00000032157		1.254114496	1.139877791	3.34E-05	ENSCAFG00000009095		-1.02891249	1.807460762	0.00252046
ENSCAFG00000008652	SHROOM3	-1.211436684	1.013364633	3.63E-05	ENSCAFG00000030056		-1.465761782	1.84740634	0.002976074
ENSCAFG00000000768	EGFL8	-1.095336788	1.19401763	3.89E-05	ENSCAFG00000029384		1.583990553	9.920755566	0.004228405
ENSCAFG00000005806	SGO1	1.215258539	1.841372354	4.18E-05	ENSCAFG00000032276		1.726794128	10.29581232	0.004513936
ENSCAFG00000001417	KIF27	1.074174637	1.338237248	4.85E-05	ENSCAFG00000029369		1.721937533	10.68782437	0.004530178
ENSCAFG00000006526	LMNTD2	-1.052625811	1.188327213	5.26E-05	ENSCAFG00000030374	C6orf141	-1.089277907	3.247877627	0.004845985
ENSCAFG00000023682	PCDHGA1	-1.027177819	2.02208212	5.40E-05	ENSCAFG00000029657		1.762668234	11.17191056	0.008742589
ENSCAFG00000000681	FBN2	1.044032141	1.414377407	5.42E-05	ENSCAFG00000028748		2.119408538	9.644239659	0.009237534
ENSCAFG00000007578	TP53INP2	-1.263161358	2.451223027	7.03E-05					

Table S3 and S4: differentially expressed genes between primary cell cultures and a non-neoplastic mammary gland tissue. For Tables S3 and S4, refer to the online version of the manuscript. Available in https://www.ncbi.nlm.nih.gov/pubmed/28834169.

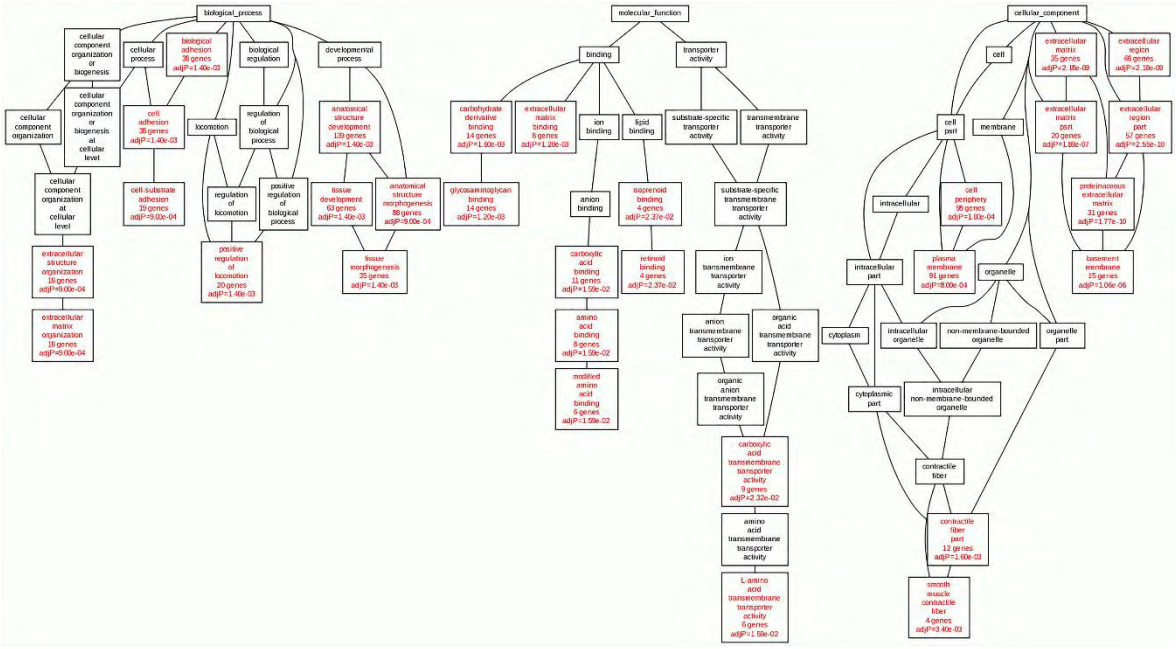

Figure S1: gene ontology analysis from gene set of 647 DE genes between M5 and M25 samples. GO categories in red are the enriched GO categories while the black ones are their non-enriched parents.

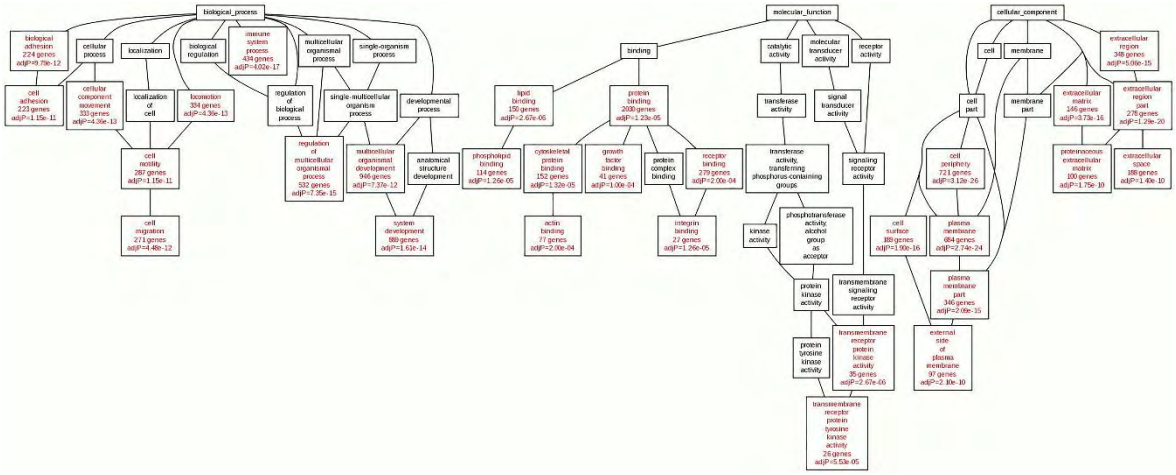

Figure S2: gene ontology analysis from gene set of 5,328 DE genes between M5 and a normal mammary gland. GO categories in red are the enriched GO categories while the black ones are their non-enriched parents.

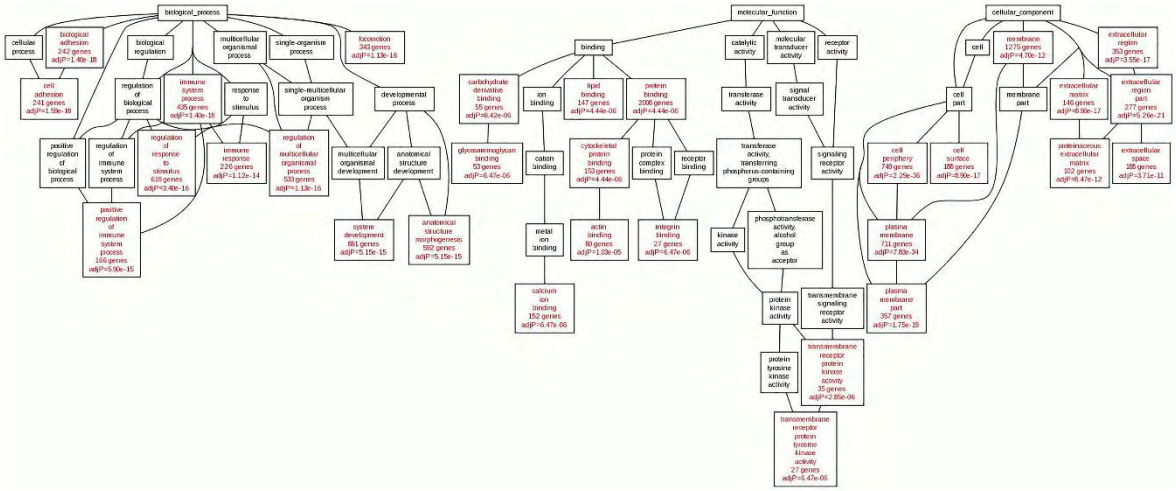

Figure S3: gene ontology analysis from gene set of 5,417 DE genes between M25 and a normal mammary gland. GO categories in red are the enriched GO categories while the black ones are their non-enriched parents.

APÊNDICE B – MATERIAL SUPLEMENTAR CAPÍTULO 2

Table S1 – Discriminative peaks between well differentiated and poorly differentiated tumor ROIs (AUC > 0.70 and FDR < 0.05).

m/z	AUC	FDR	**1508.676561**	0.73	1.28E-15	**1657.787989**	0.72	4.40E-12	**1636.829666**	0.71	3.26E-15
2216.035598	0.76	4.53E-15	**1839.872016**	0.73	1.86E-12	**1736.828248**	0.72	1.30E-12	**1694.860442**	0.71	1.14E-14
2854.37454	0.76	1.90E-15	**1407.654275**	0.73	9.64E-14	**1054.498777**	0.72	5.18E-14	**1559.686714**	0.71	4.18E-13
2217.031475	0.76	7.59E-15	**2705.225135**	0.73	2.41E-13	**1832.84783**	0.72	5.66E-12	**1127.55267**	0.71	1.26E-10
2855.379509	0.76	3.26E-15	**1735.825844**	0.73	9.16E-13	**1707.766039**	0.72	2.22E-11	**1992.91962**	0.71	6.19E-12
2130.07433	0.75	4.29E-15	**1289.651791**	0.73	4.26E-11	**1558.684573**	0.72	1.88E-10	**2720.210881**	0.71	1.16E-13
1864.862203	0.75	3.69E-15	**1560.804534**	0.73	2.30E-11	**1758.724996**	0.72	4.72E-12	**2003.99189**	0.71	7.05E-11
2105.035291	0.75	2.47E-13	**1577.802405**	0.73	1.11E-12	**1798.804963**	0.72	1.88E-11	**2002.988775**	0.71	2.93E-11
1863.857636	0.75	3.80E-15	**1886.844926**	0.73	6.51E-13	**2243.969071**	0.72	4.94E-15	**2121.991809**	0.71	1.86E-13
1585.762918	0.75	2.43E-14	**1812.871458**	0.73	1.45E-12	**1454.739696**	0.72	2.07E-11	**1993.92237**	0.71	5.28E-12
2104.043339	0.75	2.02E-12	**2059.969842**	0.73	9.77E-12	**1653.833087**	0.72	3.07E-12	**1428.710805**	0.71	4.18E-13
2853.370786	0.75	3.80E-15	**1281.612621**	0.73	1.79E-11	**1475.667479**	0.72	1.89E-12	**2219.961116**	0.71	2.87E-13
3186.466054	0.75	3.69E-15	**2020.962343**	0.73	3.21E-16	**1267.669808**	0.72	3.54E-11	**2127.030594**	0.71	1.85E-11
3187.474765	0.75	3.26E-15	**1453.735904**	0.73	1.27E-11	**1509.679731**	0.72	2.36E-15	**1799.807537**	0.71	3.13E-12
2121.035924	0.75	5.94E-14	**1561.809082**	0.73	1.38E-11	**2342.172249**	0.72	4.40E-13	**1117.543231**	0.71	8.09E-11
1586.76598	0.75	3.70E-14	**2104.985988**	0.73	2.02E-12	**1268.673643**	0.72	8.84E-11	**1289.581578**	0.71	1.05E-12
2218.042007	0.75	9.56E-15	**2154.084205**	0.73	9.04E-13	**2253.101145**	0.72	3.26E-15	**1849.843371**	0.71	2.00E-10
2106.020516	0.75	1.24E-13	**1473.663429**	0.73	1.90E-12	**1562.815325**	0.72	2.48E-12	**1721.876398**	0.71	2.03E-11
2057.9639	0.74	1.30E-12	**2126.027117**	0.73	3.22E-11	**1566.741248**	0.72	6.00E-11	**1495.6452**	0.71	8.68E-12
2056.961085	0.74	1.05E-12	**1096.565158**	0.73	1.79E-13	**2343.165087**	0.72	1.54E-12	**1105.570795**	0.71	2.99E-11
2131.094299	0.74	2.05E-13	**1836.859223**	0.73	1.38E-11	**1677.766836**	0.72	8.43E-12	**1848.840699**	0.71	3.01E-10
1656.78673	0.74	9.41E-13	**1813.877101**	0.73	1.05E-12	**1578.805738**	0.72	3.26E-12	**2081.946023**	0.71	1.11E-12
2132.099275	0.74	6.85E-13	**1835.859196**	0.73	2.69E-12	**1840.87512**	0.72	3.52E-11	**1081.582843**	0.71	6.76E-13
1607.744481	0.74	1.14E-12	**2215.950647**	0.73	1.12E-11	**1786.771394**	0.72	1.74E-13	**1953.886507**	0.71	4.94E-15
2218.018896	0.74	1.15E-13	**2706.231046**	0.73	7.97E-13	**2079.950241**	0.72	1.39E-11	**1258.620543**	0.71	3.12E-12
1655.784675	0.74	2.41E-12	**2134.104702**	0.72	1.09E-12	**2216.991653**	0.72	4.80E-12	**2707.240337**	0.71	3.17E-11
2058.966347	0.74	1.45E-12	**1465.684371**	0.72	5.09E-11	**2114.076457**	0.72	8.01E-12	**1678.772768**	0.71	1.45E-11
2122.040064	0.74	1.86E-13	**1466.687912**	0.72	4.97E-11	**2423.143391**	0.72	8.06E-12	**1530.660111**	0.71	4.18E-13
2133.101436	0.74	1.03E-12	**1885.839526**	0.72	1.73E-12	**2822.327563**	0.72	3.40E-12	**2152.022668**	0.71	2.58E-12
2856.381796	0.74	7.51E-15	**1834.889484**	0.72	3.38E-11	**1261.623035**	0.72	1.57E-10	**1954.889431**	0.71	3.26E-15
2120.034449	0.74	1.45E-13	**1608.748376**	0.72	5.06E-13	**1684.827739**	0.72	7.37E-16	**2195.976813**	0.71	8.19E-12
1095.561071	0.74	1.16E-13	**1474.666162**	0.72	1.08E-12	**1865.867345**	0.72	1.40E-14	**1599.78521**	0.71	2.23E-11
3185.45292	0.74	3.69E-15	**2704.219117**	0.72	5.85E-14	**1727.766574**	0.72	1.83E-14	**1593.752402**	0.71	5.53E-11
1834.86719	0.74	3.40E-12	**2252.099829**	0.72	3.80E-15	**2612.223536**	0.72	1.18E-09	**970.4752787**	0.71	1.16E-11
1587.769542	0.74	6.31E-15	**1818.891464**	0.72	2.06E-12	**1567.743688**	0.72	1.59E-11	**2242.965165**	0.71	6.44E-15
2106.000438	0.74	1.79E-13	**3188.483712**	0.72	6.54E-14	**2214.945965**	0.72	6.80E-10	**1475.715869**	0.71	1.27E-12
1332.648959	0.74	1.55E-13	**2019.960213**	0.72	3.53E-15	**1909.905973**	0.72	1.57E-12	**1759.728493**	0.71	3.40E-12
2153.079398	0.73	1.87E-13	**1257.616389**	0.72	3.26E-13	**1429.635137**	0.72	2.71E-12	**1106.574309**	0.71	4.23E-11
2242.965292	0.73	5.10E-15	**1279.599711**	0.72	2.20E-12	**1819.885863**	0.71	4.15E-13	**1588.724517**	0.71	1.09E-11
1706.762613	0.73	1.52E-11	**1111.592518**	0.72	2.20E-12	**2078.945919**	0.71	1.01E-11	**1264.534638**	0.71	7.00E-11
1908.902626	0.73	1.16E-13	**1728.771412**	0.72	3.26E-15	**1841.879496**	0.71	3.74E-12	**2115.079972**	0.71	4.47E-11
1576.799299	0.73	1.91E-12	**1408.657225**	0.72	5.18E-13	**1333.651356**	0.71	5.18E-13	**1833.869705**	0.71	4.01E-11

1652.832112	0.71	3.20E-11	**2821.34895**	0.71	6.37E-12	**1487.664271**	0.70	1.86E-09	**2109.004245**	0.70	7.15E-08
1530.658953	0.71	1.65E-12	**2155.090722**	0.71	2.27E-11	**1889.904801**	0.70	1.05E-11	**1192.625927**	0.70	2.76E-12
1115.540864	0.71	3.69E-15	**2876.363891**	0.71	1.20E-13	**2021.965181**	0.70	5.18E-13	**2820.339471**	0.70	7.60E-11
1337.674103	0.71	2.30E-11	**1467.690589**	0.70	3.06E-10	**2272.031287**	0.70	3.61E-11	**1177.563935**	0.70	1.06E-12
2199.952426	0.71	2.87E-12	**1737.830993**	0.70	9.21E-12	**1240.670741**	0.70	1.05E-09	**1686.851913**	0.70	3.80E-14
1112.596269	0.71	1.09E-11	**1720.872799**	0.70	4.03E-11	**1142.588502**	0.70	1.23E-11	**2200.955334**	0.70	7.29E-12
1598.781714	0.71	1.46E-10	**1833.897314**	0.70	5.00E-11	**1649.773368**	0.70	3.59E-08	**2281.042915**	0.70	4.97E-11
1290.655034	0.71	1.42E-10	**2110.006386**	0.70	5.48E-09	**1888.903191**	0.70	3.40E-12	**1700.737274**	0.70	6.59E-12
2421.15544	0.71	3.67E-11	**1262.626941**	0.70	2.45E-09	**2420.153107**	0.70	8.84E-11	**1750.852115**	0.70	2.03E-10
1648.770089	0.71	1.72E-08	**1121.610774**	0.70	3.17E-11	**1311.563208**	0.70	8.94E-12	**3184.42491**	0.70	1.03E-13
1708.769438	0.71	4.20E-11	**1685.831339**	0.70	5.53E-16	**1455.742732**	0.70	1.81E-10	**1084.559882**	0.70	1.07E-11
1401.639318	0.71	2.80E-13	**1994.925559**	0.70	1.19E-11	**2120.979445**	0.70	6.40E-12	**2041.014506**	0.70	2.59E-09
1749.847654	0.71	1.16E-10	**2169.952021**	0.70	4.94E-15	**2719.209834**	0.70	8.19E-12	**1258.620978**	0.70	1.21E-10
1814.877752	0.71	1.27E-11	**1096.516204**	0.70	8.62E-11	**2611.221451**	0.70	2.49E-09	**1642.732242**	0.70	3.63E-12
2196.978328	0.71	9.71E-12	**1214.586772**	0.70	1.94E-12	**2703.215773**	0.70	5.73E-13	**2290.069997**	0.70	1.18E-10
1850.849786	0.71	2.23E-11	**2198.947777**	0.70	8.19E-12	**2316.02914**	0.70	4.42E-12	**2151.00248**	0.70	1.81E-13
1132.482169	0.71	1.84E-10	**2422.158826**	0.70	1.83E-11	**2244.971251**	0.70	1.85E-13	**1201.579621**	0.70	1.85E-11
1827.893274	0.71	9.41E-13	**1440.700434**	0.70	3.21E-16	**1586.736464**	0.70	3.13E-11	**2435.176079**	0.70	1.33E-11
1290.584653	0.71	9.66E-13	**2424.145021**	0.70	7.62E-10	**2280.041805**	0.70	1.20E-10	**2106.99092**	0.70	5.43E-12
1637.833673	0.71	7.05E-15	**2613.22658**	0.70	4.66E-10	**2125.02373**	0.70	1.38E-07	**2268.091442**	0.70	3.38E-11
1837.860314	0.71	5.25E-11	**1757.803623**	0.70	7.60E-12	**2089.016734**	0.70	5.83E-11			
1120.606475	0.71	3.13E-11	**2317.0313**	0.70	9.85E-11	**2042.018145**	0.70	5.34E-09			

Table S2 – Protein identification extracted from LC-MS/MS data of discriminative m/z signals between WD and PD tumor regions

Observed m/z	Theoretical m/z	Error (ppm)	Protein	Symbol
1290.584653	1290.58484	0.145	40S ribosomal protein S3a	RPS3A
2217.031475	2217.04183	4.671	ABI family member 3 binding protein	ABI3BP
1567.743688	1567.75582	7.739	Adhesion regulating molecule 1	ADMR1
1813.877101	1813.87152	-3.077	Apolipoprotein A-I	APOA1
1578.805738	1578.80098	-3.014	Apolipoprotein A-I	APOA1
1473.663429	1473.65644	-4.742	BCL2 associated athanogene 3	BAG3
1585.762918	1585.77174	5.563	Beta-casein	CSN2
3188.483712	3188.48256	-0.361	Caldesmon 1	CALD1
1428.710805	1428.70775	-2.138	Calnexin	CANX
1818.891464	1818.88281	-4.758	Catenin alpha 1	CTNNA1
1281.612621	1281.6182	4.353	Collagen alpha-1(I) chain	COL1A1
1560.804534	1560.81288	5.347	Collagen alpha-1(I) chain	COL1A1
2002.988775	2003.00533	8.265	Collagen alpha-1(I) chain	COL1A1
2089.016734	2089.00927	-3.573	Collagen type VI alpha 3 chain	COL6A3
2104.985988	2105.00419	8.647	Collagen type VI alpha 3 chain	COL6A3
2056.961085	2056.96443	1.626	Collagen type XII alpha 1 chain	COL12A1
2110.006386	2110.00472	-0.790	Collagen type XII alpha 1 chain	COL12A1
2153.079398	2153.0808	0.651	Collagen type XII alpha 1 chain	COL12A1
1401.639318	1401.64923	7.072	Elastin microfibril interfacer 2	EMILIN2

1558.684573	1558.69547	6.991	Eukaryotic translation elongation factor 1 delta	EEF1D
1736.828248	1736.84497	9.628	Eukaryotic translation initiation factor 4 gamma 1	EIF4G1
1509.679731	1509.6863	4.351	Ezrin	EZR
1454.739696	1454.72742	-8.439	Galectine 3 binding protein	LGALS3BP
1833.897314	1833.90897	6.356	Heat shock protein family A (Hsp70) member 5	HSPA5
1841.879496	1841.89158	6.561	Heterogeneous nuclear ribonucleoprotein H1	HNRNPH1
1201.579621	1201.58815	7.098	Insulin like growth factor binding protein 5	IGFBP5
1888.903191	1888.91094	4.102	Jupiter microtubule associated homolog 2	JPT2
1707.766039	1707.77214	3.573	Keratin, type I cytoskeletal 10	KRT10
1834.867190	1834.85257	-7.968	Laminin subunit beta 2	LAMB2
1214.586772	1214.576	-8.869	LIM domain and actin binding 1	LIMA1
1598.781714	1598.79081	5.689	Marginal zone B and B1 cell specific protein	MZB1
1648.770089	1648.78131	6.806	NSFL1 cofactor	NSFL1C
2104.043339	2104.05569	5.870	PDZ domain-containing protein	AHNAK2
1096.516204	1096.50917	-6.415	Peptidylprolyl isomerase	FKBP10
1694.860442	1694.85553	-2.898	Perilipin	PLIN3
1653.833087	1653.82311	-6.032	Pro-interleukin-16	IL16
1084.559882	1084.56734	6.877	Protein disulfide-isomerase	PDIA3
1799.807537	1799.80441	-1.738	Rho GDP dissociation inhibitor alpha	ARHGDIA
1111.592518	1111.59937	6.164	SERPINE1 mRNA binding protein 1	SERBP1
1656.786730	1656.7936	4.146	Solute carrier family 7 member 5	SLC7A5
1587.769542	1587.76895	-0.373	Spectrin alpha non-erythrocytic 1	SPTAN1
1105.570795	1105.57488	3.695	Spectrin alpha, non-erythrocytic 1	SPTAN1
1106.574309	1106.58405	8.803	Spectrin alpha, non-erythrocytic 1	SPTAN1
1258.620978	1258.62737	5.079	Tankyrase 1 binding protein 1	TNKS1BP1
1120.606475	1120.61093	3.976	T-complex protein 1 subunit gamma	CCT3
1268.673643	1268.68449	8.550	TRAF2 and NCK interacting kinase	TNIK
1279.599711	1279.59132	-6.557	Transgelin	TAGLN2
1332.648959	1332.639	-7.474	Tropomyosin 1	TPM1
1636.829666	1636.83044	0.473	Tubulin beta chain	TUBB4B
2125.023730	2125.02703	1.553	Tubulin beta chain	TUBB
2106.990920	2106.98008	-5.145	Uncharacterized protein	LOC607207
1177.563935	1177.55242	-9.779	Versican	VCAN

Table S3 – Network of WD tumor regions sorted by degree.

ID	Average Shortest Path Lenght	Betweeness Centrality	Degree
CALD1	1.97435897	0.01555121	50
TPM1	1.74358974	0.27082132	49
BAG3	1.83760684	0.0375886	49
APOA1	1.97435897	0.0087969	49
LOC100687619	1.98290598	0.01518979	48
LIMA1	1.98290598	0.0093089	48
COL12A1	2	0.01487083	47
SLC7A5	1.99145299	0.00700513	47
IL16	1.94871795	0.03378387	46
TAGLN2	2.00854701	0.02213383	45
ADMR1	2.03418803	0.00649077	45
HSPG2	1.96581197	0.02869934	44
CAPG	2.01709402	0.00952195	44
EPB41L2	2.03418803	0.01185066	42
MZB1	2.17948718	0.01678541	41
CANX	2.05128205	0.00600304	41
LGALS3BP	2.05128205	0.003428	41
HSPA5	1.93162393	0.0314195	40
RBMX	2.05982906	0.00279846	40

KRT10	2.13675214	0.01140968	39
AHNAK2	2.05128205	0.01118311	39
FLNA	2.07692308	0.00818234	39
NSFL1C	2.08547009	0.01146019	38
PDIA3	2.09401709	0.01149288	37
MPST	2.08547009	0.00470091	37
RBM3	2.23076923	0.02477451	34
SPTAN1	2.05982906	0.02205622	34
MPO	2.08547009	0.01726755	34
ARHGDIA	2.18803419	0.00227017	33
IGFBP5	2.11111111	0.02373189	32
ABI3BP	2.1965812	0.00216929	32
JPT2	2.27350427	0.00349974	31
EEF1D	2.24786325	0.00204314	31
HIST1H1A	2.11111111	0.01979409	30
C3	2.27350427	0.00514534	30
VCAN	2.03418803	0.03257419	29
EMILIN2	2.22222222	0.00689659	28
F2	2.32478632	0.00619417	28
COL1A2	2.4957265	0.00597674	27
FETUB	2.13675214	0.13976597	25
SF3B2	2.21367521	4.50E-04	25
H2AFZ	2.25641026	0.0739495	24
HIST1H4G	2.78632479	0.01880684	24
ARPC1B	2.78632479	0.00686318	24
CMAS	2.78632479	0.00686318	24
VASP	2.31623932	0.00685848	24
ARPC5	2.27350427	0.08020641	23
MFGE8	2.29059829	0.02995825	23
ATP6V1B2	2.8034188	0.00640826	23
HNRNPC	2.79487179	0.00171283	23
KRT18	2.79487179	0.00171283	23
HIST1H2BB	2.79487179	0.00171283	23
ANXA6	2.30769231	0.01990764	22
LRRC47	2.8034188	0.00160792	22
HIST1H1C	2.8034188	0.00160792	22
A1BG	2.8034188	0.00156444	22
H2AFY	2.8034188	0.00156444	22
PDLIM5	2.36752137	3.11E-04	22
TNC	2.4957265	0.00265392	21
HMGN3	2.83760684	4.87E-04	21
RPSL29	2.83760684	4.25E-04	21
CAVIN1	2.55555556	0.00110773	20
TUBB4B	2.5982906	0.0451903	19
WDR1	2.33333333	0.01490134	19
ADAR	2.42735043	0.00886392	19
TNIK	2.58974359	0.00180232	19
ANXA4	3.02564103	0.01743005	18
VCL	2.25641026	0.00840011	18
CA3	2.87179487	9.00E-04	18
MACF1	2.5042735	1.66E-04	18
MYH9	2.7008547	1.32E-04	18
YBX3	2.7008547	1.32E-04	18
LOC102157231	3.04273504	0.05132465	17
DNAJB11	2.66666667	0.00310077	16
ACTB	3.02564103	4.20E-04	16
LSM14A	2.42735043	0.00129939	15
ELOB	2.68376068	0.01727207	14
HSPA8	2.43589744	0.00756822	14
NUP107	2.61538462	5.77E-05	14
SERBP1	2.52136752	0.0233697	12
TUBB	2.81196581	0.00641467	12
FKBP10	2.47008547	0.00603258	11
KRT5	2.73504274	3.63E-04	10
DCTN2	2.69230769	2.99E-04	10
RPS3A	2.57264957	0.0156627	9
KANK2	2.79487179	7.63E-04	9
YBX1	2.76068376	8.73E-04	8
ANXA1	2.77777778	5.66E-04	7
AHNAK	2.8974359	1.85E-04	7
LDHA	2.82905983	3.64E-05	6
HDGF	2.76923077	0	6
VIM	1	0.23333333	5
JCHAIN	1	0.025	5
ATP5F1B	1	0.025	5
RPL8	1	0.025	5
DDAH2	1	0.025	5
DSP	3.17948718	0.00140417	5
HNRNPH1	2.85470085	1.81E-04	5
PLIN3	3.13675214	1.23E-04	5
LMNB1	1.2	0.1	4
APOE	1	0.05555556	4
KRT8	1	0.05555556	4
DDX17	1	0.05555556	4
COL2A1	1.2	0.03333333	4
DPT	1.2	0.03333333	4
PDXDC1	3.55555556	0.00979632	4
EIF2S1	3.47008547	7.97E-05	4
PDIA4	3.72649573	0	4
FGB	1.2	0	4
TUBB2A	1.2	0	4
HNRNPM	4	0.03404067	3
COLGALT1	3.56410256	0.00722401	3
CCT3	3.4957265	0	3

CGREF1	1.4	0	3
KHDRBS1	1.25	0	3
CLU	1.25	0	3
DBN1	2.94871795	0	3
RRBP1	3.23076923	0.03389331	2
CSN2	4.20512821	0.01709402	2
EZR	1.6	0	2
COTL1	4.53846154	0	2
COL3A1	1	0	2
LOC475521	1	0	2
SH3BGRL3	1	0	2
RPS10	4.99145299	0	1
ACTA2	4.01709402	0	1
LTF	3.77777778	0	1
OGN	3.1025641	0	1
HNRNPA3	4.99145299	0	1
LOC480784	3.67521368	0	1
LOC491263	5.1965812	0	1

Table S4 – Network of PD tumor regions sorted by degree.

ID	Average Shortest Path Lenght	Betweeness Centrality	Degree
CALD1	1.75438596	0.04815243	65
APOA1	1.78070175	0.01803336	61
TAGLN2	1.78947368	0.02139953	60
COL12A1	2.06140351	0.01958745	60
CAPG	1.78947368	0.01566516	60
IL16	1.78947368	0.01562958	60
CTNNA1	1.78947368	0.0344978	59
LAMB2	1.85087719	0.01293907	59
BAG3	1.80701754	0.01264562	59
SLC7A5	1.80701754	0.01147142	59
COL1A1	1.80701754	0.01374398	58
LGALS3BP	2.0877193	0.00691208	58
EIF4G1	1.88596491	0.00978421	57
FLNA	1.87719298	0.00957975	56
EPB41L2	1.83333333	0.00827358	56
LIMA1	1.88596491	0.00603774	56
ADMR1	1.88596491	0.00603774	56
RBMX	2.10526316	0.00431386	56
AHNAK2	1.83333333	0.01623457	55
HSPG2	1.83333333	0.01336667	55
TPM1	1.83333333	0.01032732	55
PDIA3	1.88596491	0.00701852	55
KRT10	1.9122807	0.00584977	55
JPT2	1.89473684	0.00559182	55
IGFBP5	1.84210526	0.01388891	54
ARHGDIA	1.92105263	0.00557788	54
ABI3BP	1.90350877	0.00521186	54
HSPA5	1.92105263	0.00718489	53
HSPA8	1.93859649	0.00489449	52
SPTAN1	2.14912281	0.0054545	51
VCAN	1.87719298	0.01261153	50
C3	1.95614035	0.00468533	50
EEF1D	1.96491228	0.0033504	49
SERBP1	1.94736842	0.00620161	48
EMILIN2	1.97368421	0.00405402	48
RPS3A	2.18421053	0.00268927	48
MPST	2.23684211	0.00123852	48
HIST1H1A	2.18421053	0.00379494	47
MZB1	2.26315789	0.0018386	47
CAVIN1	2.28070175	9.19E-04	45
LSM14A	2.28070175	3.47E-04	45
MACF1	2.00877193	0.00287545	44
TNC	2.00877193	0.00237135	44
DCTN2	2.28947368	0.00175921	44
CANX	2.26315789	0.00583979	43
VCL	1.78070175	0.40954944	42
FKBP10	2.03508772	0.00445363	42
CCT3	2.28947368	6.97E-04	41
F2	2.24561404	0.02465422	40
EIF2S1	2.34210526	0.00200728	39
TNKS1BP1	2.28070175	0.04783408	35
NSFL1C	2.3245614	0.00101992	35
COL1A2	2.30701754	0.00137986	33
MYH9	2.39473684	4.71E-04	32
TUBB4B	2.3245614	0.04281873	30
YBX1	2.33333333	0.00962342	30
PDLIM5	2.42982456	8.75E-05	30
LOC102157231	2.97368421	0.00746382	28
LRRC47	2.99122807	0.00596302	27
HIST1H1C	2.99122807	0.00596302	27
HIST1H4G	2.99122807	0.00596302	27
MFGE8	2.28947368	0.07049233	26
ANXA6	2.28947368	0.07049233	26
LTF	3	0.00582504	26
H2AFZ	3	0.00272785	26
ARPC1B	2.99122807	0.00100483	26

HIST1H2BB	2.99122807	0.00100483	26
H2AFY	2.28947368	0.09378407	25
RPSL29	2.30701754	0.05720247	25
FETUB	2.30701754	0.05720247	25
RBM3	2.36842105	0.0213842	25
ARPC5	3.00877193	0.00263433	25
WDR1	3.01754386	4.33E-04	25
A1BG	3.01754386	4.33E-04	25
ACTB	3.01754386	4.33E-04	25
CMAS	3.01754386	4.33E-04	25
ATP6V1B2	3.01754386	4.33E-04	25
HNRNPC	3.00877193	3.73E-04	25
CA3	3.00877193	3.73E-04	25
HMGN3	3.03508772	2.96E-05	24
KRT18	3.03508772	2.96E-05	24
LDHA	2.47368421	8.75E-06	24
DBN1	2.5	7.50E-05	23
PDIA4	3.04385965	3.11E-04	22
ENO1	3.05263158	0	22
KRT5	2.53508772	4.70E-04	19
DSP	2.5877193	7.10E-05	17
HDGF	2.5877193	6.98E-05	16
ANXA4	3.0877193	0.03166826	15
TNIK	2.51754386	0.00688287	13
ALDOA	3.13157895	0.01754386	12
DNAJB11	3.00877193	0.00144926	11
COL3A1	2.34210526	0.01790682	10
TUBB	3.14035088	0.00909297	10
HNRNPM	3.85964912	0.00217025	10
PLIN3	3.10526316	5.12E-04	10
ADAR	3.15789474	0.00595532	8
RPS10	3.87719298	0.00148639	8
SH3BGRL3	2.37719298	5.77E-04	8
AHNAK	3.24561404	0.00287303	7
KANK2	2.60526316	4.06E-04	7
ELOB	3.16666667	1.79E-04	7
LOC100687619	2.62280702	0.01847556	6
VASP	2.57017544	7.60E-04	6
THRAP3	2.5877193	0	6
RPL8	1.16666667	0.2	5
DDAH2	1.16666667	0.2	5
EZR	1	0.025	5
VIM	1	0.025	5
DPT	1	0.025	5
LMNB1	1	0.025	5
SF3B2	2.76315789	0	5
HNRNPA3	4.04385965	0.01754386	4
MPO	3.19298246	1.90E-04	4
TAGLN	1.2	0	4
FGB	1.5	0	4
JCHAIN	1.5	0	4
CGREF1	1.2	0	4
ATP5F1B	1.5	0	4
TUBB2A	1.5	0.33333333	3
APOE	1	0	3
ANXA1	4.10526316	0	3
KHDRBS1	1	0	3
KRT8	1	0	3
CLU	1	0	3
ACTA2	5.03508772	0	1
NUP107	1	0	1
FN1	2.33333333	0	1
LOC475521	3.33333333	0	1
SFPQ	1	0	1
CSN2	1	0	1
HNRNPH1	3.61403509	0	1
ACAN	4.12280702	0	1
LOC480784	3.23684211	0	1
LOC491263	1	0	1

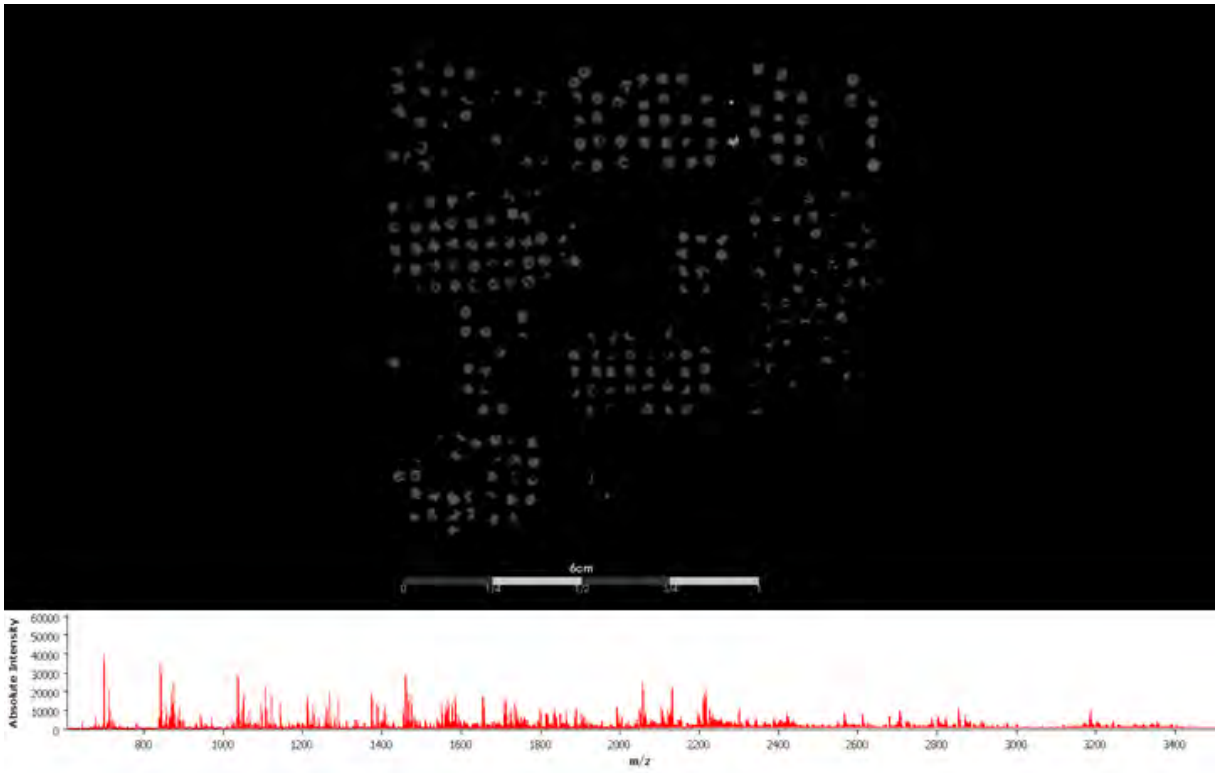

Supplementary Figure S1 – Overview of mass spectrometry imaging data set consisting in tissues of 17 primary tumors surgically removed from five animals diagnosed with metastatic mammary carcinomas.

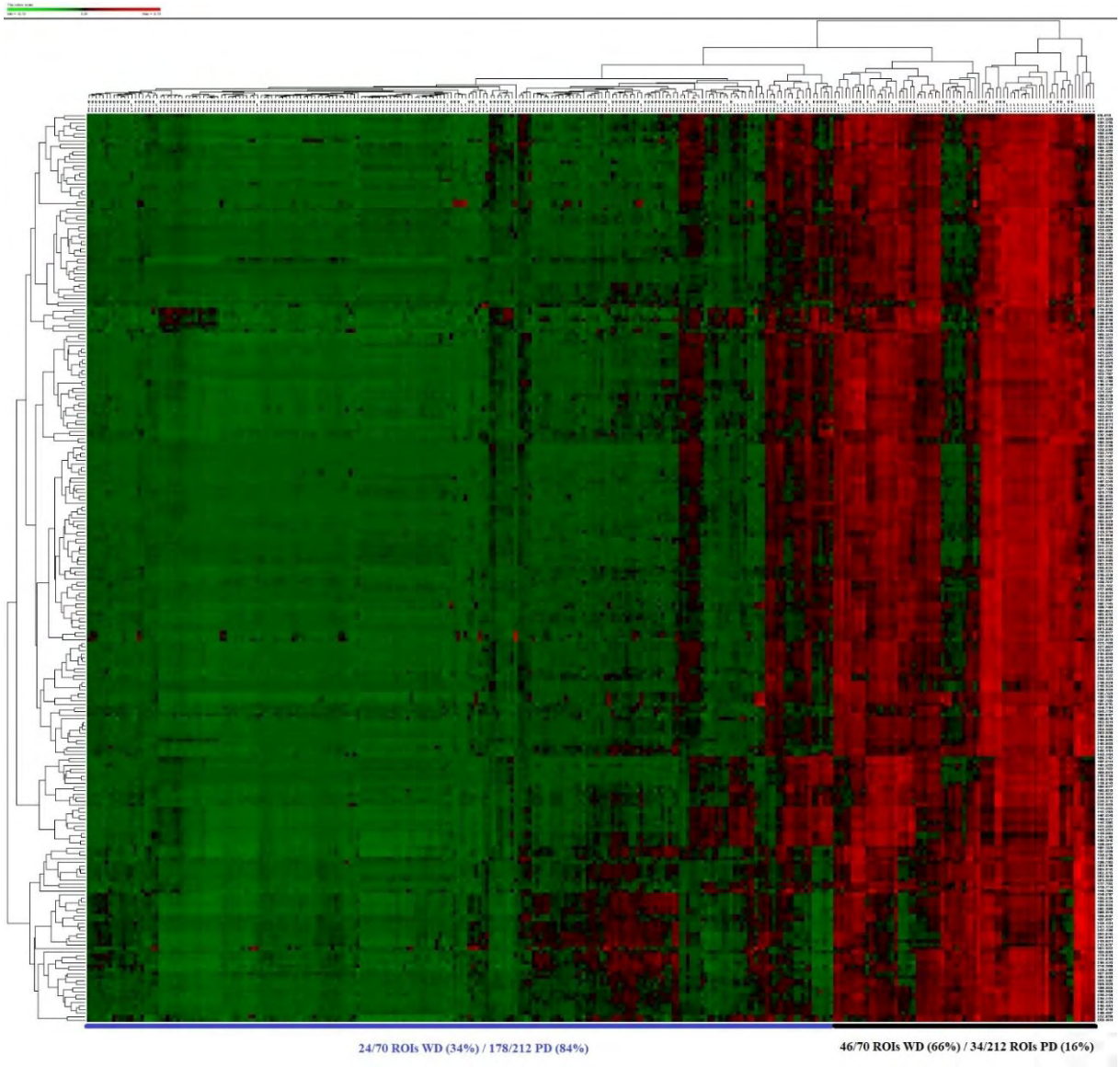

Supplementary Figure S2 – Heatmap showing the average expression per ROI of the 254 m/z differentially expressed signals between 70 well-differentiated ROIs (WD) and 212 poorly-differentiated ROIs (PD). ROC analysis and statistics results showed all m/z values as being more expressed in WD regions (AUC > 0.70 and FDR < 0.05). We also observed tumor heterogeneity, with 16% of PD ROIs clustering with the majority of WD populations (black bar).

APÊNDICE C – MATERIAL SUPLEMENTAR CAPÍTULO 3

Table S1 – Protein assingment of 108 *m/z* signals (tolerance = ±10 ppm) obtained from MALDI imaging dataset

Observed m/z	Theoretical m/z	Error (ppm)	Protein	Symbol
976.4489895	976.44828	-0.727	Actin cytoplasmic 1/Actin alpha 2 smooth muscle	ACTB/ACTA2
1198.70636	1198.7055	-0.718	Actin cytoplasmic 1/Actin alpha 2 smooth muscle	ACTB/ACTA2
2040.043861	2040.02439	-9.545	Annexin	ANXA1
1858.878632	1858.87522	-1.836	ATP synthase subunit beta	ATP5F1B
1061.575492	1061.57382	-1.575	Complement C4 A	C4A
1050.552407	1050.55783	5.162	Capping actin protein gelsolin like	CAPG
1280.621243	1280.61509	-4.805	Capping actin protein gelsolin like	CAPG
1875.976372	1875.96715	-4.916	Chromodomain helicase DNA binding protein 4	CHD4
1232.610452	1232.61172	1.029	Clusterin	CLU
1427.639032	1427.64712	5.665	Clusterin	CLU
2014.942371	2014.92937	-6.452	Clusterin	CLU
1281.630711	1281.6182	-9.762	Collagen alpha-1(I) chain	COL1A1
1690.78509	1690.77795	-4.223	Collagen alpha-1(I) chain	COL1A1
1223.618059	1223.61272	-4.363	Collagen alpha-2(I) chain	COL1A2
1261.635922	1261.62837	-5.986	Collagen alpha-2(I) chain	COL1A2
1427.719002	1427.71337	-3.944	Collagen alpha-2(I) chain	COL1A2
2023.942396	2023.93626	-3.031	Collagen type II alpha 1 chain	COL2A1
1114.505019	1114.49458	-9.367	Collagen type IV alpha 3 chain	COL4A3
1359.620078	1359.62091	0.612	Casein alpha s1	CSN1S1
1375.618071	1375.61582	-1.636	Casein alpha s1	CSN1S1
1773.844292	1773.84359	-0.396	Casein alpha s1	CSN1S1
2065.924124	2065.92686	1.324	Casein alpha s1	CSN1S1
1002.572525	1002.57309	0.563	Beta-casein	CSN2
1014.572002	1014.57309	1.072	Beta-casein	CSN2
1585.77562	1585.77174	-2.447	Beta-casein	CSN2
1564.67832	1564.67215	-3.943	D-aminoacyl-tRNA deacylase	DTD1
1225.562426	1225.56952	5.788	Filamin A	FLNA
1697.895781	1697.89292	-1.685	Glyceraldehyde-3-phosphate dehydrogenase	GAPDH
1274.701323	1274.69639	-3.870	Histone H2A	H2AC11
944.5340232	944.53123	-2.957	Histone H2A	H2AFZ
1325.75716	1325.75357	-2.708	Histone H4	H4C1
1166.621198	1166.61641	-4.104	H15 domain-containing protein	HIST1H1C
1198.670099	1198.66778	-1.935	H15 domain-containing protein	HIST1H1C
1326.760753	1326.76274	1.498	H15 domain-containing protein	HIST1H1C
1092.607712	1092.60479	-2.674	Histone H2B	HIST2H2BF/ HIST1H2BB

1137.551295	1137.54627	-4.418	Histone H2B	HIST2H2BF/ HIST1H2BB
1227.675041	1227.66918	-4.774	Histone H2B	HIST2H2BF/ HIST1H2BB
1751.059187	1751.04255	-9.501	Histone H2B	HIST2H2BF/ HIST1H2BB
1013.448777	1013.44353	-5.178	Heterogeneous nuclear ribonucleoprotein A2/B1	HNRNPA2B1
1221.558391	1221.55283	-4.552	Heterogeneous nuclear ribonucleoprotein A2/B1	HNRNPA2B1
1313.60623	1313.59814	-6.159	Heterogeneous nuclear ribonucleoprotein A2/B1	HNRNPA2B1
1377.639433	1377.62944	-7.254	Heterogeneous nuclear ribonucleoprotein A2/B1	HNRNPA2B1
1664.786279	1664.80206	9.479	Heterogeneous nuclear ribonucleoprotein A2/B1	HNRNPA2B1
2205.919963	2205.90027	-8.928	Heterogeneous nuclear ribonucleoprotein A2/B1	HNRNPA2B1
1194.704762	1194.69935	-4.530	Heterogeneous nuclear ribonucleoprotein K	HNRNPK
1459.697859	1459.7032	3.659	Heterogeneous nuclear ribonucleoprotein M	HNRNPM
1114.639293	1114.64665	6.600	Heterogeneous nuclear ribonucleoprotein M	HNRNPM
1714.926765	1714.91226	-8.458	Heterogeneous nuclear ribonucleoprotein U	HNRNPU
2171.164078	2171.14551	-8.552	Heterogeneous nuclear ribonucleoprotein U	HNRNPU
986.5159128	986.5153	-0.621	Heat shock protein family A (Hsp70) member 5	HSPA5
1677.80738	1677.80785	0.280	Heat shock protein family A (Hsp70) member 5	HSPA5
1487.691822	1487.70126	6.344	Heat shock protein family A (Hsp70) member 8	HSPA8
917.5012336	917.49384	-8.058	Canine mammary tumor	HSPB1
1614.808599	1614.80819	-0.253	Canine mammary tumor	HSPB1
1635.862654	1635.86016	-1.525	Immunoglobulin heavy constant mu	IGHM
1960.927809	1960.91746	-5.278	Immunoglobulin heavy constant mu	IGHM
1415.709446	1415.70529	-2.936	Ig-like domain-containing protein	IGLL5
1361.677936	1361.6907	9.373	Keratin	KRT
1082.59162	1082.59931	7.103	IF rod domain-containing protein	KRT
1203.6275	1203.63681	7.735	IF rod domain-containing protein	KRT
1265.629288	1265.63721	6.260	Keratin type II cytoskeletal 1	KRT1
2367.277463	2367.26266	-6.253	Keratin type I cytoskeletal 10	KRT10
2101.989575	2101.98187	-3.666	Keratin 14	KRT14
1138.597245	1138.59635	-0.786	IF rod domain-containing protein	KRT18
1936.999583	1936.98353	-8.287	IF rod domain-containing protein	KRT18
1577.779731	1577.76666	-8.285	Keratin 19	KRT19
1779.837479	1779.82965	-4.399	Keratin 19	KRT19
1380.713918	1380.71177	-1.556	IF rod domain-containing protein	KRT5
1517.694933	1517.69005	-3.218	IF rod domain-containing protein	KRT5
1824.908896	1824.91986	6.008	IF rod domain-containing protein	KRT5
2246.159292	2246.14115	-8.077	IF rod domain-containing protein	KRT5
2470.158419	2470.15146	-2.817	IF rod domain-containing protein	KRT5

1107.545118	1107.54291	-1.993	IF rod domain-containing protein	KRT6A
1126.667473	1126.66912	1.462	IF rod domain-containing protein	KRT7
941.4325757	941.4323	-0.293	IF rod domain-containing protein	KRT8
1473.780368	1473.77951	-0.582	IF rod domain-containing protein	KRT8
1489.704677	1489.703	-1.125	IF rod domain-containing protein	KRT8
1473.675903	1473.67507	-0.565	LIM and SH3 protein 1	LASP1
1203.568429	1203.57394	4.579	Lamin A/C	LMNA
1507.730427	1507.74208	7.729	Lamin A/C	LMNA
1605.821015	1605.81188	-5.689	Lamin A/C	LMNA
1945.935998	1945.93624	0.124	Lamin A/C	LMNA
1371.622841	1371.63464	8.602	Lamin B2	LMNB2
1045.565213	1045.56365	-1.495	Peptidase S1 domain-containing protein	LOC475521
1108.519496	1108.51907	-0.384	Lipocln_cytosolic_FA-bd_dom domain-containing protein	LOC491263
1745.925817	1745.9392	7.665	LRR binding FLII interacting protein 1	LRRFIP1
1215.605872	1215.60764	1.454	Latent transforming growth factor beta binding protein 2	LTBP2
1571.814078	1571.82753	8.558	Microtubule-associated protein	MAP4
1322.658618	1322.65465	-3.000	N-Myc downstream regulated gene 1	NDRG1
1565.795546	1565.78779	-4.953	N-Myc downstream regulated gene 1	NDRG1
1648.774715	1648.78131	4.000	NSFL1 cofactor	NSFL1C
1757.863468	1757.87767	8.079	Proline rich coiled-coil 2A	PRRC2A
1237.555182	1237.54839	-5.489	RNA binding motif protein 14	RBM14
1144.640453	1144.64732	5.999	60S ribosomal protein L6	RPL6
1769.989999	1769.98682	-1.796	60S ribosomal protein L6	RPL6
1749.091616	1749.07451	-9.780	Ribosomal protein L8	RPL8
1187.645695	1187.65313	6.260	Ribosomal protein S16	RPS16
1219.64741	1219.64296	-3.649	40S ribosomal protein S8	RPS8
1117.507023	1117.50211	-4.397	Serum amyloid A protein	SAA1
1274.647305	1274.64475	-2.005	Serum amyloid A protein	SAA1
1730.781746	1730.76884	-7.457	Small nuclear ribonucleoprotein U1 subunit 70	SNRNP70
1399.620113	1399.6093	-7.725	Transgelin	TAGLN2
1769.831449	1769.83092	-0.299	Transgelin	TAGLN2
1245.592025	1245.59323	0.967	Tubulin beta chain	TUBB4B
1088.539886	1088.53308	-6.253	Vimentin	VIM
1510.711046	1510.7067	-2.877	Vimentin	VIM
1900.962831	1900.95116	-6.140	Vimentin	VIM
1897.811353	1897.80462	-3.548	CSD_1 domain-containing protein	YBX1

Table S2 – Significant m/z signals between ILM and LNM regions, considering FDR < 0.01

m/z	**P value**	**Mean1**	**Mean2**	**Difference**	**SE of difference**	**t ratio**	**df**
944.53402	0.0111034	13692.6	19230.7	-5538.11	2102.93	2.63352	52
1013.4488	0.00395638	488.047	1060.27	-572.219	189.727	3.01602	52
1045.5652	4.3088E-06	9931.64	5660.22	4271.42	832.057	5.13357	52
1050.5524	0.00052017	677.451	1193.26	-515.804	139.384	3.70058	52
1061.5755	0.0150363	635.393	986.019	-350.626	139.418	2.51492	52

1114.6393	0.0160082	818.662	1278.88	-460.217	184.825	2.49001	52
1117.507	0.00330793	411.375	662.018	-250.643	81.3888	3.07957	52
1144.6405	0.00115719	23225.7	40614	-17388.3	5055.83	3.43926	52
1166.6212	0.00312257	4249.58	6859.02	-2609.44	841.785	3.09989	52
1187.6457	7.2089E-05	1272	2502.18	-1230.18	285.214	4.31318	52
1194.7048	0.00039486	691.154	1226.33	-535.175	141.259	3.78861	52
1221.5584	1.1821E-06	803.621	2085.66	-1282.04	233.207	5.49746	52
1232.6105	0.00042948	527.341	939.94	-412.599	109.679	3.76187	52
1237.5552	0.00041063	869.576	1696.12	-826.546	218.885	3.77616	52
1274.7013	6.5664E-05	9024.83	16679.9	-7655.02	1763.34	4.3412	52
1313.6062	4.338E-06	1683.77	5478.34	-3794.57	739.444	5.13165	52
1322.6586	0.0147305	1133.58	1735.45	-601.861	238.544	2.52306	52
1326.7608	0.00360624	3327.49	4861.05	-1533.56	502.97	3.04901	52
1361.6779	0.00039891	778.288	1590.15	-811.859	214.473	3.78536	52
1377.6394	0.010154	702.303	1825.58	-1123.28	421.037	2.66788	52
1473.7804	0.00024743	669.172	1319.91	-650.743	165.341	3.93576	52
1507.7304	0.00804612	752.199	1104.38	-352.177	127.779	2.75615	52
1565.7955	0.00850978	822.938	1388.87	-565.929	204.856	2.76257	52
1585.77539	0.00790978	9731.64	5780.22	3951.42	743.136	2.76351	52
1635.8627	0.00916429	1650.14	965.775	684.365	252.813	2.70699	52
1648.7747	0.00505938	1125.82	1868.07	-742.256	253.548	2.92748	52
1690.7851	0.00237572	914.2	1602.54	-688.341	215.427	3.19524	52
1697.8958	5.8703E-06	6771.99	2057.5	4714.49	934.374	5.04561	52
1749.0916	0.00016855	5490.15	2837.38	2652.77	654.228	4.05482	52
1751.0592	4.0187E-06	17337.5	6078.22	11259.3	2184.86	5.15334	52
1769.8314	4.2378E-05	843.697	1837.37	-993.676	222.213	4.47172	52
1773.8443	0.00905785	801.043	1204.53	-403.487	148.81	2.71143	52
1897.8114	1.061E-05	3041.86	6238.86	-3197	655.653	4.87605	52
1936.9996	0.0112458	1544.81	2375.31	-830.499	315.947	2.6286	52
1945.936	0.0016686	1020.78	1667.67	-646.897	195.067	3.31627	52
2171.1641	0.00829131	2622.61	4091.89	-1469.28	535.285	2.74486	52
2205.92	0.00044784	2140.86	6039.87	-3899.01	1040.15	3.74852	52